ELSEVIER

Solar Energy Materials & Solar Cells 60 (2000) 201–262

Solar Energy Materials & Solar Cells

www.elsevier.com/locate/solmat

Electrochromic tungsten oxide films: Review of progress 1993–1998

C.G. Granqvist

Uppsala University, The Ångstrom Laboratory, Department of Materials Science, P.O. Box 534, SE-751 21 Uppsala, Sweden

Received 25 May 1999

Abstract

W oxide films are of critical importance for electrochromic device technology, such as for smart windows capable of varying the throughput of visible light and solar energy. This paper reviews the progress that has taken place since 1993 with regard to film deposition, characterization by physical and chemical techniques, optical properties, as well as electrochromic device assembly and performance. The main goal is to provide an easy entrance to the relevant scientific literature.

Keywords: Electrochromism; W oxide; Thin film; Smart window

1. Introduction

An electrochromic material is characterized by its ability to sustain reversible and persistent changes of the optical properties when a voltage is applied to it. The electrochromic phenomenon was discovered in W oxide thin films, and this material remains the most promising candidate for electrochromic devices. A thorough review of electrochromic W oxide was given in the earlier "Handbook of Inorganic Electrochromic Materials" [1], treating previous studies until mid-1993. The reader is referred to this book for background material. The present treatise ventures to cover the more recent work, i.e., from 1993 and onwards. The motivations for this new review are that much progress has taken place lately so that the Handbook tends to be

E-mail address: claes-goran.granqvist@angstrom.uu.se (C.G. Granqvist)

0927-0248/00/$ - see front matter
PII: S0927-0248(99)00088-4

somewhat outdated as regards W oxide (but less so for most other electrochromic oxides), and that the numerous overview papers that have appeared during the past few years are far from exhaustive [2–64].

It is convenient to introduce electrochromism in W oxide by reference to the simple reaction

$$WO_3 + xM^+ + xe^- \leftrightarrow M_xWO_3 \quad (1)$$

with $M^+ = H^+$, Li^+, Na^+, or K^+, and e^- denoting electrons. Thus when W oxide, which is transparent as a thin film, incorporates electrons and charge-balancing ions it can be reversibly transformed to a material with radically different properties, being absorbing if the material is heavily disordered and infrared-reflecting if it is sufficiently crystalline. It should be pointed out already here that relation (1) is a gross oversimplification, and the thin films of practical interest normally are hydrous — i.e., contain hydroxyl groups and incorporated water molecules — and may deviate to some extent from the stated WO_3 stoichiometry.

It is obvious that a detailed theoretical understanding of the electrochromism hinges on reliable theoretical modeling of the electronic structure of WO_3 and M_xWO_3. This modeling has advanced significantly during the past few years, and recent data on single crystalline materials are discussed in Section 2. Section 3 then considers practical thin film manufacturing and surveys data on samples prepared by a multitude of techniques such as evaporation, sputtering, sol–gel deposition, chemical vapor deposition, anodization, etc. In Section 4 we turn to the physical (excepting the optical) properties of ion intercalated films and discuss items such as diffusion constants and structural modifications. Optical properties are dealt with in Section 5, with detailed accounts of reflectance modulation in crystalline W oxide — which can be given a thorough discussion starting from the electronic structure — and absorptance modulation in heavily disordered W oxide. Polaron effects are considered in some detail. Finally, Section 6 covers electrochromic device aspects and lists characteristic data for a large number of practical arrangements for modulating optical transmittance. A "case study" runs throughout Sections 3–5; it gives detailed information on W oxide films made by sputter deposition under a set of well-specified conditions.

2. Calculated electronic structure of crystalline WO_3 and MWO_3

The electronic structure of a material is the foundation on which its electromagnetic properties can be understood and modeled, and WO_3-based materials have been subject detailed studies several times [65–73]. The early work can be criticized for being non-self-consistent and for other reasons, while the recent one represents state-of-the-art. The exposition below is strongly focused detailed computations by Hjelm et al. [71]. We will return to the electronic structure several times later in this review; in particular, it will be employed for the computations of the optical properties of crystalline M_xWO_3 in Section 5.1.

2.1. Theoretical and computational aspects

Some technical details are needed in order to explain the computations of the electronic structure, which were carried out fully self-consistently using the local density approximation to density functional theory [74–77] and employing a parameterized exchange-correlation potential [78,79]. Basis functions and matrix elements were constructed using a full-potential linear muffin-tin orbital method [80,81]. The charge density and potential were expanded in symmetry-adapted spherical harmonics up to eighth order in a muffin-tin sphere around each atomic site. The spheres were non-overlapping, and the charge density and potential were expanded in 24^3 Fourier waves in the interstitial region. The basis set consisted of augmented muffin-tin orbitals [82,83]. The tails of the basis functions outside their parent spheres were linear combinations of Hankel or Neuman functions with non-zero kinetic energy. Tungsten-site-centered 5p, 6s, 6p, and 5d wave functions were used as well as 2s and 2p functions centered on oxygen sites. When H, Li, or Na were included in the calculations, the s and p functions were employed with appropriate principal quantum number. A double-basis set was used, i.e., two-basis functions of the same quantum numbers were taken to be connected to tails with different kinetic energy. Furthermore, the W 5p constituted a pseudo-valence state and used tail energies considerably lower than those of the true valence wave functions, although fully hybridizing with the valence states. Relativistic effects were treated in a scalar relativistic approximation, implying that spin–orbit coupling was not included [84]. The core states were relaxed in each iteration, using a fully relativistic equation. The Brillouin zone integrations used a special point method with Gaussian smearing over a width of 1 mRy [85,86]. In all calculations, except those for the hexagonal structure to be discussed below, a $\boldsymbol{k}$-point density corresponding to 56 points in $\frac{1}{48}$ of the cubic Brillouin zone was adopted. Fifty points were used for the hexagonal phase.

The computational method outlined above was applied to appropriate structural models. These models must be developed with care since WO_3 and related materials can be found in a large variety of crystal structures. The tungsten oxides consist of WO_6 octahedra arranged in various corner-sharing or edge-sharing configurations [1,87–90]. The simplest form is the defect perovskite or ReO_3 structure shown in Fig. 1(a). The figure also illustrates the positions of intercalated ions occupying symmetry positions; clearly a perovskite structure is then formed. Pure, bulk-type WO_3 does not generally exist in a cubic structure, though, but instead a monoclinic phase appears to be most stable at room temperature [91]. In thin films, however, it is most likely that the octahedra are ordered hexagonally in crystallites with sizes depending on the fabrication route and deposition temperature [92–95]. The monoclinic phase requires a large unit cell (containing eight tungsten atoms) and hence too much computing power, and the cubic structure was chosen as a model system. However, it is the ubiquitous octahedral order that dominates the electronic properties, and this approximation therefore should be adquate. The differences in the electronic structure caused by various atomic arrangements were illuminated by calculations for the hexagonal phase, which requires three tungsten atoms per unit cell.

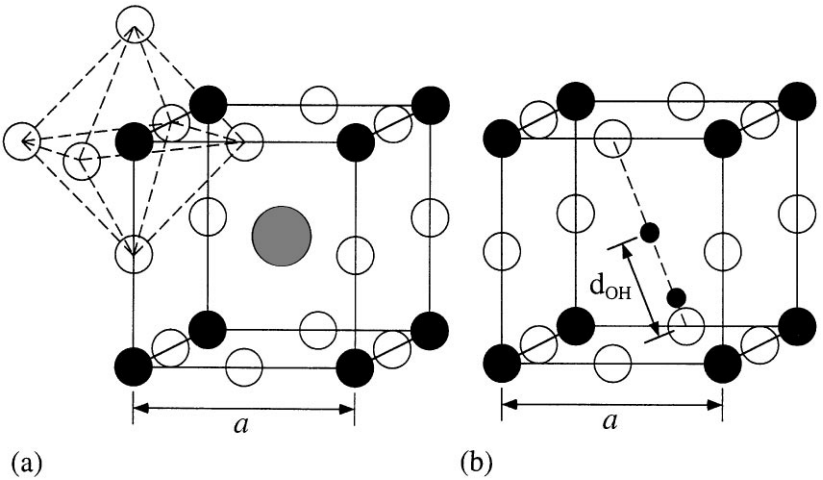

Fig. 1. Unit cells for cubic (Li,Na)WO_3 (part a) and HWO_3 (part b) with tungsten atoms as large solid circles, oxygen atoms as open circles, lithium or sodium atoms as large dashed circle, and hydrogen atoms as small solid circles located on a line between an oxygen site and the central position. The distance between the hydrogen and oxygen sites is denoted d_{OH}. The ReO_3 structure, used as an approximation for monoclinic WO_3, is obtained by considering only the tungsten and oxygen atoms. The lattice constant a is defined, and the octahedron, built up by oxygen atoms surrounding the tungsten atom, is shown.

Intercalation of H, Li, or Na in WO_3 leads to intricate structural changes that are not yet fully investigated and understood. Cubic structures have been reported for $H_{0.5}WO_3$, Li_xWO_3 with $0.1 < x < 0.4$, and Na_xWO_3 with $0.3 < x < 1$. The Li and Na atoms are expected to lie at the centers of the perovskite units (cf. Fig. 1(a)), whereas the H atoms are significantly off-center and are attached to oxygen atoms in hydroxyl groups as illustrated in Fig. 1(b) [96]. Our computations of electronic structure, to be discussed below, were confined to cubic HWO_3, $LiWO_3$, and $NaWO_3$.

Structural information of WO_3-related materials is almost endless, and we note, mainly for completeness, that recent data have been given on cubic WO_3 [97–100]; orthorhombic WO_3 [97], $W_{1-x}Mo_xO_3$ [97] and Ti-stabilized $WO_3 \cdot \frac{1}{3}H_2O$ [101]; monoclinic WO_3 [102]; hexagonal WO_3 [103–107], $Ce_{0.3}WO_3$ [108], $Cs_xW_{2-x/6}O_3$ [109–111], $(NH_4)_{0.3}WO_3$ [112] and Sn_xWO_3 [113]; and pyrochlore WO_3 [114] as well as this structure containing various ionic species [115–118]. Furthermore, structural data are available for a novel supermetastable WO_3 phase [90], substoichiometric WO_3 [119–122], Bi_2O_3–WO_3 [123], Nb_2O_5–WO_3 [124], Ta_2O_5–WO_3 [125,126], W_3O_8 [127], $WO_3 \cdot \frac{1}{3}H_2O$ [128–130], $W_{56}(O,F)_{156}$ [131], Li_2WO_4 [132], $Na_{0.10}WO_3$ [133], Ba_xWO_3 [134,135], Zn_xWO_3 [136], $Sb_{0.16}WO_3$ [137], $Sn_{0.23}WO_3$ [138], $Pb_{0.29}WO_3$ [135], $Nb_8W_9O_{47}$ [139], $Ta_8W_9O_{47}$ [139,140], $H_xV_xW_{1-x}O_3 \cdot q\ H_2O$ [141,142], $Li_xWO_{3+x/2} \cdot qH_2O$ [142], $Li_{1-x}Na_{1-x}W_xO_3$ [143], $Ag_2O \cdot WO_3 \cdot TeO_2$ [144], Keggin-type $[C_{12}H_{25}N(CH_3)_3]_6(H_2W_{12}O_{40}) \cdot q\ H_2O$ [145], Pt-containing WO_3 [146], phosphate tungsten bronzes [147], and for surface structures of WO_3 [148–152] and Na_xWO_3 [153–155].

2.2. Density of states data

We first consider cubic WO_3 whose density of states (DOS) is shown in Fig. 2(a). The data are consistent with the material being a semiconductor, in agreement with experiments. The O 2p and W 5d projected contributions to the total DOS are included in the figure. It is found that, as expected, the valence band is dominated by the O 2p states, while W 5d states dominate the conduction band. In addition, there is considerable hybridization between the valence and conduction bands. The O 2s levels are not included in the figure; they are positioned at -17.5 eV in energy. The calculated band gap is 0.6 eV, which is much smaller than the experimentally

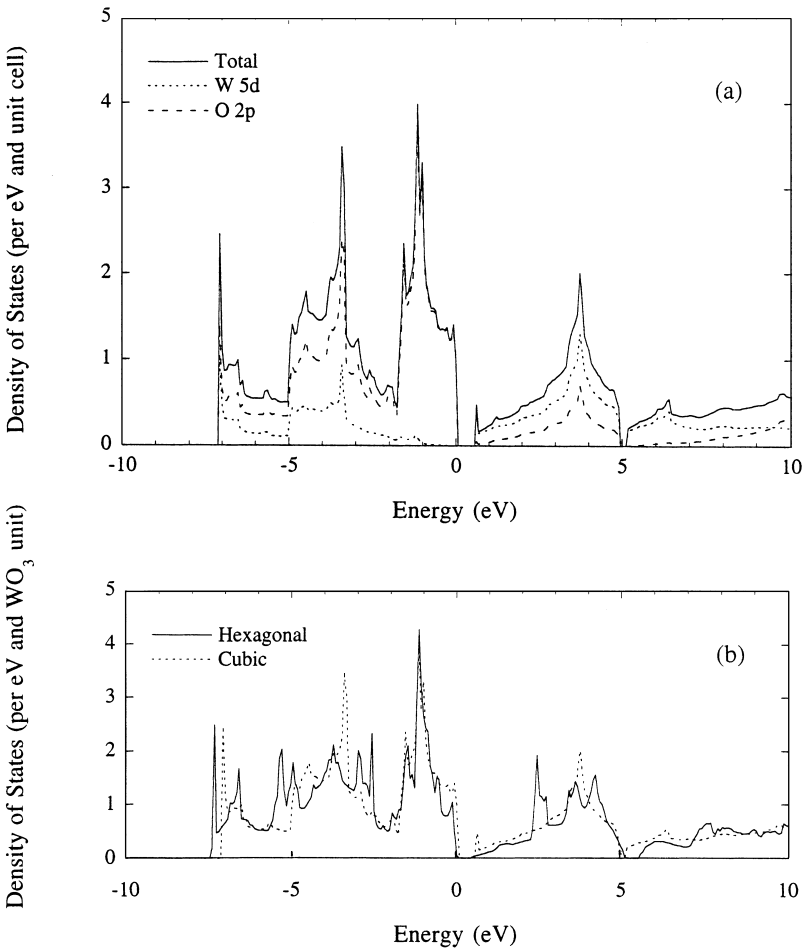

Fig. 2. Density of states for cubic WO_3 (part a) and comparison of data for the hexagonal and cubic structures (part b). Filled states are found at energies below zero and empty states above zero. Also shown are the O 2p and W 5d projected state densities for cubic WO_3.

determined value of 2.6–2.7 eV for the indirect band gap [1,156]. This difference points at a common failure when the local density approximation is applied to semiconducting systems [157]. Furthermore, the present approximation of the crystal structure as being cubic seems to reduce the band gap compared to that of the experimentally found structures [65,66]. The calcuated total energy of cubic WO_3 displays a minimum for a lattice constant of 3.84 Å; this is a value of the expected magnitude [71].

As pointed out above, it is of interest to carry out calculations also for hexagonal WO_3. In fact, two hexagonal phases are known [87]: one hydrated wherein the hexagonal layers of WO_6 octahedra are shifted from one layer to another, and one dehydrated for which the hexagonal layers are stacked directly on top of each other. Only the latter phase was subjected to computations; it comprises three WO_3 entities per unit cell. All W–O distances are equal in the basal plane, following the hexagonal symmetry, while the W–O distance along the *c* axes is slightly larger. The calculated DOS is presented in Fig. 2(b) together with the data for the cubic phase. The most important difference between hexagonal and cubic WO_3 is that the bottom of the conduction band shows a smooth onset above the gap in the hexagonal structure, while the cubic phase has a peak at this position. The width of the O 2p bands is somewhat broader in the hexagonal phase than in the cubic one. The splitting between the t_{2g} and e_g components of the W 5d bands (using conventional notation) appears at a somewhat higher energy in the hexagonal structure, and the gap is slightly larger. The total energy calculated for the cubic and hexagonal structures differ by 0.1 Ry, where the cubic structure has the lowest energy. This is consistent with the fact that the monoclinic phase of WO_3 is the normal one when the material is in bulk from. The present results strongly support the view that the octahedral ordering in WO_3 dominates its electronic properties, so that a confinement of the following DOS computations to the simpler cubic structure is very likely to provide insights into the electronic structure of real materials.

We now turn to $LiWO_3$, whose DOS is given in Fig. 3(a). The Li 2s band is found to be centered at 8.2 eV above the top of the valence band, and the Fermi energy lies at 2.9 eV, i.e., in the conduction band. This gives a very low occupation of the Li band, implying that the Li ion essentially remains ionized in the oxide, while the charge-balancing electron occupies the bottom of the conduction band. This large charge transfer is in sharp contrast to the interaction between the W and O wave functions, where the dominating mechanism in the transferring of electrons to lower energies is hybridization. In general, the occupied part of the conduction band is very similar to that of the pure oxide, implying that a rigid-band filling picture is appropriate. However, the valence band is narrower than in the pure oxide; the bandwidth is reduced from 7.1 to 6.4 eV. The band gap, now located in the occupied part of the spectrum, is increased to 1.6 eV. The calculated equilibrium lattice constant is slightly larger than for the pure oxide, viz., 3.88 Å. This is in contrast to the experimental situation for which it is found that the crystal contracts with increasing Li content, at least up to a concentration of 0.56 Li ions per unit cell where the contraction is 0.4% [158].

From a chemical point of view, sodium is very similar to lithium, with almost identical ionization potentials. This feature is clearly exhibited in the similarity of the

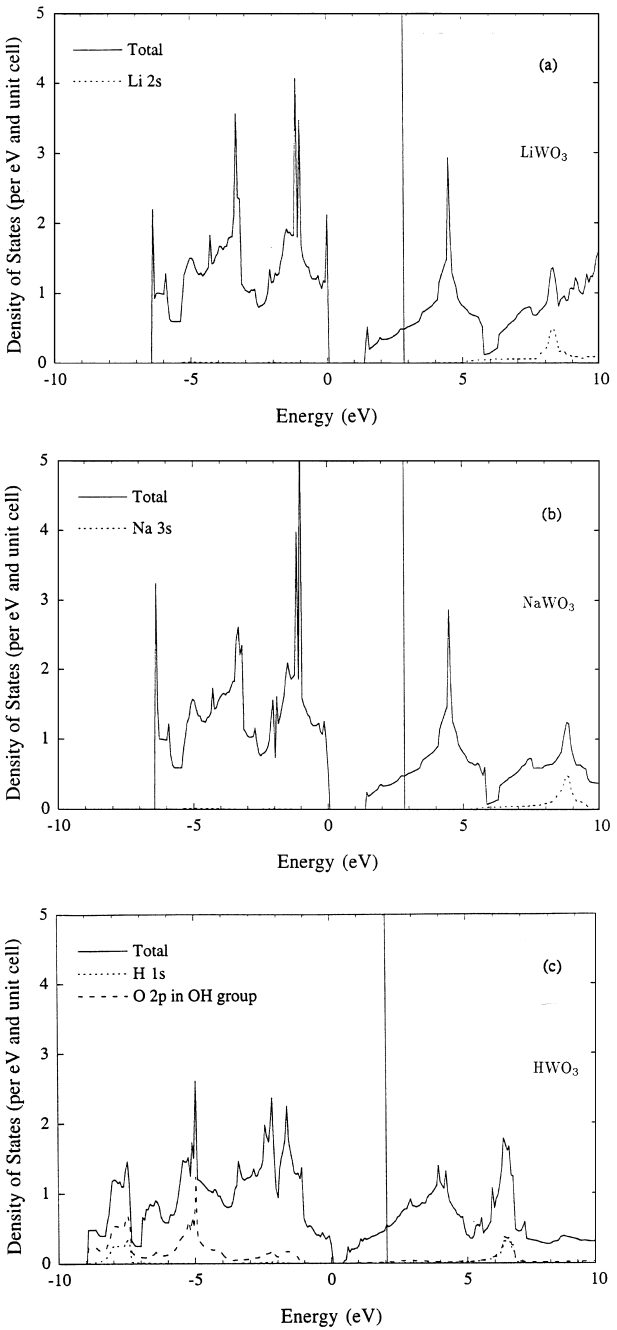

Fig. 3. Density of states for $LiWO_3$ (part a), $NaWO_3$ (part b), and HWO_3 (part c). Projected states are indicated by dashed curves, and Fermi levels are marked by vertical lines.

DOS plots in parts (a) and (b) of Fig. 3, referring to $LiWO_3$ and $NaWO_3$, respectively. The calculated lattice constants are the same for the two materials.

Hydrogen behaves differently from Li or Na in WO_3, though, and neutron diffraction data showed that the hydrogen atom is located near an oxygen atom with a maximum distance of 1.1 Å, i.e., that a hydroxide unit is formed [96]. The hydroxide formation was studied theoretically through calculations of total energy as a function of the O–H distance d_{OH}, with the H position being varied from the center in the perovskite cube along a straight line towards one oxygen atom as illustrated in Fig. 1(b). A minimum in total energy was found for $d_{OH} = 1.03$ Å, as shown in Fig. 4. If the calculations were performed using the central position for the hydrogen atom, a large hydrogen-projected peak in the DOS was seen to be present at the Fermi energy. Such a system supports spin polarization, with a calculated spin polarization energy of ~ 0.5 eV and a total magnetic moment of 0.84 Bohr magnetons. However, the total energy of the magnetic state is still larger than for the hydroxide forming state. When d_{OH} is decreased, the hydrogen peak moves away from the Fermi level towards higher energies, while a second hydrogen peak originating from the hybridization with the oxygen atom in the O–H pair grows at low energies. This implies that the hydrogen contribution to the DOS, and the support for spin polarization, vanishes as d_{OH} decreases. Fig. 3(c) displays the calculated DOS for the hydrogen position at which the total energy is minimized. Clearly, the oxygen states in the hydroxide pair is much lowered in energy, thus yielding a broadening of the valence band. The bottom of the conduction band, which now is occupied by one electron, resembles the cases for $LiWO_3$ or $NaWO_3$, and thus the physical properties should not be too different regardless of whether hydrogen or alkali ions are intercalated into the WO_3 host.

The hydrogen atom in HWO_3 does not occupy the central position, and there might be room for more than one hydrogen atom in the crystal. A total energy study of various plausible hydrogen contents shows that the energy gain when one hydroxide unit is formed amounts to 2.6 eV. If an additional hydrogen atom is inserted near

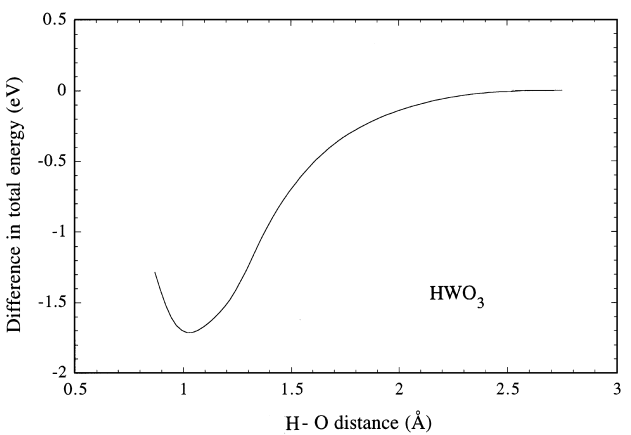

Fig. 4. Total energy for HWO_3 as a function of the O–H distance, denoted d_{OH} in Fig. 1(b).

to an oxygen atom already in a hydroxyl unit, thus forming a water molecule, the energy is lowered by 2.4 eV compared to the case of pure WO_3. On the other hand, if the second hydrogen atom forms another hydroxyl unit, the energy gain is 3.9 eV. From the differences in total energy one can draw the conclusion that the formation of a hydroxide is favored compared to a hydrate (water molecules around the oxygen sites) when hydrogen is inserted into WO_3. From the trends in total energies given above one can predict an energetically favorable uptake of hydrogen until all oxygen atoms participate in hydroxide pairs.

3. Thin film preparation and characterization

Electrochromic W oxide films can be prepared by a variety of different techniques, often leading to somewhat different properties as discussed in detail before [1]. Section 3.1 of this chapter gives a survey of the work in 1993–1998 and discusses, in order, films made by evaporation, sputtering, and electrochemical and chemical techniques. This overview is then followed by a more detailed presentation of W oxide films made by reactive sputtering in the presence of O_2 and CF_4, following work by Azens et al. [159–164].

3.1. Survey of data

Evaporation is a convenient technique for the production of electrochromic W oxide films. Deposition from an electrically heated Mo boat, as well as electron-beam evaporation, are used frequently, especially to fabricate samples for scientific purposes. The vapor species are molecular in nature, and recent mass spectrometric work has shown a preponderance of WO_2, WO_3, W_2O_6, and W_3O_9, implying that the tungsten is mainly in $+4$ and $+6$ states [165]. The as-deposited films are heavily disordered with a porosity that can be varied by deposition in the presence of a small amount of gas. In particular, evaporation in the presence of 5×10^{-4} Torr of H_2O yields a relative density of 0.6, whereas deposition in a good vacuum produces films with a relative density of 0.8 [166]. Similar porosities have been found by deposition in N_2 and O_2 [1]. Evaporated electrochromic W oxide films tend to be hydrous even if they are produced without deliberately adding water to the deposition unit, as seen by infrared spectroscopy [167–169] and other means [170]. A particularly elaborate study by Bohnke et al. [171] used Rutherford backscattering spectrometry (RBS) and elastic recoil detection analysis for W, O, and H profiling and proved that the stoichiometry could be expressed as $WO_x \cdot qH_2O$ with $x = 3.00 \pm 0.03$ at the substrate and $x = 3.10 \pm 0.03$ at the film's surface. The water was loosely bound with a H/W ratio of 0.8 for as-deposited films. This ratio dropped strongly upon annealing, especially in the range between 150°C and 180°C. The porous W oxide films could be crystallized by heating, and it was shown by Klein and Yen [172] that deposition onto a substrate at 200°C followed by a post-deposition anneal at 430°C in O_2 led to a monoclinic WO_3 film which became infrared reflecting after Li^+ intercalation (cf. Section 5.1 below). Interestingly, direct in situ annealing at 400°C yielded films that

were less suited for electrochromic applications. Annealing at 400°C, 500°C, and 600°C was reported to give a triclinic crystalline structure [173]. These latter films were somewhat substoichiometric, as detected by X-ray photoelectron spectroscopy (XPS). Atomic force microscopy (AFM) indicated that the crystalline films developed a surface roughness that became coarser at elevated annealing temperatures. An epitaxial tetragonal phase was found for films grown on sapphire at 600°C [174]. Densification of W oxide films is possible not only by annealing but also through ion beam irradiation [175]. The threshold for compaction was reported to be as low as 10^{12} ions/cm^2, thus indicating that a single ion is able to displace $\sim 10^5$ W oxide "molecules". Evaporated W oxide films have been investigated also in a large number of other studies [176–254]; the most pertinent results will be referred to below in different contexts. Evaporated films of $K_{0.3}WO_{3.15}$ have been reported [255]. Nanocrystalline films were prepared by evaporation in the presence of Ar or N_2 followed by annealing at 400°C in air [256], and directly by the evaporation of tungsten in the presence of O_2 [257].

Sputtering is considered next. This is a well established method for making thin films of practically all kinds of materials. DC and RF powering of the sputter plasma are convenient for deposition from conducting (metallic) and non-conducting (oxidic) targets, respectively, and the deposition can proceed in the presence of a reactive gas in order to make oxides, etc. Reactive DC magnetron sputtering is especially well suited for large-scale, large-area manufacturing. It has been combined with roll coating in the production of W oxide films [258]. Deposition rates in the 2–3 nm/s range have been reported [259,260]. Films deposited by this technique onto substrates at temperatures between 70°C and 100°C were found by Witham et al. [261] — who used a somewhat indirect method involving optical measurements — to have a columnar morphology and an intercolumnar void network, i.e., to exhibit a two-phase structure. The void content of these films was strongly dependent on the oxygen pressure in the sputtering plasma, denoted p_{O_2}, and increased from 5% at $p_{O_2} = 10$ mTorr to 12% at $p_{O_2} = 30$ mTorr. A similar effect was found also by Wang et al. [241], who reported a lowest relative density of 0.75; these films had an O/W ratio of 3.1 ± 0.1, as found from RBS. A growth of the mean crystallite size in films deposited onto substrates at temperatures up to 200°C was inferred from Raman spectra indicating the presence of O–W–O and W=O bonds [262]. Crystallization of the films took place at temperatures between 300°C and 350°C [263–265]. An addition of Ti to the W oxide tended to stabilize the disordered structure to higher temperatures [260].

It is of interest to comment on some recent results for films prepared by RF sputtering and subjected to a careful structural analysis by Nanba et al. [94,95]. The density of their films was close to that of bulk WO_3, and no structural water appeared to be present. Vibrational spectroscopy and X-ray diffractometry disclosed that the films basically consisted of three, four, and six-membered rings of WO_6 octahedra sharing corners in almost the same way as for hexagonal WO_3 crystals. The occurrence of a hexagonal structure was dependent on the magnitude of p_{O_2}, though, and high oxygen pressures led to the stabilization of a tetragonal phase with four-membered rings. It is unfortunate that no analogous study has yet been made on

porous W oxide films made by reactive DC magnetron sputtering. Elevated substrate temperatures led to crystalline structures [174,266]; for 350°C it was reported that the structure was mixed monoclinic and orthorhombic [266]. Film thickness dependent effects on the crystal structure are also known [267]. The importance of the details in the sputtering process are often significant — and poorly understood — and, for example, Batchelor et al. [268] showed that RF sputtering from metallic and oxide targets gave different film properties. Films made by different varieties of sputtering are discussed in numerous other works as well [167,187,198,269–316].

Electrochemical and chemical techniques are convenient and widely employed for preparation of electrochromic W oxide films. Electrodeposition from a solution of W powder dissolved in aqueous H_2O_2 was used in several investigations [317–330]; a detailed technical description was given by Monk et al. [325]. An addition of isopropanol, in order to improve the storage properties of the solution, has been studied [331–336]; the work by Meulenkamp [331] describes the technique at length. The as-deposited films were not analyzed in detail, but it is known that the porosity can be very large, with data indicating relative densities between 0.4 and 0.7 [331,335,336]. Electrodeposition from solution is practical for making mixed oxides, with additions of Mo, Ni, Co, Cr, Fe, Ru, and Zn [317,327–329,337], Co + Ni, Co + Zn, Ni + Zn, as well as of three of the metals Mo, Ni, Co, Cr, and Zn [325], having been reported. The substrate adherence depended strongly on the specific metal additive, with particularly good results stated for Ni, Fe, and Zn [337]. Furthermore, it was demonstrated that it is possible to make composites of W oxide and phosphomolybdic acid [333] and to prepare tandem samples with a film of W oxide onto which a layer of polyaniline-polyvinyl alcohol [326], polyaniline [338], or polyvinyl sulfate [338] was grown. Another way to electrodeposit W oxide films makes use of $Na_2WO_4 \cdot 2H_2O$ aqueous electrolytes. XPS spectra of such films showed evidence for tungsten in different valence states, specifically W^{4+}, W^{5+}, and W^{6+} [244].

Anodization in electrolytes of H_3PO_4, H_2SO_4, HNO_3, $HClO_4$, or methanesulfonic acid represent other routes to make W oxide films [128,129,339–343]; growth conditions rather than ensuing film properties were in focus. Stress evolution can be substantial during the anodization [341]; it can be affected by additions to the electrolyte, and one example with NaCl added to H_2SO_4 yielded evidence for the formation of W oxychlorides [342].

Chemical vapor deposition (CVD) and spray pyrolysis are two closely related techniques with specific pros and cons. CVD using the decomposition of $W(CO)_6$ was used to make crystalline W oxide films [344–348]. Low-temperature processing made it possible to prepare porous films with good electrochromic properties, and work by Maruyama and Arai [349] and Riaz [350] — using W carbonyl and alkoxide complexes, respectively — led to X-ray amorphous and smooth films grown at ~ 0.5 nm/s onto substrates kept below 300°C to 350°C. The carbon content was low even in the film made from a $W(CO)_6$ precursor, as seen from XPS [350]. Two methods have been adopted to enhance the deposition rate: photo-CVD [351] and plasma enhanced CVD. Specifically, Maruyama and Kanagawa [352] used the former technique with ultraviolet (UV) irradiation from a low-pressure mercury lamp

and performed depositions at a rate of ~ 5 nm/s onto substrates kept at 200°C. Still larger rates were possible at higher temperatures, but the film quality deteriorated. XPS was employed to verify that the UV radiation promoted the oxidation of W in addition to enhancing the rate of film formation. Henley and Sachs [353] used plasma enhanced CVD with a parallel-plate reactor in which a rf discharge took place in a gas mixture of O_2, H_2, and WF_6. High-quality films were produced at rates up to 10 nm/s; again higher rates were possible if film quality was sacrificed. Relative film densities between 0.59 and 0.78 were accomplished depending on the O_2/WF_6 ratio, with the lowest density occurring at the highest amount of WF_6.

Spray pyrolysis can be viewed as a variety of CVD since the spray droplets are likely to evaporate before striking the substrate to be coated. Depositions using H_2WO_4 in aqueous ammonia, sprayed onto substrates at 150°C, yielded X-ray amorphous deposits, while annealing at 400°C gave monoclinic WO_3 [354]. Spray depositions at higher substrate temperatures led directly to crystalline structures [211,355].

Sol–gel deposition can be made form colloidal solutions by dipping, spin coating, or spraying, followed by heat treatment to consolidate the film. There are numerous routes to prepare the precursor solution, such as by acidification of an aqueous salt or by hydrolysis of an organometallic compound. Properties of the precursor solutions and of the film formation processes have been studied in considerable detail for films based on $Na_2WO_4 \cdot 2H_2O$ [167,356,357], $WOCl_4$ [358] and $W_2[OC(CH_3)_3]_6$ [359]. The structure of films made by the former of these techniques was analyzed by Nanba et al. [94], who found that the relative film density was 0.57 before heat treatment and 0.64 after annealing at 190°C. The material was comprised of microcrystallites with a hexagonal-like structure, analogously to the case of W oxide films made by several other techniques. Similar, or somewhat lower, porosities have been reported also by others [356,360]. After low-temperature curing, the films contain loosely bound water that disappears at ~ 100°C; structurally bound water or H_2O_2 leaves at 200–300°C [361,362]. A tetragonal structure has been reported for the annealed material [363]. The O/W ratio was studied in one experiment [360] and was found to be 3 to within experimental uncertainties. Films made by using organic precursors are known to contain some percent of carbon [359,360]. The sol–gel technique is well suited for making mixed oxides, and work on W–Ti oxide [260,364,365], W–V oxide [366], and W–Si oxide [367] has been reported. Annealed W–Ti oxides displayed hexagonal and monoclinic structures as well as an intermediate orthorhombic phase for which the Ti addition appeared crucial [365]. In addition to the already cited work, films made by sol–gel-related techniques have been studied in [368–388].

The methods discussed so far by no means exhaust the possibilities to make electrochromic W-oxide-based films and devices. Thus oxide films have been prepared by thermally treating bulk tungsten [389], W-coated bulk titanium [390], and thin metal layers of W, W–Ti, and W–Ni [391]. A novel and interesting technique used hydrothermal synthesis to make films with a pyrochlore structure [392]. WO_3 colloids and films made of them have been discussed [393–396]. Colloids can be incorporated in pastes [397] and used for screen printing [398]. Polymer-WO_3

composites offer interesting possibilities; data have been reported for materials incorporating polyvinyl alcohol with $KHCO_3$ [399], polypyrrole [400,401], polyaniline [402], and polymethyl methacrylate [403]. Other interesting materials are peroxopolytungstic acid films [404,405], silicotungstic acid [406], composites of phosphotungstic acid and titanium oxide [407–409], and polytungstate-polymer composites [410,411]. Finally, WO_3-based powders made by milling technology and gas evaporation have shown interesting properties [115,257,412].

3.2. Case study on sputter deposited W-oxide-based films

The lapidary coverage of deposition tecniques and ensuing film properties in the previous section is supplemented here with a case study on sputter deposited W-oxide-based films, based on work by Azens et al. [159–164]. The focus is on high-rate deposition and means for achieving durability; we consider specifically the roles of fluorine in the sputter plasma, electron bombardment of the growing film, deposition from heated targets, and oblique incidence of the sputtered flux. The films prepared by these techniques will be further discussed in Sections 4.2 and 5.3 below. One may note that still another high-rate technology, suitable for electrochromic Mo oxide [413,414] as well as for other oxides [415], has been explored recently; it involves joint deposition from several closely positioned and partly facing targets.

The role of a bias voltage U_{bias} applied to the substrate was investigated in some detail, and oxide films with good electrochromic properties were produced by sputtering in $Ar + O_2$. The deposition rate r was ~ 0.5 nm/s for $25 < U_{bias} < 80$ V, as seen from Fig. 5. These conditions correspond to a bombardment of 1–10 electrons per incident atom forming the film. Oxyfluoride films made with 17 vol% of CF_4 in the sputter plasma, on the other hand, had deposition rates up to 1.2 nm/s for $U_{bias} < 0$ but low deposition rates for $U_{bias} > 50$ V. Most likely, the relation between r and U_{bias} for the oxyfluoride films depends on electron bombardment making the film surface very active for reactions with F-containing radicals, thus leading to volatile etch

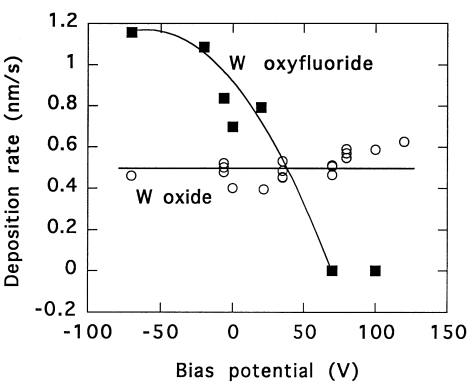

Fig. 5. Deposition rate vs. applied substrate bias for films made by sputtering of W in $Ar + O_2$ ($+ CF_4$). Filled and open symbols denote experimental data, and curves were drawn for convenience.

products. The present films were made in a special research coater, and the deposition rates are not as high as those one can expect in a large-area production machine.

Atomic force microscopy was used to investigate surface topographies of ~ 0.6-μm-thick samples produced under different conditions. Oxide films showed surface roughness with an average distance of ~ 0.1 μm between the protrusions; these features are believed to mirror a columnar microstructure of the film. A similar surface topography was found in oxyfluoride films made by sputtering in $Ar + O_2 + CF_4$. Electron bombardment through the application of a positive substrate bias of 70 V had a more drastic influence on the roughness, and AFM data indicated a column size of ~ 0.5 μm. One should notice that the effect of the electron bombardment is opposite to that expected for ion bombardment, which is generally known to disrupt the columnar structure thereby giving rise to denser and smoother films [416].

X-ray diffraction studies were made on films similar to those mentioned above and also on crystalline W oxide films that had undergone annealing in vacuum for 2 h at 420°C. Diffractograms for the electron bombarded and annealed samples showed clear features due to long-range lattice order, whereas no such features were apparent for the as-deposited oxide and oxyfluoride samples. The diffraction peaks were in principle agreement with those earlier found in crystalline W oxide films made by several different techniques [1].

Infrared spectrophotometry was applied to the different types of films discussed above. Data are given in Fig. 6(a). The absorptance spectrum for the as-prepared W oxide film exhibits a dominating peak at a wave number of $\sim 600\ cm^{-1}$, which is characteristic for the vibrational properties of a disordered tungsten-oxygen framwork [1,267]. The annealed and crystalline counterparts, on the other hand, have absorption peaks at ~ 700 and $\sim 800\ cm^{-1}$, in good agreement with the phonon spectrum in WO_3 crystals. An electron bombarded film prepared with $U_{bias} = 35$ V shows an interesting absorption spectrum with unmistakable features of *both* the highly disordered and the crystalline states. The oxyfluoride film, finally, displays a very broad absorption structure between 600 and $1000\ cm^{-1}$.

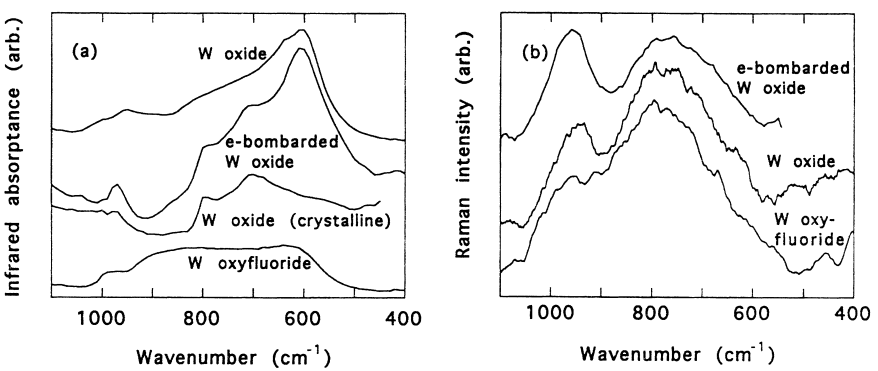

Fig. 6. Spectral infrared absorptance (part a) and Raman intensity (part b) of films made by sputtering of W in the presence of $Ar + O_2$ ($+ CF_4$). Electron bombardment took place at $U_{bias} = 35$ V (part a) and $U_{bias} = 70$ V (part b).

Raman spectrometry, yielding complementary information on the vibrational properties, was applied to ~ 0.7-μm-thick films. As found from Fig. 6(b), the as-prepared W oxide film has a broad peak at $\sim 780\ cm^{-1}$, characteristic of the W-O stretching modes in a disordered material [1,417]. Crystallization of such a sample made this feature split into two separate peaks, the one at $\sim 950\ cm^{-1}$ being caused by asymmetric stretching vibrations of W=O bonds mainly on internal surfaces. An oxide film grown under electron bombardment at $U_{bias} = 70$ V maintained the broad peak at $\sim 780\ cm^{-1}$ — i.e., crystallization was not apparent — whereas the influence of the W=O bonds was clearly augmented. The latter effect is both interesting and unexpected, since even a partial crystallization ought to have diminished the W=O feature, and since the AFM data referred to above pointed at grain growth under electron bombardment and hence a decrease of any internal surface. The oxyfluoride film, finally, shows less pronounced features due to W=O bonds.

Enhanced sputtering rates in the presence of CF_4 were first reported by Harding [418–420]. The basic processes underlying the phenomenon are expected to be of chemical nature, possibly related to reactive ion etching [421–427], and it is then reasonable to expect that r is a function of the target temperature. The relation was studied by Azens et al. [159,162], who carried out depositions with targets kept at 5°C and 50°C in the presence of varying amounts of CF_4. Fig. 7 shows that when the target was cooled to 5°C, the rate had a peak at ~ 20 vol% CF_4 both for sputtering in $O_2 + CF_4$ and $Ar + O_2 + CF_4$. The rate reached ~ 0.6 nm/s for the latter gas mixture, which is in line with the data in Fig. 5. Having the target heated to 50°C yielded significantly higher rates, with maxima at ~ 1.1 nm/s irrespective of the Ar content when the CF_4 admixture was ~ 40 vol%. Clearly, the data in the left-hand part of Fig. 7 shows that r is affected by chemical factors, since the CF_4 content is of

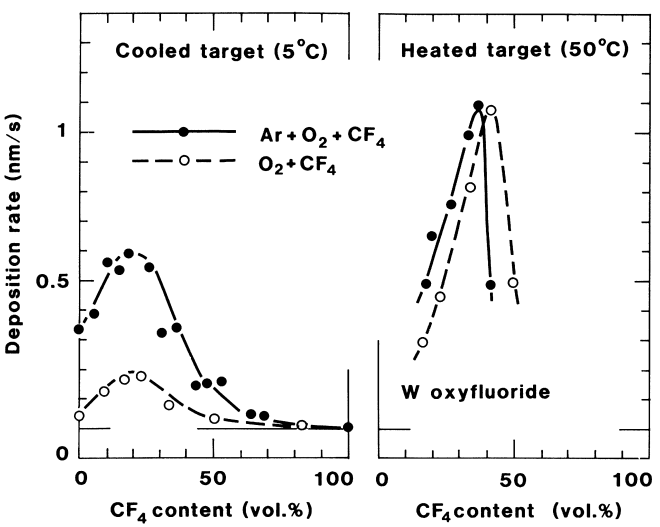

Fig. 7. Deposition rate for W oxyfluoride films made by sputtering of W in (Ar) + O_2 + CF_4. Filled and open circles denote experimental data, and curves were drawn for convenience.

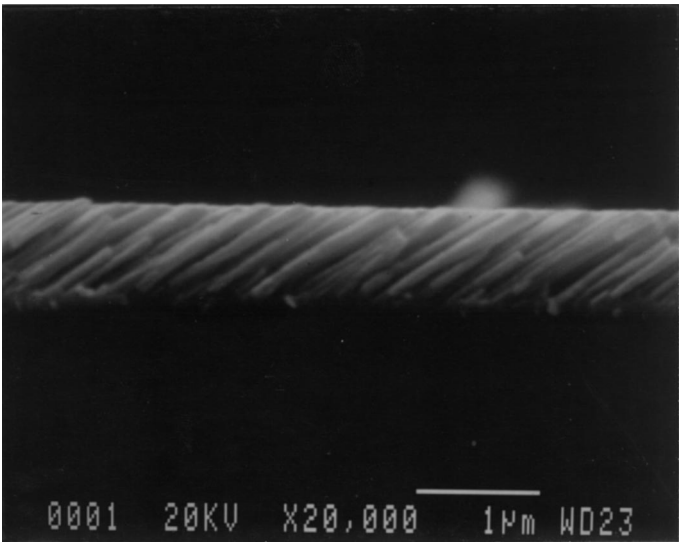

Fig. 8. Scanning electron micrograph of the cross section of an obliquely sputter deposited W oxide film. The horizontal bar corresponds to 1 μm.

importance, but physical sputtering (by ion impact) is also significant since different rates are obtained depending on whether Ar is present. For a warm target, the right-hand part of Fig. 7 demonstrates that the Ar content is irrelevant, and the sputtering is dominated by chemical effects. The elemental compostion of the oxyfluoride films was probed by RBS. A maximum fluorine content of ~ 30 at% was found for films made under conditions giving the largest deposition rates.

A special study was made by Le Bellac et al. [164] of W oxide films produced by sputtering in $Ar + O_2$ onto substrates positioned so that the sputtered flux formed an average angle between 75° and 85° to the substrate normal. Cross sections of these films were studied by scanning electron microscopy (SEM). A columnar structure was found, as illustrated in Fig. 8, with an inclination angle of about 56° to the substrate normal. The incidence angle for the sputtered flux and the column orientation are in fair agreement with the well known "tangent rule" [428,429]. Oblique angle deposition is known to promote porosity [430,431], and, as we will see in Section 5.3 below, the column inclination also introduces important optical features.

4. Properties of ion-intercalated films

Electrochromism is associated with ion intercalation, as pointed out in connection with relation (1), and the properties of the ion intercalated films — that also contain excess electrons — are of great importance. In this section we first survey recent data obtained by electrochemical and physical techniques (Section 4.1); optical properties

are not covered, but are treated separately below. We then turn to a case study of sputter deposited W-oxide-based films (Section 4.2), being a direct continuation of the exposition in Section 3.2. This latter part is based on work by Azens et al. [161] and Strømme Mattsson [432].

4.1. Survey of data

Ion intercalation is normally investigated in an electrochemical three-electrode set-up with the W oxide film as "working electrode". A voltage is applied with regard to a reference electrode, and reliable potential readings are taken against a standardized reference electrode. The intercalation phenomenon is not a simple one but embraces effects of ion diffusion, electron diffusion, charge transfer at the film's two surfaces, as well as transitions of ions between different sites in the WO_3 lattice. Discussions on these matters can be found in [208,287,291]. Rate enhancing effects due to pulsed polarisation with microsecond pulses were discussed in [433].

The voltage measured between a film with a nominal composition H_xWO_3 and a reference electrode is a function of the ionic content and goes down when x is increased. The drop is monotonic if the W oxide film is highly disordered but step-like if the film is crystalline [1,166]. A theoretical model for the voltage dependence in disordered materials was forwarded recently by Kudo and Hibino [434]. It makes it possible to understand the phenomenon quantitatively; we return to this important subject shortly in connection with the case study in Section 4.2.

The kinetics of the ion intercalation/deintercalation is complicated, as noted above. Several encompassing studies on this issue have been reported during the past few years [240,250,251,372–374,380], and theoretical models have been offered. We do not attempt to go into the various intricacies of these theories but simply observe that an overall description of the kinetics can be provided by a (chemical) diffusion constant D_{M+}, which depends on the ionic species, the intercalation level, the temperature, etc. Diffusion constants can be measured by numerous techniques. It is convenient to start by looking at some data by Wang et al. [241], who investigated films made by reactive DC magnetron sputtering. Fig. 9 shows D_{H+} vs relative film density for two magnitudes of x in H_xWO_3. The effect of increasing porosity is a dramatic one, and by going from a relative density of ~ 0.9 to ~ 0.75 the magnitude of D_{H+} is changed from the range 10^{-11}–10^{-10} cm^2/s up to the range 10^{-9}–10^{-8} cm^2/s, i.e., by two orders of magnitude. This is a very significant difference with regard to possible device performance. The diffusion coefficient drops by about a factor two when x is increased from 0.1 to 0.3. Similar D_{H+}s have been noted also for films made by evaporation [240], sputtering [307], and sol–gel deposition [380], whereas diffusion constants as large as 2×10^{-7} cm^2/s have been reported for electrodeposited films [337]. By adding Co, Cr, Ni, Ru, or Zn to the electrodeposited films, the diffusion constant became somewhat lower. In contrast with the data in Fig. 9, it was found that D_{H+} went up from 10^{-10} cm^2/s to 10^{-9} cm^2/s when x was increased from ~ 0.1 to ~ 0.3 in some sputter deposited films [309]. It has also been stated that D_{H+} can stay essentially independent of the intercalation level [213]. Water can play an accelerating role for proton

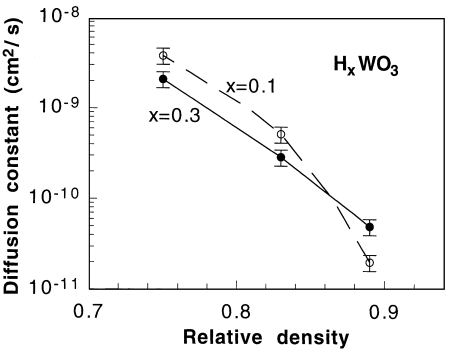

Fig. 9. Chemical diffusion constant vs relative film density for sputter deposited W oxide films. The ion intecalation level is represented as x in H_xWO_3. Symbols with error bars denote experimental data, and curves were drawn for convenience.

insertion [435]. Bulk-type WO_3 showed diffusion constants in the range from 10^{-14} to 10^{-12} cm^2/s [436].

In general, Li^+ diffusion is slower than proton diffusion, but some films made by hydrothemal synthesis in order to stabilize an open pyrochlore structure yielded D_{Li+} as high as $\sim 10^{-7}$ cm^2/s for $x = 0.01$ [392]; the diffusion constant dropped rapidly upon lithiation and was $\sim 10^{-10}$ for $x = 0.5$. A hexagonal type film had $D_{Li+} \approx 10^{-9}$ cm^2/s [106,142]. A decrease of D_{Li+} from $\sim 10^{-9}$ cm^2/s at low intercalation level to $\sim 10^{-11}$ cm^2/s for $x = 0.3$ was noted for films evaporated in the presence of water vapor [166]; films made in the absence of H_2O had $D_{Li+} \approx 2 \times 10^{-11}$ cm^2/s at low x. Electrodeposited films with a relative density of ~ 0.7 showed $D_{Li+} \approx 1.2 \times 10^{-9}$ cm^2/s [335,336]. Several other studies have stated D_{Li+}s in the range between 5×10^{-13}/s and 10^{-11} cm^2/s [94,213,240,308, 378–380,383,437]. The lowest value was quoted for a sputter deposited film that was known to be very dense [94]. Work by Pyun and Bae [308] reported an increase of D_{Li+} from 10^{-12} to 10^{-11} cm^2/s when x went from 0.1 to 0.3, but another study [213] was unable to record any significant effect of x on D_{Li+}.

Whereas the role of a lowered density to promote rapid diffusion appears unambiguous, it may seen confusing that some studies state decreased diffusion coefficients upon ion intercalation whereas other ones report increased diffusion coefficients. A drop of D_{Li+} under ion insertion has been found many times (cf. earlier work reviewed in the Handbook [1]), and the effect has been explained as due to a blocking of "channels" for easy diffusion in an inhomogeneous material [438]; these channels have been associated with grain boundaries [213,439]. However, it is also possible to envisage that ion diffusion is promoted by intercalation acting so as to open up a compact oxide structure. The latter mechanism was forwarded recently by Yebka et al. [365] to explain enhancements of D_{Li+} upon lithiation of crystalline powders of W oxide with hexagonal, orthorhombic, and monoclinic structures. An entirely clear picture for the ion-content-dependent magnitude of D_{M+} has not emerged yet, but it

seems that if the film is porous enough in as-prepared state the net effect of ion intercalation will be one to hinder further diffusion, whereas if the film is initially compact the ion intercalation can serve so as to render the structure more prone to easy diffusion.

Ion diffusion in a static field obviously leads to mass transfer that can be detected by different techniques. Clear information on lithium transport in W oxide was found by Goldner et al. [289] who employed nuclear reaction analysis using the $^7Li(p,\gamma)^8Be$ reaction. Similar results were found by Bechinger et al. [183]. Direct evidence for Li^+ intercalation was documented recently also by scanning force microscopy [440]. Microbalance measurements using a vibrating quartz resonator with a W oxide film immersed in a liquid electrolyte can provide valuable — but sometimes rather ambiguous — information on ion transport [186,205,207,287,292]. The emerging picture is one of reversible Li^+ intercalation occurring jointly with the expulsion of anions from the electrolyte. The charge transfer is slower for Na^+ and still slower for K^+ [207]. The heavier, and larger, alkali ions may induce obscuring stress effects [441].

Ion insertion polarizes the lattice. The ensuing deformations can be probed by various methods. X-ray absorption fine-structure spectroscopy is a powerful technique that has been used extensively [187,228,442–450]. The effects of H^+ intercalation in evaporated W oxide films provide convincing evidence in favor of polaron formation, as we return to in Section 5.2 below. Reversible changes in the crystal structure have been seen also by straightforward X-ray diffraction applied to heat-treated W oxide films [172,266]. Infrared absorption spectroscopy is capable of giving information on lattice properties. The status of the data, as reported in the Handbook [1], can best be termed confusing, but a careful study by Paul and Lassègues [303] has clarified the situation and given a consistent model with local lattice distortions around W^{5+} sites, as expected for polarons. The infrared spectrum depends markedly on the specific crystalline structure [451]. Structural changes have been detected also by Raman spectroscopy [452] applied to proton-containing and deuterium-containing W oxide films [168,169,233,234]. Further data supporting polaron formation can be found from electrical measurements [181,237].

Surface structures of W oxide films have been determined by scanning force microscopy applied to samples with and without Li^+ intercalation. The results reported thus far are conflicting, with claims both that lithiation causes changes [229] and that it does not [207].

Ion intercalation occurs jointly with electron insertion. In disordered W oxide, the electrons are strongly localized to tungsten sites, and a transition from W^{6+} to W^{5+} is, at least in principle, possible to detect by several different techniques. The Handbook [1] quoted, among other things, XPS data that could be explained in a consistent manner by regarding films of H_xWO_3 to be of mixed valency. Recent studies by Jeong et al. [209] of evaporated W oxide films showed broadened XPS spectra that looked similar to the earlier ones, and an analogous explanation would seem possible. However, the new data were given an alternative interpretation in terms of final states effects. It appears that this alternative explanation relies on a non-rigid-band behavior of the electronic density of states and on the presumed

existence of mid-gap states in H_xWO_3. None of these presumptions were substantiated in our detailed computations reported in Section 2, and we believe that hydrogen insertion being accompanied by a $W^{6+} \rightarrow W^{5+}$ transition remains a valid model. We also note that Jeong et al. [209] offered sample inhomogeneities as an alternative cause of their observed line broadenings. XPS has been used also to detect sub-stoichiometry in W oxide films made by several different techniques [244,353] and to document W^{5+} formation upon reaction with H_2S [286]. Similar results have been reported for powder samples [453].

4.2. Case study on sputter deposited W-oxide-based films

We now consider the intercalation of Li^+, Na^+, and K^+ from electrolytes of $LiClO_4$, $NaClO_4$, and $KClO_4$ in propylene carbonate into ~ 0.3-μm-thick W oxide films prepared by sputter deposition under the same conditions as in Section 3.2. The voltage between the film (i.e., the working electrode) and a reference electrode was measured under ion intercalation progressing slowly enough that quasi-static conditions prevailed. The films were deposited onto substrates that were unheated or heated to 350°C. The corresponding films were X-ray amorphous and monoclinic crystalline, respectively, with relative film densities being 0.78 and 0.90. Only a summary of the experimental data and their interpretation is given here; full detail can be found in a paper by Strømme Mattsson [432].

Fig. 10 shows data for the two types of films. The voltages are seen to decrease when the ionic content goes up; the relationship is monotonic and characterized by a large initial drop for the heavily disordered film, whereas the relationship is progressing in a step-like manner for the crystalline film. X-ray diffraction studies for x being 0.08, 0.31, and 0.53 indicated predominantly monoclinic, tetragonal, and cubic structures, respectively, for each of the ionic species. An analogous structural evolution for lithiated samples was found in earlier work by Zhong et al. [454].

The results of the heavily disordered film can be understood in terms of a novel model by Kudo and Hibino [434]. They showed that standard theories [455,456] for well-ordered materials had to assume unrealistically strong repulsive energies between the intercalated ions and chose to consider instead a relatively large distribution of site energies while repulsive interaction was neglected. Assuming the site energies in the heavily disordered material to have a Gaussian distribution with a standard deviation σ, the working electrode potential U_{WE} follows a relation

$$U_{WE} = -\left[E_0 + \sqrt{2}\sigma \,\mathrm{erf}^{-1}(2x-1) + k_B T \ln\left(\frac{\xi(1-x)}{x(1-2x+\xi)}\right)\right]. \tag{2}$$

The parameter E_0 denotes the mean energy in the distribution, erf^{-1} is the inverse error function, k_B is Boltzmann's constant, and T is the temperature. The parameter ξ is the ratio of the number of ion pairs occupying neighboring sites to the number of available sites, as elaborated and explained in more detail by Kudo and Hibino [434]. Presently ξ is used only as a fitting parameter.

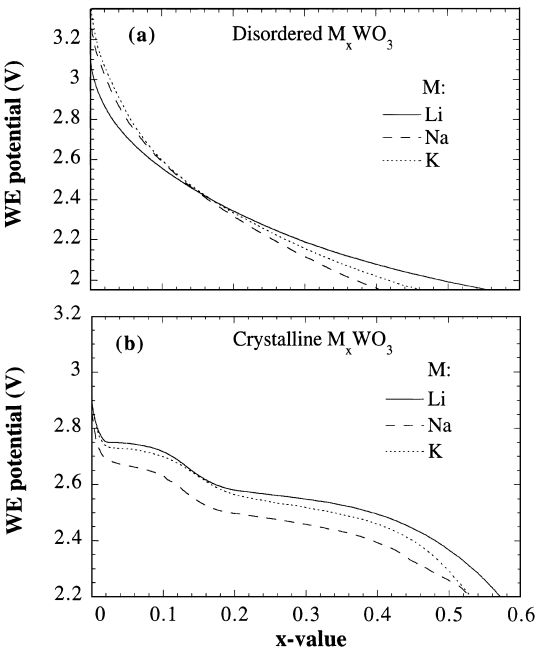

Fig. 10. Working electrode (WE) potential for sputter deposited W oxide films vs ionic content x representing the M/W atom ratio with M denoting Li, Na, and K. Parts (a) and (b) refer to heavily disordered and crystalline films, respectively.

Fig. 11 shows a fit between the experimental values in Fig. 10 and the Kudo-Hibino model with the shown magnitudes of E_0 and σ. The agreement is very good, which speaks in favor of the distribution of site energies being Gaussian. The actual values of σ and E_0 for the present sputter deposited films are very similar to the corresponding parameters for some evaporated W oxide films [434]. The distribution width appears to be larger for Na^+ and K^+ intercalation than for Li^+ intercalation. The magnitude of E_0 is more negative for Li^+ than for the other ionic species, which shows that intercalation is energetically most beneficial for the small Li^+ ions.

For the crystalline W oxide film reported on in Fig. 10(b), it is possible to treat U_{WE} in terms of standard notions [456] based on statistical mechanics. Assuming that ions are intercalated randomly into equivalent sites and that each intercalated ion is exposed to a mean interaction or field from its intercalated neighbors [455,456], the working electrode potential can be expressed within a "lattice gas model" as

$$U_{WE} = \varepsilon + k_B T \ln\left(\frac{1-y}{y}\right) - Uy + U_{el}. \tag{3}$$

Here ε is the site energy required to put an isolated ion and its electron into the host. The ions occupy a fraction y of all available and energetically equivalent sites in the host. U is the total interaction that an intercalated ion would experience if all the

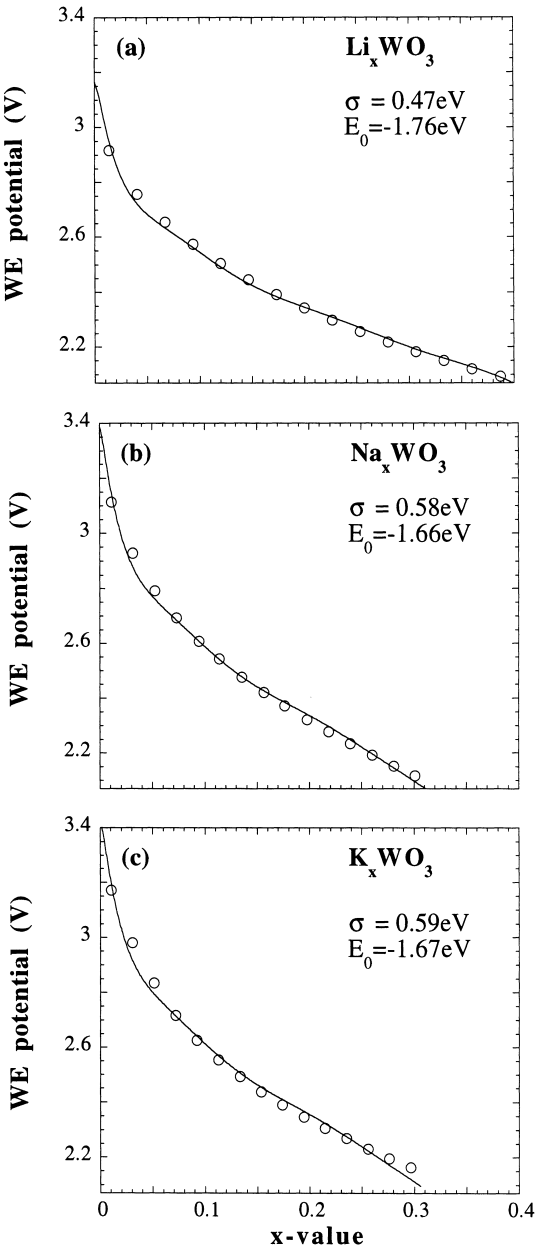

Fig. 11. Working electrode (WE) potential for sputter deposited W oxide films vs ionic content x representing the M/W atom ratio with M denoting Li, Na, and K. Circles signify experimental data from Fig. 10(a), and curves were obtained by fitting to the Kubo–Hibino model in Eq. (2) using the shown parameter values.

other sites were full. Hence U includes both the repulsive Coulombic interactions between intercalated ions and strain fields caused by expansion or contraction of the lattice; it provides information about whether the net force on an intercalated ion tends to attract it towards (negative U) or repel it from (positive U) other intercalated ions, and whether this force is strong or weak. U_{el} denotes the electronic contribution to the potential. This latter contribution may be complex, but at least for metallic compounds one can argue [456] that the U_{el} term may be neglected. This contribution to U_{WE} was omitted to simplify the analysis below.

A detailed analysis is fairly lengthy and is not justified here since the compact crystalline W oxide films are not prime candidates for electrochromic devices; details can be found in the report by Strømme Mattsson [432]. Fig. 12 gives the end result of the fit between experimental data and predictions based on the lattice gas theory, i.e. equation (3). The comparison is made for the x dependence of $-\mathrm{d}x/\mathrm{d}U_{WE}$ in order to give a clear picture of the quality of the fit. In general terms, the agreement is satisfactory, especially for Na^+ intercalation. The ensuing differences for Li^+ and K^+ emerge from a phase separation in the film. The interaction between the ions was found to be attractive at low intercalation levels and repulsive for high intercalation.

Cyclic voltammetry was applied to sputter deposited W-oxide-based films in work by Azens et al. [161] with the aim of providing complementary information. Fig. 13 shows data for Li^+ intercalation/deintercalation in 0.6 to 0.7-μm-thick films. Part (a) refers to an oxyfluoride film and shows that the initial charge capacity is large. However, the voltammograms evolve during the cycling, and the charge capacity has decreased very much after 10^3 cycles. The change is more rapid than for typical W oxide films. The oxyfluoride still can be used after $\sim 10^4$ cycles, but significant ion intercalation/deintercalation can be maintained only by increasing the limits of the potential sweep. Fig. 13(b) reports data for an electron bombarded W oxide film produced with $U_{bias} = 22$ V. The voltammogram is very different from that of the oxyfluoride, and the charge capacity does not show any signs of decline even after 10^4 cycles. The main cycle-dependent evolution takes place in the part of the voltammogram that corresponds to Li^+ deintercalation. A charge imbalance for the intercalation/deintercalation reaction was found during the intitial cycling, whereas the inserted and extracted charge remained stable at ~ 15 mC/cm^2 after 10^4 cycles between 2.5 and 4.5 V vs Li.

Particularly interesting results were obtained with a tandem film having a 0.6-μm-thick W oxyfluoride layer covered with a 0.05-μm-thick protective film of electron bombarded W oxide made with $U_{bias} = 22$ V. The voltammogram in Fig. 13(c) shows that the tandem combines the assets of the constituent layers, viz., the large charge capacity of the oxyfluoride and the good durability of the electron bombarded oxide. The overall shape of the voltammogram is similar to that of heavily disordered W oxide [1]. It is noteworthy that the top layer does not prevent the Li^+ ions from penetrating easily into the underlying film. Another experiment was carried out on a 0.7-μm-thick film of electron bombarded W oxide in 0.1 M H_2SO_4 under potentiostatic switching between $+1$ and -1 V vs Ag/AgCl at 0.2 Hz. The film remained functional as an intercalation/deintercalation host even after 10^5 cycles, which points at a remarkable durability.

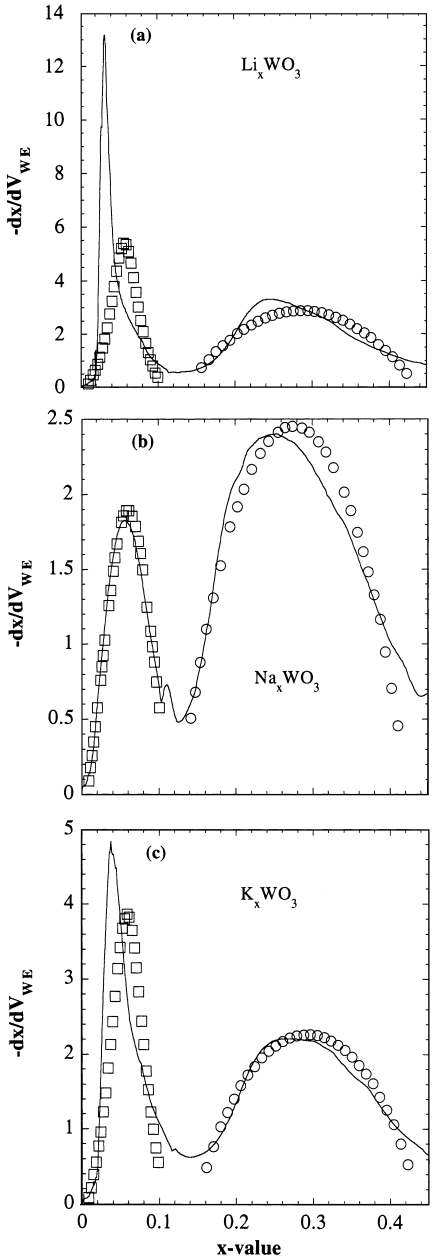

Fig. 12. Derivative of the composition x — representing the M/W atom ratio with M denoting Li, Na, and K — with regard to the working electrode (WE) potential vs x for sputter deposited W oxide films. Symbols signify experimental data based on Fig. 10(b), and curves were drawn as fits to the lattice gas model in Eq. (3).

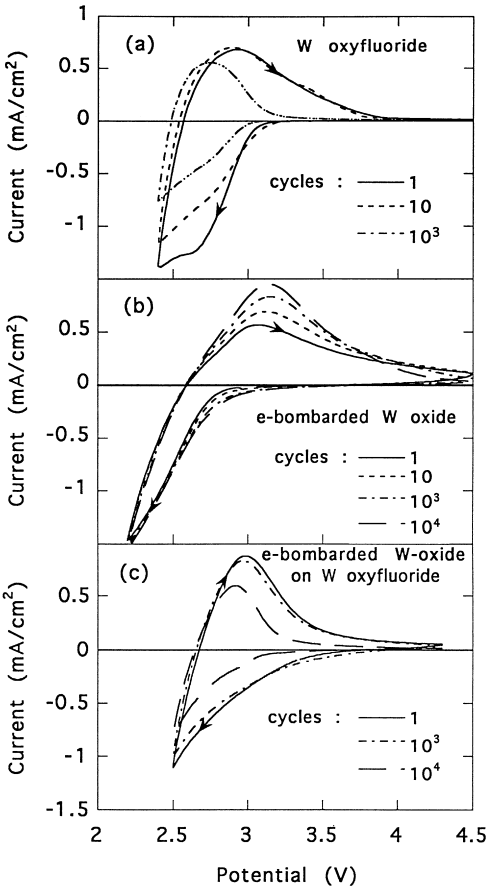

Fig. 13. Cyclic voltammograms for a W oxyfluoride film (part a), a W oxide film prepared under electron bombardment with $U_{bias} = 22$ V (part b), and a tandem with a W oxyfluoride film covered with a thin layer of electron bombarded W oxide (part c). Data are given for different numbers of voltammetric cycles. The voltage scan rate was 50 mV/s. Arrows indicate scan direction.

5. Optical properties

The optical properties of W oxide films with varying degree of ion intercalation are considered next. Section 5.1 regards experimental data and theoretical modelling for crystalline W-oxide-based materials. This is followed in Section 5.2 by a discussion of the optical properties of heavily disordered W-oxide-based films. Section 5.3 provides a case study devoted to the optical properties of sputter deposited films; it is based on work carried out by Azens and others [160,161,163,164, 457–459].

5.1. *Reflectance modulation in W-oxide-based crystals: experimental data and theoretical model*

Crystalline ion-containing W oxide can exhibit a high reflectance, especially in the infrared. Fig. 14(a) illustrates data for Li_xWO_3 and Na_xWO_3 as reproduced from Cogan et al. [460,461] and Goldner et al. [462,463]. Consistent data have been reported also in other work [172,190,265,266,300]. These properties can be explained — at least semi-quantitatively — from computations based on the electronic structure reported in Section 2 above, as considered next.

The response of a material to electromagnetic radiation depends on many different effects, and it is not the aim to try account for them all here. Rather we concentrate on the interband transitions, and represent intraband contributions in terms of a Drude model [464]. The interband contribution to the imaginary part of the dielectric

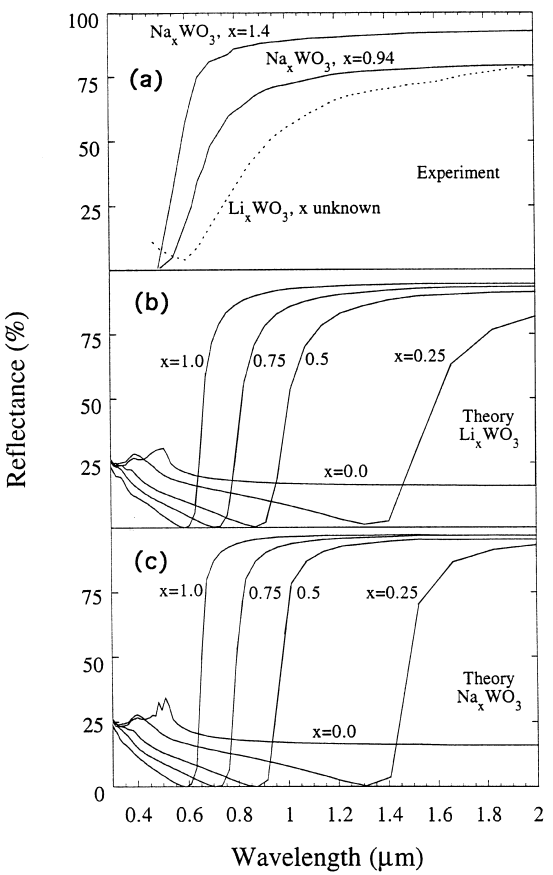

Fig. 14. Spectral reflectance for lithium and sodium containing W oxide. Part (a) refers to experimental data and parts (b) and (c) to computations for Li_xWO_3 and Na_xWO_3, respectively.

function, ε_2, is calculated by summing transitions from occupied to unoccupied states (with fix $\boldsymbol{k}$ vector) over the Brillouin zone, weighted with the matrix element giving the propability for the transition, according to $\langle\psi_f|\boldsymbol{p}|\psi_i\rangle$ where i and f denote initial and final states, respectively, and $\boldsymbol{p}$ is the momentum operator. The real part of the dielectric function, ε_1, is then found by using Kramers-Kronig relations. The reader is referred to Wooten [464] for a general discussion on these techniques.

Considering first bulk WO_3, the optical properties in the visible region are dominated by the absorption threshold, detemined by the band gap E_g. For frequencies lower than $E_g/\hbar$, where $\hbar$ is Planck's constant divided by 2π, the material is essentially transparent, since there are no free electrons present to give a metal-like repsonse, and since interband transitions cannot be exited. However, when the photon energy is increased and reaches the band gap width, absorption from interband transitions will start to take place. For photon energies slightly larger than E_g (sufficiently large to avoid the Urbach effect [465]) the absorption coefficient α can be described by

$$\hbar\omega\alpha \propto (\hbar\omega - E_g)^{\eta}, \tag{4}$$

where $\hbar\omega$ is the photon energy and the exponent η depends on the type of optical transition in the gap region. Specifically, η is $\frac{1}{2}$, $\frac{3}{2}$, 2, and 3 for transitions being direct and allowed, direct and forbidden, indirect and allowed, and indirect and forbidden, respectively. Since the top of the valence band is completely dominated by the O 2p states, while the bottom of the conduction band is constituted by W 5d orbitals to some ninety percent, the transitions are allowed. Furthermore, the band gap is indirect, so the exponent is expected to be 2. This is in accordance with experiments [1]. For higher energies, nearer to the ultraviolet region, the optical properties are governed by the interband transitions. The reflectance for WO_3, calculated from interband transitions, has a peak around a wavelength corresponding to the onset of transitions across the direct band gap (indirect transitions were neglected in the study reported on here). This effect results in a greenish color of bulk WO_3. As mentioned above, the calculated band gap is smaller than the experimentally determined value, and thus the calculated "color" of WO_3 is shifted to longer wavelengths.

For Li containing and Na containing WO_3, the optical properties can be radically different from those of the unintercalated oxide as already noted. It would be extremely time consuming to perform selfconsistent calculations for varying Li or Na content, but since a filling of a rigid conduction band seems to be appropriate it is possible to approximate the situation of varying ion content simply by adjusting the Fermi energy to the desired degree of band filling, using the band structure calculated selfconsistently for $x = 1$. Using a value of zero for x thus corresponds to pure WO_3, but derived from a calculation for a metallic state. The two curves for this case — computed from Li and Na containing oxide, respectively — are included in Fig. 14(b) and (c). The two sets of data are similar, though not identical, and this similarity serves as a measure of the correctness of the rigid band model. Compared to the reflectance calculated from a self-consistent solution for WO_3, the present values show better agreement with experiments since the calculated band gap is larger for the metallic state.

When free electrons are present in Li_xWO_3, and Na_xWO_3, their contribution to the dielectric function can be approximated by the Drude model. This model includes three parameters: the density of conduction electrons, the average relaxation time, and the optical effective mass, m^*. Only the electron density is easy to estimate in the present case. However, the effective mass can be represented as the enhancement of the calculated DOS at the Fermi level compared to the DOS from the free-electron model. In the range $0 < x < 1$ one thus uses the ratio of the calculated DOS to the DOS calculated with the free-electron model for the corresponding band filling. This ratio is well approximated by $m^* = 1.5m$, with m being the free-electron mass, over the concentration range of interest for both Li_xWO_3, and Na_xWO_3.

In the free-electron model, the DC conductivity depends on the ratio of the effective mass to the relaxation time. Starting from the value found for m^*, it is possible to deduce the relaxation time by comparison with conductivity measurements, and by using published data [158,466] one finds the value 9.7×10^{-15} s for the Li containing material, while the value 4.8×10^{-14} s was obtained [467] for the corresponding Na containing compound. Provided that these quantities are used for all concentrations, the plasma frequency and hence the contribution to the dielectric function depends only on the electron concentration.

The reflectance spectra in Fig. 14(b) and (c) were obtained by adjusting the Fermi level to give the electron density corresponding to the x values 0.25, 0.5, 0.75, and 1. These spectra can be directly compared with the experimental ones in Fig. 14(a). The agreement between the two sets of data is satisfactory, especially when one contemplates the uncertainties that enter the theoretical model, and hence the optical properties of crystalline W-oxide-based films can be understood to a large extent from first principles. It is worthwhile to note, however, that the computed reflectivities are larger than the measured ones. Another way to extract ε_1 and ε_2 as a function of wavelength is by electron energy loss measurements [468]; such data can — at least in principle — be compared with the computations presented above.

The optical properties of ion intercalated WO_3 have also been studied [469] from the perspective of a dynamic resistivity [470] with ionized impurity scattering accounted for by the Gerlach theory [471]. For low electron concentration, one finds that the present theory and the Gerlach theory agree much better with each other than any one of them do with experimental data.

The quantitative disagreement between the present calculations and experiments, clearly illustrated in Fig. 14, can be ascribed to several causes. Firstly, it is possible that the rigid band filling of the band structure for $x = 1$ is not sufficiently accurate. However, a comparison of the curve for $x = 0$ with the self-consistent calculation for WO_3 shows only some small differences, and the main features are the same. Secondly, polaron absorption might make a non-negligible contribution to the optical properties. Indeed, highly disordered W oxide with intercalated ions exhibit strong polaron absorption in a band centered around a wavelength of 1 μm, and polaron absorption is responsible for the absorptive electrochromism in heavily disordered W oxide films, as discussed at length below. With such a contribution superimposed on the curves presented in Fig. 14(b) and (c), one could get better agreement with experiments. Furthermore, it is conceivable that the real material comprises local

environments with $x = 1$ and 0. By making linear combinations of the two reflectance curves to match the desired concentration, one can indeed obtain a very good agreement with the experimental data. Further work is needed to shed light on these issues.

5.2. Absorptance modulation in disordered W-oxide-based films

Ion intercalation/deintercalation in disordered W oxide films leads to a modulation of the optical properties. This effect can be ascribed to polaron absorption and arises as a result of excess electrons localized on metal ion sites. The absorption is pronounced provided that the overlap of the pertinent wave functions is weak and if disorder is strong [472–474]. The stability of the polaronic state has been ascertained through recent work by Iguchi and Miyagi [475]. Bipolarons (i.e., paired polarons) can also be formed, particularly in the low-temperature phase (ε-phase) of W oxide [476]. We note in passing that the occurrence of single polarons and bipolarons under different conditions may be the underlying cause to the long-standing problem as to why some electron spin resonance measurements [477–480] yielded clear evidence for W^{5+} whereas other measurements [481] gave no detectable signals — a fact that then may be associated with W^{5+}–W^{5+} pairs.

It is generally accepted that polaron absorption — due to the transfer of electrons and accompanying lattice polarization between adjacent tungsten ion sites — can take place and indeed is the cause of the electrochromism following reversible electron insertion/extraction according to relation (1) [1]. Nevertheless, it has been difficult to carry out detailed investigations to unambiguously prove the occurrence of the polaronic effects. This difficulty has been caused by the use of too simplified theoretical models for polaron absorption and to their application to poorly characterized samples. However, one should notice recent efforts by Kubo and Nishikitani [262] to study polaron absorption in W oxide films sputter deposited onto heated substrates and inferring the crystallite sizes from Raman spectroscopy (specifically using the W=O modes assumed to be associated with crystallite surfaces [482]).

Spectral transmittance through W oxide films, that is of direct relevance for device performance, has been reported a number of times; characteristic data are available for films made by evaporation [166], sputtering [259,300], chemical vapor deposition [349,352], and sol–gel deposition [361]. It is convenient to express the film properties in terms of optical constants, n and k, or, equivalently, ε_1 and ε_2. The two sets of data are related by

$$\varepsilon_1 + i\varepsilon_2 = (n + ik)^2. \tag{5}$$

A particularly clear and illustrative set of optical constats as a funtion of charge insertion was given by von Rottkay et al. [239] who used variable-angle spectroscopic ellipsometry to obtain the data reproduced as "three-dimensional" plots in Fig. 15. It is evident that charge injection leads to the growth of k — i.e., of the absorption — especially in the near infrared. With regard to n, the magnitude is ~ 2 across most of the spectral range for the unintercalated state. Charge insertion leads to a drop of

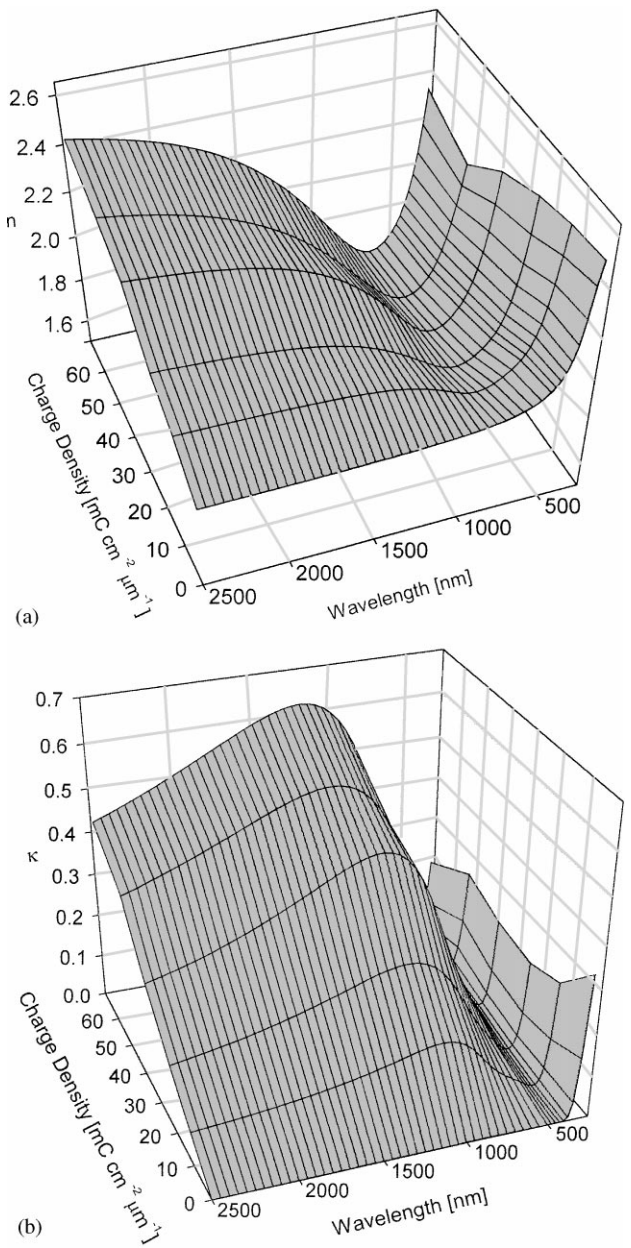

Fig. 15. Spectral optical constants, n and k, as a function of inserted charge density for evaporated W oxide films. From von Rottkay et al. [239].

n at wavelengths centered around 0.6–0.7 μm and an increase of n at longer wavelengths. Analogous, though less comprehensive, data can be found elsewhere for films made by evaporation [178,210,226,229], sputtering [261,263–266,269,294,300,

301], and sol–gel technology [301,384,385]. A dispersion analysis of the optical properties was given in [344].

It is common to represent the absorption by an optical density OD which is related to k, wavelength λ, and film thickness d by

$$\mathrm{OD} = (4\pi/\lambda)kd. \tag{6}$$

Recent work by Burdis et al. [259], who studied sputter deposited films, showed that the OD exhibits a characteristic dependence on film thickness and levels off at a certain charge insertion that becomes progressively lower in the thinner films. Data pertaining to an averaging over the solar spectrum are shown as symbols in Fig. 16. Analogous results on OD as a function of ionic content at $\lambda = 788$ nm have been reported by Zhang et al. [166] for evaporated films, and a similar tendency can, in fact, be inferred for several sets of data given in the literature already several years ago [483,484]. The saturation of the optical density can be understood from a conceptually simple model by Denesuk and Uhlmann [485]. Their model pertains to highly localized electrons causing absorption by jumping to a neighboring site, i.e., a polaron picture applies. The electron transfer must take place from an occupied site (W^{5+}) to an empty site (W^{6+}), and hence saturation becomes important at such high charge insertion that the fraction of W^{5+} states is significant. Around $x = 0.5$ it is prediced that OD would be independent of charge insertion. This simple model is readily transformed to treat the relation between OD and d, and a fitting yielded the set of curves in Fig. 16 that are in good agreement with the experimental data. Saturation in the OD can be inferred also from studies of dry lithiation of evaporated W oxide films [176].

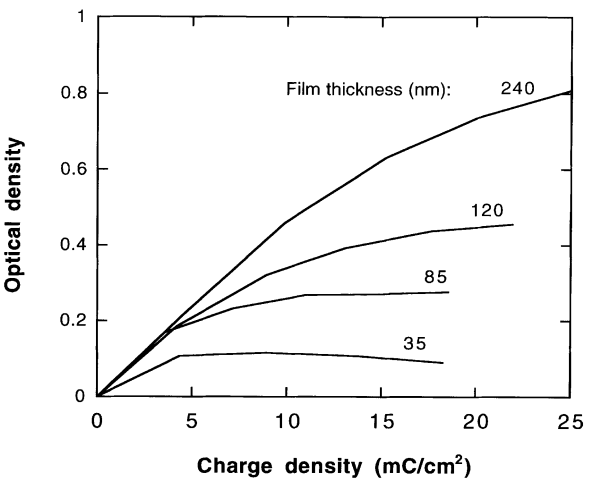

Fig. 16. Optical density pertinent to solar irradiation vs inserted charge density for W oxide films made by reactive DC magnetron sputtering. Symbols denote experimental data by Burdis et al. [259] and curves represent fits to the site saturation model due to Denesuk and Uhlmann [485].

A quantitative measure of the change of optical density Δ(OD) as a function of fractional charge insertion ΔQ is given by the coloration efficiency CE defined as

$$CE = \Delta(OD)/\Delta Q. \quad (7)$$

Values of CE are often quoted in the literature but are not always straightforward to interpret since they depend on the amount of charge insertion, as implied in the site saturation model discussed above. Furthermore, CE is a function of wavelength. Most of the CEs quoted recently for films made by evaporation [166], sputtering [259–261,265], electrodeposition [337], and sol–gel technology [260,360] are in overall agreement. An exception has been stated for the case of chemical vapor deposition, and Maruyama et al. [349,352] reported CEs as large as $\sim 230\ cm^2/C$; these magnitudes are about a factor five larger than those reported in other work — using CVD [354] as well as other techniques — and should be reproduced in independent experiments before being generally accepted.

The coloration efficiency can be dependent on film preparation conditions, and Fig. 17 illustrates data from Burdis et al. [259] on the CE (based on an OD averaged over the solar spectrum) as a function of the Ar/O_2 gas mixture for reactive DC magnetron sputtering. When this ratio is $\gtrsim 10\%$, the coloration efficiency is about $30\ cm^2/C$. However, there is a narrow range with approximately 5% oxygen admixture within which the CE exhibits larger values. These enhanced CEs occur concomitantly with a lowering of the luminous transmittance [259].

The peak in the CE values shown in Fig. 17 may have a bearing on the model for explaining electrochromism in heavily disordered W oxide. As pointed out before, the prevailing model is that absorption takes place by polaron hopping and involves transitions between W^{5+} and W^{6+} states. A large amount of experimental data can be rationalized on this premise. However, there are also some results pointing towards

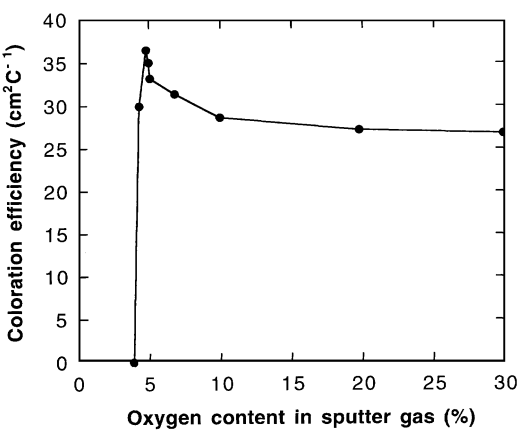

Fig. 17. Coloration efficiency pertinent to solar irradiation vs oxygen content in the sputter plasma for W oxide films made by reactive DC magnetron sputtering. Symbols denote experimental data, and the curve was drawn for convenience. From Burdis et al. [259].

the importance of transitions between W^{4+} and W^{5+}; the latter view has been argued for in some recent articles by Bechinger et al. [273,486,487], and it has been found that enhanced CEs can be associated with oxygen deficiency. A final explanation of the data in Fig. 17 cannot yet be given, but it is tempting to ascribe the constant CE in well oxidized films to the "conventional" polaron hopping between W^{5+} and W^{6+} states, whereas the enhancement connected with oxygen deficiency can be due to additional polaron hopping between W^{4+} and W^{5+}. The possibility to boost the electrochromism by operating with substoichiometric films may be impeded by manufacturing difficulties as well as by difficulties to achieve a fully non-absorbing state.

5.3. Case study on sputter deposited W-oxide-based films

This section follows up the film preparation discussed in Section 3.2 and the electrochemical analysis in Section 4.2 by presenting optical properties of sputter deposited W-oxide-based films. The exposition below is kept brief; full detail can be found in articles by Azens and others [160,161,163,457–459].

Spectral optical transmittance was measured in the $300 < \lambda < 2500$ nm wavelength range by spectrophotometry. Fig. 18 shows data for a ~ 0.6-μm-thick film of electron bombarded W oxide prepared with $U_{bias} = 35$ V; the colored and bleached states were obtained by applying 2.3 and 4.3 V vs Li, respectively, for 100 s. The range of optical modulation is large, and the luminous transmittance was 74% for the bleached state and 3% for the colored state. The coloration efficiency was 30–40 cm^2/C at $\lambda = 550$ nm for electron bombarded W oxide films and ~ 60 cm^2/C for oxyfluoride films.

The color/bleach dynamics is critically dependent on the technique for making the film, as can be understood from voltammetry data. Fig. 19 reports transmittance at $\lambda = 550$ nm when the films earlier reported on in Fig. 13 were subjected to 2.3 V vs Li for 50 s followed by 4.3 V vs Li for another 50 s. The W oxyfluoride film was in virgin state, while the other films had undergone 5000 voltammetric cycles.

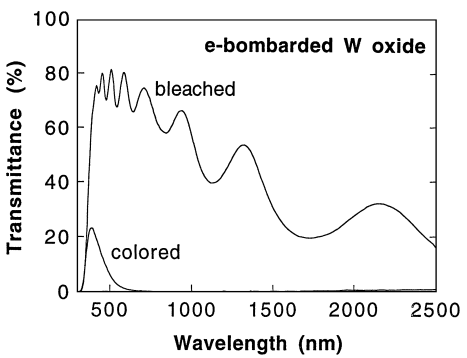

Fig. 18. Spectral transmittance for an electron bombarded W oxide film prepared at $U_{bias} = 35$ V. The curves refer to the sample in colored and bleached states.

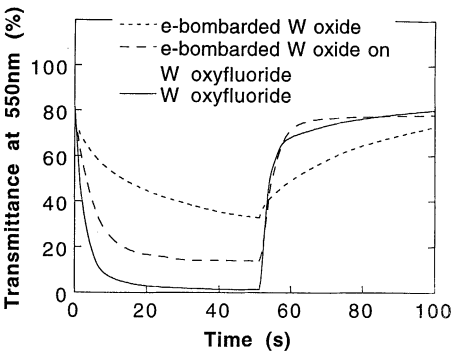

Fig. 19. Transmittance at a wavelength of 550 nm during coloration and bleaching of the shown types of films.

The dynamics of the individual electron bombarded oxide and oxyfluoride films are remarkably different, with the latter being capable of going from 75% to 10% in 5 s and returning from a low to a high transmittance in a comparable time span. The tandem film has a similar dynamics, though it does not attain as low a transmittance as the oxyfluoride. Fig. 19 is a striking illustration of the good properties obtainable in tandem films. It is possible that the top layer prevents dissolved oxyfluoride species from leaving the film, in analogy with the effect that polymeric Nafion layers can have on W oxide films [488]. The slow response of the electron bombarded W oxide films can be partly alleviated if they are used in an electrolyte of 0.1 M H_2SO_4. It was then possible to reach a transmittance below a few percent under experimental conditions analogous to those underlying Fig. 19.

Specular optical properties, such as those given above, are presented in almost all work on electrochromism However, practical fenestration must avoid perceivable haze, implying that light scattering is of importance. Such properties were investigated in detail for films deposited onto transparent substrates by Kullman et al. [457] and Rönnow et al. [459]; a complementary investigation by Lindström et al. [458] considered analogous films backed by metallic reflecting substrates. The main results of these studies are reported next. Total and diffuse transmittance (T_t and T_d, respectively) were studied as a function of wavelength using a total integrated scattering instrument. Diffusely transmitted light was focused onto the detector by a spherical mirror, while the directly transmitted light went through an aperture into a beam dump. Total transmittance was obtained by putting a plug in the aperture. A detailed description of this newly developed equipment is given elsewhere [489]. Spectra were recorded at $400 < \lambda < 1000$ nm for the three types of films in their as-deposited (ad) state and after 10, 100, and 1000 voltammetric cycles.

Fig. 20 shows $T_t^\gamma(\lambda)$ and $T_d^\gamma(\lambda)$ (where the superscript γ denotes ad, 10, 100, 1000, and hence refers to the sample treatment). The electrochromic films were in their fully bleached states. $T_t^\gamma(\lambda)$ is close to unity for all samples, irrespective of treatment, with the exception of a decrease at $\lambda < 450$ nm for the electron bombarded W oxide. The magnitudes of $T_d^\gamma(\lambda)$ are different for the three samples. Fig. 20(a), pertaining to

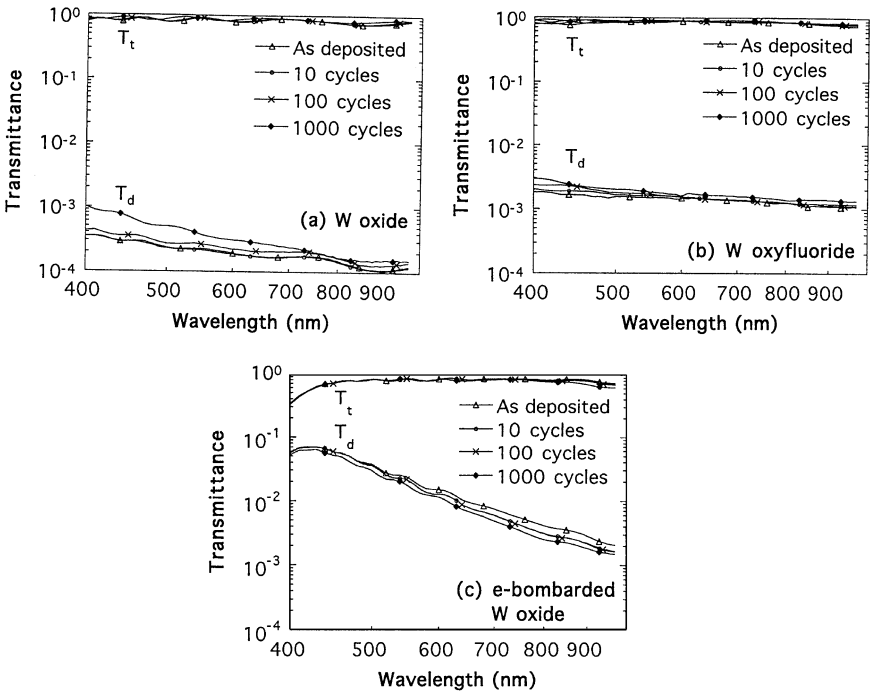

Fig. 20. Spectral total and diffuse transmittance (T_t and T_d, respectively) for films in the as-deposited state and after voltammetric cycling. Parts (a), (b), and (c) refer to W oxide, W oxyfluoride, and electron bombarded W oxide prepared with $U_{bias} = 120$ V, respectively.

"standard" W oxide, shows that T_d^γ is as low as 3.5 to 9×10^{-4} at $\lambda = 400$ nm, and this quantity decreases with increasing wavelength so that even lower values (down to $1–2 \times 10^{-4}$) are found at $\lambda = 900$ nm. The W oxyfluoride film, reported on in Fig. 20(b), has a weaker spectral dependence of T_d^γ with magnitudes lying between 1×10^{-3} and 3×10^{-3}. The electron bombarded W oxide sample in Fig. 20(c) shows a qualitatively different performance, with T_d^γ approaching 10^{-1} at $\lambda = 450$ nm. The scattering falls off rapidly with increasing wavelength, and is as small as $1–2 \times 10^{-3}$ at $\lambda = 900$ nm. The data for T_d^{ad}, T_d^{10}, T_d^{100}, and T_d^{1000} are not significantly different, and hence the degradation observed for W oxide and oxyfluoride does not lead to a change in scattering. The largest effect was observed in T_d^{1000} for W oxide, as seen from Fig. 20(a), but similar differences could be observed for measurements at different parts of the sample so that this effect cannot be taken to be significant.

The diffuse and total transmittance of rough surfaces can be related to each other through different theories. Scalar scattering theory gives

$$T_d = T_t[2\pi(1 - n)(\delta//\lambda)]^2, \tag{8}$$

where δ is the root-mean-square roughness [490]. The data in Fig. 20 can be interpreted in terms of a surface roughness that, quantitatively, is as low as a few

nanometer for W oxide and W oxyfluoride and about an order of magnitude larger for electron bombarded W oxide. As pointed out in Section 3.2 above, AFM profiles revealed that electron bombarded W oxide has larger grains than W oxide and W oxyfluoride and is rougher on lateral length scales of the order of the wavelength of light and longer; this is in qualitative agreement with the results based on light scattering.

A rule-of-thumb states that haze becomes visible when T_d exceeds $\sim 10^{-2}$. Hence the electron bombarded film is not ideal, whereas both the conventionally prepared W oxide film and the W oxyfluoride film have a clear appearance. It is noteworthy that the roughness does not seem to increase during the degradation. It should also be remarked that the simplistic scalar theory underlying the formula for T_d above can be replaced by an elaborate vector perturbation theory applicable to multilayers with rough interfaces [491] and volume inhomogeneities [492]. In fact, vector perturbation theory was used recently to investigate the elastic light scattering of W oxide films on transparent and reflecting substrates, and features of scattering spectra for both colored and bleached samples could be modeled [457–459].

Obliquely sputter deposited W oxide films were subjected to spectrophotometric measurements. The samples were fixed so that the light was incident in the deposition plane, i.e., the plane normal to the substrate surface that contains the direction of the deposition flux and the column axes. Optical transmittance was measured for $300 < \lambda < 2500$ nm for s and p polarized light incident at the angles 0° and $\pm 60^\circ$; positive angles are taken to be on the same side of the substrate normal as the deposition direction and the column tilt. Transmittance of unpolarized light was obtained as the arithmetic mean of the values for s and p polarized compontents.

Fig. 21 reports measured transmittance for the sample whose microstructure was shown in Fig. 8. Part (a) refers to the as-deposited film. The transmittance increases strongly in the luminous range. This feature is not typical for electrochromic W oxide films (cf. Fig. 15), and the short-wavelength absorption in the obliquely sputtered sample is ascribed to unoxidized tungsten. Such absorption is instrumental in oxide-based films with pronounced angular selectivity [164,493–501]. The most important result shown in Fig. 21 is the observation of angular selectivity, i.e., the fact that the p polarized transmittance is much larger when the incidence angle is $+60^\circ$ than when it is -60°. The relative difference is enhanced in the colored film. Specifically, the luminous transmittance of unpolarized light is 46% at $+60^\circ$ and 35% at -60° in the as-deposited state, whereas the corresponding numbers are 15% and 9% in the colored state. This clearly manifested angular selectivity may be of interest for applications of electrochromic smart windows to inclined windows, glass blinds, and louvres. Data can be readily taken also outside the incidence plane [501].

6. Devices

Electrochromic device design is conveniently discussed with regard to a five-layer stack on a substrate or between two substrates. The central layer is a pure ionic conductor for small ions such as H^+, Li^+, or Na^+. The optically functional

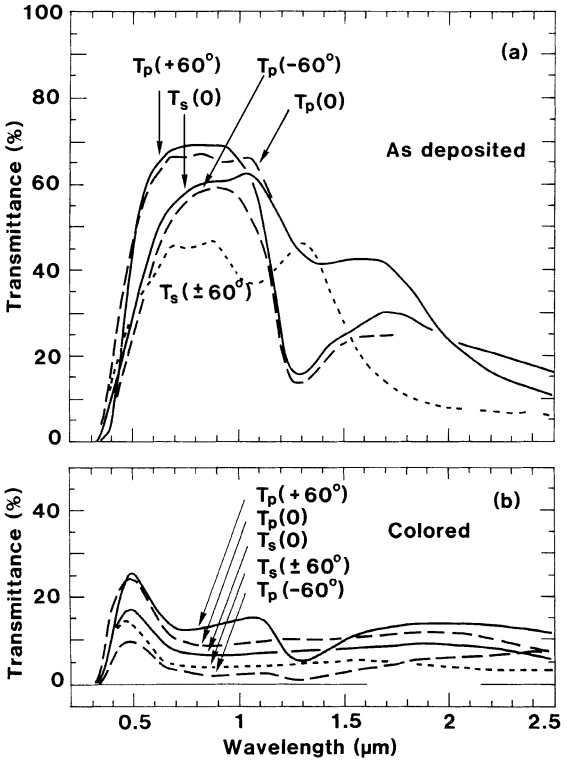

Fig. 21. Spectral and angular transmittance T of s and p polarized light through electrochromic W-oxide-based films in as-deposited (part a) and Li^+ intercalated (part b), and hence colored, states.

electrochromic layer is located on one side of the ion conductor, and an ion storage layer serves as counter electrode on the other side of the ion conductor. The optical modulation takes place when ions are moved back and forth between the electrochromic layer and the counterelectrode. This movement is induced by a static electric field applied between electrically conducting layers, one being on the outer side of the electrochromic material and the other on the outer side of the counterelectrode. Both of these electrical conductors must be transparent if optical transmittance modulation is desired. The voltage needs to be applied only when optical changes are to take place, i.e., the device has open-circuit memory. The analogy between the electrochromic device and the electrical battery should be evident, the essential difference between the two being that the electrochromic device is a thin-film stack in which the charging state manifests itself as an optical effect. While the above mentioned five-layer design is used in the great majority of the prototype devices, it does not represent the only possibility, and interesting results on "three-layer electrochromics" has been demonstrated by use of WO_3–Ta_2O_5–Li_2CO_3 composites [42].

The electrochromic device can be used in different ways. Perhaps the most striking — and potentially most important — is to modify the optical transmittance of

architecural smart windows in order to avoid overheating and to achieve good indoor lighting conditions. Window applications of electrochromism have been surveyed several times with special attention to energy savings potential [502], control strategies [503], color rendering [504], directional optical performance [315], durability issues [9,505,506], and visual quality assessment [507]. The possibilities to have self-powering by integration of photovoltaic cells has been considered; studies have been performed on design goals [14,508] as well as on the implementation of semi-transparent solar cells of amorphous hydrogenated SiC [183,509,510] and dye sensitized nanocrystalline TiO_2 [179]. In addition to smart windows applications, there has been recent work on devices that modulate specular reflectance [277], diffuse reflectance [214], and thermal emittance [190,264]. The latter devices are of interest with regard to anti-dazzling rear view mirrors for cars and trucks, to non-emissive information display, and to thermal control of space vehicles, respectively.

It should be mentioned, mainly for the sake of completeness, that W oxide films are of much concern also in several non-electrochromic applications. For example, they exhibit a photochromic effect [11,180,181,196,211,212,511] which operates well with ultraviolet irradiation. Visible light photochromism is possible with WO_3-CdS composites [182,223] as well as with W oxide pretreated in a solution of KNO_3 and propylene carbonate [512]. Photochromism has been found also in peroxopolytungstic films [404] and in WO_3 particle suspensions [394]. Thermochromism caused by pulsed laser heating has been discussed [512]. Coloration can be achieved by exposure to H_2, and this "gasochromic" effect is of interest for smart windows [198,231,405]. Coloration can be obtained by ion implantation [290,298], and coloration by mechanical forces has been demonstrated using ultrasonics ("sonolytic coloration") [396], piezoelectrics [513], and mechanical milling [412]. WO_3-based gas sensors have been studied for H_2S [272,286,311,314,514], NO_x [173,282,284, 285,299,304–306,312,398,515–518], CO_2 [278,399], NH_3 [312], and H_2 [346,519]. Multi-material array sensors incorporating W oxide have been mentioned [520]. Still other applications of W oxide concern pH sensing [389,521], electron-beam lithography [188], and focused-ion-beam lithography [202,203,522].

6.1. All-inorganic electrochromic devices

It deserves to be mentioned at the outset that liquid electrolytes are convenient for fundamental studies of electrochromism but are not of much interest for practical devices owing to obvious risks of leakage and since gravity-induced forces may be excessive when large areas are of importance. The possibilities of immobilizing the electrolyte in a porous membrane should be noted, though, and a foil of such a material can appear fully transparent provided that there is a matching of the refractive indices for the liquid electrolyte and the solid membrane [377].

There has been much recent work on all-solid-state electrochromic devices for transmittance modulation and potential use in smart windows. Much of the initial discussion will revolve around Table 1, which summarizes the essential properties such as materials, range of transmittance modulation, and tested number of color/bleach cycles.

The first example concerns a "Deb device" [1,18], whose distinctive feature is an outer electrical conductor being a semitransparent Au film that acts so as to catalytically decompose water. Entry 1 in Table 1 refers to results in a paper by Lusis [523] that summarizes a large body of work performed at the University of Latvia. The devices are durable if operated in the presence of some humidity, and 10^5–10^6 color/bleach cycles have been documented. A somewhat similar design, employing instead an electrolyte being an antimony hydrogen phosphate thin film, was studied by Kuwabara and Yamada [215]; cf. entry 2. Devices using proton-conducting $Sb_2O_5 \cdot qH_2O$ electrolytes are of considerable interest, and up to 10^7 color/bleach cycles have been documented with laminated constructions having the electrolyte in between films of W oxide and Ir oxide, as discussed by Vaivars et al. [238] and Lusis [523]; cf. entry 3. General design and simulation models have been formulated for such devices [230,524,525]. An antimony-based electrolyte was employed also in [214].

An interesting construction, with a TiO_2-based ion conductor and a counter electrode of Ti-Ce oxide, was reported on by Macêdo and Aegerter [381], who used sol–gel technique to make the entire device. As indicated in entry 4, the transmittance at $\lambda = 550$ nm could be modulated between 18% and 58%. The device functioned with proton transport, but Li^+ transport is another option. Degradation by delamination was noted after a few hundred cycles; this degradation was not an inherent property of the Ti-Ce oxide film, though, but symmetric devices using this material could be run through at least 3×10^4 cycles. One should note that Ti–Ce oxide is an optically passive thin film material of much interest as a counterelectrode in electrochromic materials. It can be prepared by sol–gel technique [526–538] as well as by sputtering [527,539–546]. A detailed discussion of Ti–Ce oxide is outside the scope of this review.

Recent work by Azens et al. [547] has reported on devices with a proton conducting ZrP-based electrolyte in between films of W oxide and Ni oxide; cf. entry 5. High coloration efficiency is obtained by combining the cathodically coloring W oxide with anodically coloring Ni oxide. A thin layer of ZrO_2 protects the Ni oxide surface. Fig. 22(a) shows that the mid-luminous transmittance can be varied over a range as wide as from 17% to 75%, and Fig. 22(b) reports that the color/bleach dynamics is fairly rapid.

NiO is a very important, and yet poorly understood, electrochromic material whose advantageous properties were discovered a number of years ago [548–550]. A considerable amount of work has been published recently [354,513,547,551–574]. Again, the object is to give a sampling of relevant work rather than a complete coverage. The physics of NiO has been reviewed by Hüfner [575].

Entry 6 is of particular interest. It concerns a device that has been studied in great detail for practical applications to large area smart windows by Wang et al. [241] and Mathew et al. [49]. The system operates with proton transport via a hydrous Ta_2O_5 layer between a W oxide film and a Ni oxide film. This three-layer stack is positioned between ITO layers. The luminous transmittance was modulated between 12% and 78% in in devices up to 0.18 m^2 in size. Durability for more than 2×10^4 cycles was reported. The color/bleach cycle time was ~ 10 s for small devices but is expected to

Table 1
Data for inorganic electrochromic devices showing materials, sample size, modulation range for the transmittance (T), number of color/bleach (c/b) cycles, and switching time (τ_{sw}). G denotes glass, and the subscript for T signifies the wavelength (in nm) or the averaging over wavelength to obtain luminous (lum) and solar (sol) values

Entry	Device construction	Size (cm^2)	T (%)	c/b (cycles)	τ_{sw} (s)	Reference
1	G/ITO/WO_3/SiO_2/Au	—	—	10^6	—	[523]
2	G/ITO/WO_3/$SbHP_2O_2 \cdot qH_2O$/Au	—	—	$> 10^4$	—	[215]
3	G/ITO/WO_3/$Sb_2O_5 \cdot qH_2O$/IrO_2/ITO/G	—	—	$> 10^7$	—	[238,523]
4	G/ITO/WO_3/TiO_2/TiO_2-CeO_2/ITO/G	—	$18 < T_{550} < 58$	360	—	[381]
5	G/ITO/WO_3/$ZrP \cdot qH_2O$/ZrO_2/NiO/ITO/G	20	$17 < T_{550} < 75$	—	60	[547]
6	G/ITO/NiO/Ta_2O_5/WO_3/ITO	180	$12 < T_{lum} < 78$	$> 2 \times 10^4$	10	[49,241]
7	G/ITO/V_2O_5/$LiBO_2$/WO_3/Au	3	$3 < T_{815} < 38$	~ 100	—	[176]
8	G/SnO_2/WO_3/Li_2O-CeO_2-SiO_2/V_2O_5/Au	—	$9 < T_{sol} < 25$	—	10	[253]
9	G/ITO/WO_3/MgF_2/V_2O_5/Au	1	$\Delta T \approx 50$	—	—	[183]
10	G/ITO/V_2O_5/$LiBO_2$/WO_3/ITO	3	$13 < T_{lum} < 65$ $9 < T_{sol} < 58$	—	720	[177]
11	G/ITO/V_2O_5/$LiBO_2$-LiF/WO_3/ITO/MgF_2	3	$21 < T_{lum} < 60$ $13 < T_{sol} < 52$	2000	450	[177]
12	G/ITO/VO_2/$LiAlF_4$/WO_3/ITO	3	$10 < T_{sol} < 50$	> 1000	—	[189]
13	G/ITO/WO_3/$LiNbO_3$/$LiCoO_2$/In_2O_3	2	$12 < T_{550} < 65$	1.8×10^4	—	[582–584]
14	G/ITO/CrO_z/$LiBO_2$/WO_3/ITO/ZrO_2	16	$9 < T_{lum} < 74$	> 5000	30	[191,192]

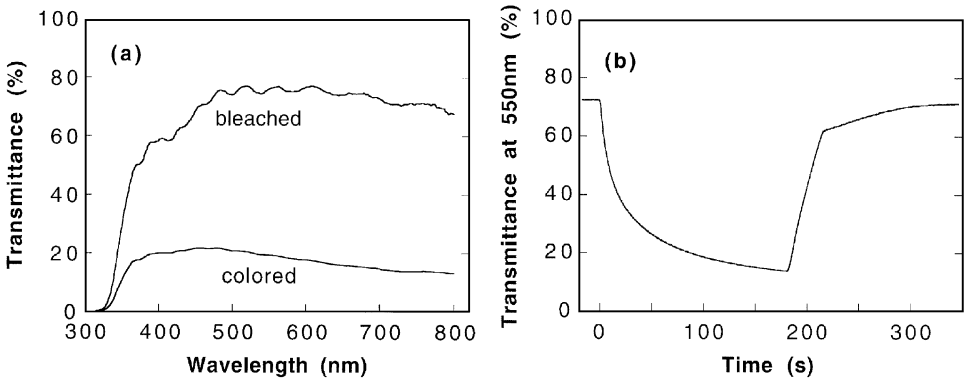

Fig. 22. Spectral transmittance (part a) and time-dependent transmittance at a wavelength of 550 nm (part b) for an electrochromic device with a proton conducting ZrP-based electrolyte between films of W oxide and Ni oxide.

be longer for larger sizes. Leakage currents were found to be small enough for practical applicability. A somewhat similar design, with an ion conductor of Ti oxide or Ta oxide and a counter electrode of Co oxide or Ni oxide, was able to show large reflectance differences when the top electrode was an Al film [277].

We now turn to devices that operate by Li^+ insertion/extraction. It is convenient to start by considering entry 7 in Table 1, which illustrates some data by Ashrit et al. [176] on an arrangement with films of W oxide and V pentoxide and an intervening $LiBO_2$ layer. The ion conductor can be represented alternatively as Li_2O–B_2O_3, which may be a more correct description [576]. A modest modulation of the transmittance was obtained. In particular, the bleached state transmittance was only 38% at $\lambda = 815$ nm, as expected from the substantial absorption in the top layer of Au [577] and the absorption inherent in V pentoxide [578]. This latter absorption is due to the non-octahedral microstructure of V_2O_5 [579]. Rather similar device data were obtained by Zhang et al. [253] who studied a related design incorporating a V pentoxide counter electrode, a Li_2O–CeO_2–SiO_2 ion conductor, and an Au top electrode; data are given in entry 8.

The design in entry 9 was studied by Bechinger et al. [183]. It includes a MgF_2 host for Li^+ transport, and was able to vary the transmittance by $\sim 50\%$. The absolute value of the transmittance was not given, though. The most conspicuous result of this device is its operating voltage being as low as ~ 1 V. As pointed out above, the Au layer is capable of a catalytic decomposition of water, and one may wonder whether proton mobility is operating along with the presumed Li^+ transport. General models for the optical and electrochemical properties of V pentoxide-based devices have been reported [579].

Improved versions of the above designs were investigated by Ashrit et al. [177]; cf. entries 10 and 11. The metallic top electrode was replaced by ITO, which enhanced the transmittance significantly. The design in entry 11 also has an ion conductor whose Li^+ conductivity was boosted by codeposition with LiF, and which is

protected by a MgF_2 layer serving the additional purpose to antireflect the underlying ITO [580,581]. The luminous and solar transmittance can be varied within rather large ranges, with maximum values of 65% for the luminous transmittance and 58% for the solar transmittance. The surface-protected device withstood more than 2000 color/bleach cycles. Temperatures up to 60° and relative humidities between 25% and 70% were used. A major concern is the slow dynamics, with switching times of the order of 10 min even at a small size. Rather similar optical properties were found by Chen et al. [189] who studied an analogous device, albeit with a V dioxide counter-electrode and a $LiAlF_4$ ion conductor; cf. entry 12. A V pentoxide counter electrode was used also in some other work [220].

The device investigated by Goldner et al. [582–584], included as entry 13 in Table 1, shows a performance similar to the one in entry 10. Goldner et al. used a counter electrode of $LiCoO_2$, an ion conductor of $LiNbO_3$, and a top electrode of In oxide. Nuclear reaction analysis was employed to assure that the optical modulation operated by Li^+ transport [289]. The devices were reported to withstand 1.8 x 10^4 color/bleach cycles.

Cogan et al. [191,192] reported good optical properties in devices with CrO_x as counter electrode, $LiBO_2$ as ion conductor, and ITO as top electrode; cf. entry 14. A protective layer of ZrO_2 was also included. The luminous transmittance could be varied over a range as large as 9–74%; hence the transparency can be almost as good as in the best proton conducting systems including Ni oxide. Several thousand color/bleach cycles were tested. The switching time was of the order of 1 min, depending on applied voltage.

The thin film devices incorporating Li normally need lithiation as a separate process step. This can be accomplished by sublimation from $LiNbO_3$ [176], direct evaporation of Li on top of the W oxide [183,189,191,192,245,253], and codeposition with Li [199]. One study pointed at a Li/W ratio of 0.14 as being suitable [245].

6.2. Polymer-laminated electrochromic devices

We now consider devices incorporating a centrally positioned polymer electrolyte and discuss a number of devices. Most of them employ two ITO-coated glass substrates, whereas a few use instead ITO-coated flexible polymer (polyester) foils; specific designs and pertinent data are summarized in Table 2, where entries 15–19 concern devices relying on H^+ transport.

A particularly simple device design was described by Pennisi and Simone [327–329]; cf. entry 15. It is based on an electrochromic W oxide film (with Mo doping to provide color neutrality), an electrolyte of hydrogenated poly perfluoro sulfonic acid (PPSA, normally known as "Nafion"), and an ITO film serving the double purpose of being counter electrode and transparent electrical conductor. The luminous and solar transmittance could be varied in a reasonable range, but high transmittance values were not reported. Furthermore, the long-term durability may be questioned, and the use of ITO films as intercalation materials could not be substantiated in a recent investigation [585]. Nevertheless, it should be observed that ITO powders can exhibit electrochromism [16,586]. A design similar to the one by

Table 2
Data for laminated electrochromic devices showing materials, sample size, modulation range for the transmittance (T), number of color/bleach (c/b) cycles, and switching time (τ_{sw}). G denotes glass, P denotes polymer, and the subscript for T signifies the wavelength (in nm) or the averaging over wavelength to obtain luminous (lum) and solar (sol) values. The abbreviations for the various polymers are explained in the main text

Entry	Device construction	Size (cm^2)	T (%)	c/b (cycles)	τ_{sw}(s)	Reference
15	G/ITO/WO_3:Mo/PPSA-H^+/ITO/G	6	$8 < T_{lum} < 58$ $7 < T_{sol} < 46$	~ 300	~ 20	[327–329]
16	G/ITO/WO_3/PAMPS/PB/ITO/G	400	$5 < T_{550} < 69$	2×10^4	60	[204,588]
17	G/ITO/PVA/PANI/ITO/G	—	$9 < T_{700} < 42$	—	1	[318]
18	P/ITO/WO_3/BPEI-H^+/FI/ITO/P	16	$25 < T_{lum} < 60$	—	20	[270,271]
19	P/ITO/WO_3-PMMA/BPEI -H^+/PANI/Au/P	2	$25 < T_{550} < 50$	—	—	[403]
20	G/ITO/WO_3/PMMA-Li^+/V_2O_5/ITO/G	25	$22 < T_{lum} < 73$ $14 < T_{sol} < 60$	—	60	[252]
21	G/ITO/WO_3/PMMA-Li^+/V_2O_5/ITO/G	64	$20 < T_{550} < 50$	—	5	[592]
22	G/ITO/WO_3/HEMA-NPG-Li^+/PB/ITO/G	2025	$20 < T_{lum} < 77$	10^5	120	[206]
23	G/ITO/WO_3/PMMA-PC-Li^+/NiO/ITO/G	—	$31 < T_{600} < 78$	10^4	—	[217]
24	G/ITO/$K_{0.3}WO_3$/PEO-PC-Li^+/WO_3-NiO/ITO/G	9	$25 < T_{550} < 80$	—	5	[608]
25	G/ITO/WO_3/PVB-Li^+/TiO_2-CeO_2/ITO/G	100	$7 < T_{lum} < 81$ $4 < T_{sol} < 73$	5×10^4	60	[313]
26	G/ITO/WO_3/Silane-Li^+/TiO_2-CeO_2/ITO/G	1225	$20 < T_{380\text{-}800} < 80$	—	> 100	[382,383]
27	G/ITO/WO_3/GLYMO-TEG-Li^+/SnO_2(Mo,Sb)/ITO/G	5	$25 < T_{550} < 75$	500	30	[611]
28	G/ITO/WO_3/PMMA-PPG-Li^+/TiO_2-ZrO_2/ITO/G	5	$20 < T_{550} < 80$	—	200	[38]
29	G/ITO/WO_3/PEO-Li^+/PODS/ITO/G	15	$9 < T_{lum} < 55$ $4 < T_{sol} < 34$	—	< 60	[323,324,330]
30	G/ITO/WO_3/PEO-ECH-Li^+/PPY-DDS/ITO/G	2	$30 < T_{700} < 60$	1.5×10^4	~ 2	[279]
31	P/ITO/WO_3/PMMA-PC-Li^+/V_2O_5/ITO/P	—	$8 < T_{600} < 65$	3×10^4	—	[217]
32	G/ITO/dye-TiO_2/electrolyte/WO_3/ITO/G	—	$54 < T_{788} < 70$	—	—	[179]

Pennisi and Simone [327–329] — with H^+ conducting polyethylene oxide (PEO) and H^+ loaded ITO — was investigated by Ingram et al. [208], in particular with regard to coloration and bleaching dynamics. Device studies using a recently developed Nafion-type ionomer was reported by Varjian et al. [587], who investigated somewhat ill-defined electrochromic devices up to 800 cm^2 in size.

Ho et al. [204,588] reported detailed results, included as entry 16, for a more conventional design with a poly-2-acrylamido-2-methyl-propane sulfonic acid (PAMPS) electrolyte and a counter electrode of hexacyanoferrate (known as "Prussian Blue", PB). The transmittance in the mid-luminous range could be varied between 5% and 69% during more than 2×10^4 color/bleach cycles. The cycle time was ~ 15 s for 20-cm^2-devices and ~ 60 s for 400-cm^2-devices. The response became more sluggish below 0°C. Electrochromic devices based on PAMPS and a counterelectrode of polyaniline (PANI), or a bilayer of PANI and PB, have been discussed in detail [317,319–321,589,590]. The optical modulation range was not as large, and the devices were smaller, in this latter work.

Alternatives to the above mentioned electrolytes have been reported by Heckner and Rothe [318] and Passerini et al. [591]. The former of these works, included as entry 17 in Table 2, regards an electrolyte based on polyvinyl alcohol (PVA) and a PANI counter electrode; a modest transmittance modulation was reported. The latter work [591] investigated prototype devices with a proton-conducting gel electrolyte of Nafion-type and a NiO counterelectrode.

Polymer electrolytes lend themselves to incorporation in flexible electrochromic devices. Work along this line has been reported by Antinucci et al. [270,271] and, more recently, by Michalak and Aldebert [403]; cf. entries 18 and 19. The substrate was ITO-coated polyester, and the electrolyte was cross-linked branched polyethylene imine (BPEI) made proton conducting by H_3PO_4. Antinucci et al. [271] used WO_3 and a counter electrode of fluoroindine (FI), i.e., 5,7,12,14-teraaza-(7H,14H)-pentacene; the luminous transmittance could be modulated between 25% and 60%. Michalak and Aldebert [403] reported on a device with an electrochromic composite of WO_3 and polymethyl methacrylate (PMMA) and a counter electrode of PANI. The counter electrode was in contact with an Au film which limited the maximum transmittance to about 50%.

We now turn to devices incorporating Li^+ conducting polymers and first consider a design by Zhang et al. [252] employing a V_2O_5 counter electrode and an electrolyte of PMMA made Li^+ conducting by the addition of $LiClO_4$ or $LiBF_4$; cf. entry 20. The luminous transmittance could be varied between 22% and 73% and the solar transmittance between 14% and 60%. An analogous design was discussed by Passerini et al. [592], who indicated a smaller range of optical modulation; cf. entry 21. Results have been given also by Bell et al. [369]. Optical absorption in V_2O_5 gives an inherent limitation to the transmittance, as pointed out above.

A number of devices have used PB as counterelectrode, in conjunction with various Li^+ conducting polymers. Detailed results were given by Inaba et al. [206] for a design incorporating a copolymer of hydroxyethyl methacrylate (HEMA) and neopentyl glyco dimethylacrylate (NPG); cf. entry 22. The luminous transmittance lay between 20% and 77% in devices as large as 45×45 cm^2. They withstood at least 10^5

color/bleach cycles. The times for coloring and bleaching were ~ 180 and ~ 90 s, respectively, and operation was tested for temperatures between 5°C and 70°C. Device-related studies on samples incorporating PB can be found also elsewhere [225,593–607]; these latter works are not confined to Li^+ conducting polymers, though, but also consider the role of larger ions such as Na^+ and K^+. We may note, in passing, the highly repetitive character of some publications [595–607].

Devices with NiO as a counter electrode are able to yield a high transmittance, as indicated earlier. Entry 23, summarizing work by Lechner and Thomas [217], shows transmittance values up to 78% in a device with an electrolyte based on PMMA and propylene carbonate (PC). A somewhat related design was developed by Lee et al. [255,608–610]. As indicated in entry 24, the device contained electrochromic $K_{0.3}WO_{3.15}$, an electrolyte based on PEO and PC, and a mixed W–Ni oxide counterelectrode. The mid-luminous transmittance was varied between 25% and 80%. A NiO-based counter electrode was used also by Passerini et al. [591].

Ti–Ce oxide is a novel and interesting material capable of serving as a transparent counterelectrode as pointed out above. It was used by Schlotter et al. [313] in devices incorporating polyvinyl butyral (PVB) made Li^+ conducting by addition of $LiClO_4$. As shown in entry 25, the luminous transmittance could be varied between 7% and 81% and the solar transmittance between 4% and 73%. Up to 5×10^4 color/bleach cycles were tested. The time for optical modulation was about one minute. The data were obtained for a construction with an ITO electrode having a resistance/square of 100 Ω, which is a moderately high value. Diminishing this resistance to 10 Ω could produce faster color/bleach dynamics, but at the same time the maximum solar transmittance was limited to 66% since the ITO had a substantial reflection in the near-infrared spectral range.

Munro et al. [382,383] also studied devices with a Ti–Ce oxide counter electrode; cf. entry 26. Their electrolyte was based on organically modified silanes, specifically glycidoxypropyl trimethoxysilane (GPTS), tetraethoxysilane (TEOS), $LiClO_4$, $Zr(O^nPr)_4$ and tetraethylene glycol (TEG), where GPTS and TEOS serve as network formers, TEG acts as a plasticizer, lithium perchlorate is the conducting salt, and $Zr(O^nPr)_4$ is added as a starter for thermal curing. The transmittance averaged over the $380 < \lambda < 800$ nm range — i.e., essentially the luminous transmittance — could be varied between 20% and 80%. The color/bleach time was ~ 100 s for devices being 150 cm^2 in size, but electrochromic smart windows as large as 1225 cm^2 were included in the study. Work on devices with a PEO-based electrolyte and a Ti–Ce oxide counter electrode was reported also by Reisfeld et al. [386].

An original design of electrochromic devices was reported recently by Orel et al. [611]. The electrolyte comprised glycidyloxypropyl trimethoxysilane (GLYMO) and TEG, and the counter electrode was a film of SnO_2 doped with Mo, Mb, or both of these; cf. entry 27. The mid-luminous transmittance could be varied between some 25% and 70%. Sn oxide capable of ion intercalation has been investigated recently for films made by sol–gel technology [612–614] and sputtering [615–619].

A very recent, and in some regards superior, alternative to Ti–Ce oxide is provided by Zr–Ce oxide [545,546,620]. A film of this material was used together with a Li^+ conducting electrolyte based on a copolymer of PMMA and polyethylene glycol

(PEG) [621]; cf. entry 28. As shown in Fig. 23(a), reproduced from a review by Granqvist et al. [38], the transmittance could be varied between widely separated extrema, and the mid-luminous value lay between 20% and 80%. The dynamics depends on the voltages for coloration and bleaching, as illustrated in Fig. 23(b).

Devices with polymeric counter electrodes have been investigated by Lampert et al. [323,324,330] who used layers of polyorganodisulfide (PODS) together with a PEO-based electrolyte. As apparent from entry 29, the luminous and solar transmittance could be modulated, but the devices were unable to attain a very high transmittance. Another alternative, using a copolymer of polypyrrole (PPY) and dodecylsulfate (DDS) as counter electrode and a Li^+ conducting copolymer of PEO and epichlorohydrin (ECH) as electrolyte, is reported in entry 30. This latter work was performed by De Paoli et al. [279], who extended earlier studies by Rocco et al. [310].

A flexible electrochromic device based on ITO coated polymer foil was studied by Lechner and Thomas [217]; cf. entry 31. It uses a PMMA-based electrolyte joining films of W oxide and V pentoxide. The transmittance at $\lambda = 600$ nm could be varied between 6% and 65%. Durability up to 3×10^4 color/bleach cycles was reported. Another design, also with a PMMA-based electrolyte and with a counterelectrode of PANI, was reported by Panero et al. [302]; the transmittance modulation was modest.

We end the detailed presentation of electrochromic devices by considering an innovative approach towards self-powering taken recently by Bechinger et al. [179,622]; cf. entry 32. They combined the electrochromic W oxide film with a dye sensitized solar cell employing, as in the normal Grätzel design, nanocrystalline TiO_2 with a dye of $Ru(II)L_2L'$, where L = 2,2′-bipyridine-4,4′-dicarboxylate and L′ = 4,4′-dimethyl-2,2′-bipyridine, and a liquid electrolyte of propylene carbonate containing 0.1 M LiI and 0.01 M tertbutylpyridine [623–625].

Some further data on polymer-based devices can be found elsewhere [190,254,368,379]. Results are available also on electrochromic bilayers of W oxide and a dibenzyl viologen polymer [293], on polymer electrolytes for windows [626],

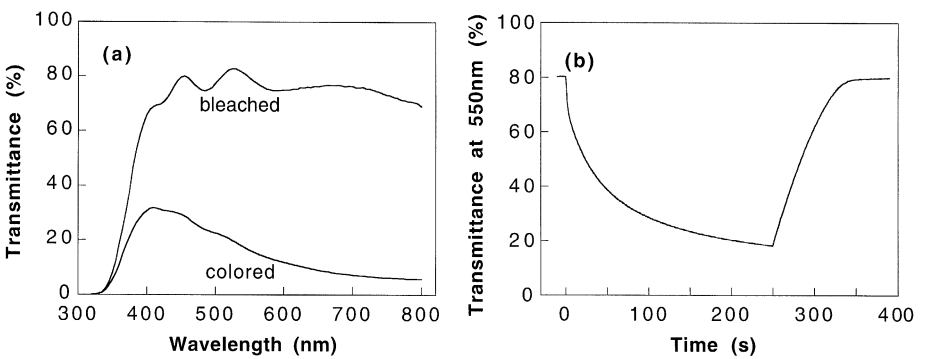

Fig. 23. Spectral transmittance (part a) and time-dependent transmittance at a wavelength of 550 nm (part b) for an electrochromic device with Li^+ conducting PMMA-PPG-based electrolyte between films of W oxide and ZrO_2–CeO_2.

and on counterelectrodes of PANI-PVA composite [326], PANI together with nitrilic rubber [236], and PPY-DDS [310].

7. Summary and remarks

This review has covered work during 1993–1998 on electrochromic W oxide films. The emphasis has been on results of particular relevance for devices such as smart windows. For crystalline WO_3, the theoretical understanding is rather good, and it is possible to present reliable calculations of optical and other properties. However, highly disordered W oxide films and their electrochromism represent areas where several unknowns still remain. The review has discussed a number of ways to achieve porosity so that the coloration/bleaching dynamics can be fast. Coloumetric titration data can be reconciled with a model involving a distribution of site energies. Optical properties cannot yet be calculated from basic models, but there has been recent progress on the understanding of effects such as the saturation of the coloration efficiency at high charge densities and the enhancement of the coloration efficiency in nonstoichiometric films.

A lot of work has been devoted to devices: all-solid-state constructions backed by one glass substrate as well as polymer-based devices involving lamination of two glass substrates. A transmittance up to 80% in the bleached state has been reported for several designs. Flexible devices based on polymer foils have been reported.

Electrochromics involves a healthy blend of basic physics and chemistry, thin film science, device technology, and market opportunities. Combining these features with the fascination surrounding smart windows and glass facades, intelligent buildings, and novel concepts such as interactive architecture, one can project that electrochromics is likely to remain a vital field for endeavors of various kinds during several years to come.

References

[1] C.G. Granqvist, Handbook of Inorganic Electrochromic Materials, Elsevier, Amsterdam, 1995.
[2] S.A. Agnihotry, S. Chandra, Indian J. Eng. Mater. Sci. 1 (1994) 320.
[3] A. Agrawal, J.P. Cronin, R. Zhang, Solar Energy Mater. Solar Cells 31 (1993) 9.
[4] C. Arbizzani, M. Mastragostino, A. Zanelli, Solar Energy Mater. Solar Cells 39 (1995) 213.
[5] C.O. Avellaneda, M.A. Macêdo, A.O. Florentino, M.A. Aegerter, Proc. Soc. Photo-Opt. Instr. Eng. 2255 (1994) 38.
[6] A. Azens, A. Hjelm, D. LeBellac, C.G. Granqvist, J. Barczynska, E. Pentjuss, J. Gabrusenoks, J.M. Wills, in: J.B. Bates (Ed.), Proceedings of the Symposium of Thin Film Solid State Ionic Devices and Materials, Vol. 95-22, The Electrochemical Society, Pennington, 1995, pp. 102–117.
[7] A. Azens, A. Hjelm, D. LeBellac, C.G. Granqvist, J. Barzynska, E. Pentjuss, J. Gabrusenoks, J.M. Wills, Proc. Soc. Photo-Opt. Instr. Eng. 2531 (1995) 92.
[8] A. Azens, A. Hjelm, D. LeBellac, C.G. Granqvist, J. Barczynska, E. Pentjuss, J. Gabrusenoks, J.M. Wills, Solid State Ionics 86–88 (1996) 943.
[9] M.E. Badding, S.C. Schulz, L.A. Michalski, R. Budziak, in: K.-C. Ho, C.B. Greenberg, D.M. MacArthur (Eds.), Proceedings of the Third Symposium of Electrochromic Materials, Vol. 96-24, The Electrochemical Society, Pennington, 1997, pp. 369–384.

[10] K. Bange, T. Gambke, G. Sparschuh, in: R.E. Hummel, K.H. Guenther (Eds.), Handbook of Optical Properties, Vol. I, Thin Films for Optical Coatings, CRC Press, Boca Raton, 1995, pp. 105–134.
[11] C. Bechinger, D. Ebner, S. Herminghaus, P. Leiderer, Solid State Commun. 89 (1994) 205.
[12] J. Bell, Opt. Laser Eng. (February 1997) 21–25.
[13] J.M. Bell, I.L. Skryabin, G. Vogelmann, in: K.-C. Ho, C.B. Greenberg, D.M. MacArthur (Eds.), Proceedings of the Third Symposium on Electrochromic Materials, Vol. 96-24, The Electrochemical Society, Pennington, 1997, pp. 396–408.
[14] D.K. Benson, H.M. Branz, Solar Energy Mater. Solar Cells 39 (1995) 203.
[15] H.J. Byker, in: K.-C. Ho, D.A. MacArthur (Eds.), Proceedings of the Symposium on Electrochromic Materials, II, Vol. 94-2, The Electrochemical Society, Pennington, 1994, pp. 3–13.
[16] J.P. Coleman, A.T. Lynch, P. Madhukar, J.H. Wagenknecht, in: K.-C. Ho, C.B. Greenberg, D.M. MacArthur (Eds.), Proceedings of the Third Symposium on Electrochromic Materials, Vol. 96-24, The Electrochemical Society, Pennington, 1997, pp. 325–337.
[17] F. Croce, S. Panero, S. Passerini, B. Scrosati, Electrochim. Acta 39 (1994) 255.
[18] S.K. Deb, Solar Energy Mater. Solar Cells 39 (1995) 191.
[19] R.B. Goldner, J. Vac. Sci. Technol. A 13 (1995) 1088.
[20] C.G. Granqvist, in: M.H. Francombe, J.L. Vossen (Eds.), Physics of Thin Films, Vol. 17, Academic, San Diego, 1993, pp. 301–370.
[21] C.G. Granqvist, Solid State Ionics 60 (1993) 213.
[22] C.G. Granqvist, Mater. Sci. Eng. A 168 (1993) 209.
[23] C.G. Granqvist, Appl. Phys. A 57 (1993) 3.
[24] C.G. Granqvist, in: E.W.A. Lingeman (Ed.), Using Energy in an Intelligent Way, Proceedings of the 111th WE-Heraeus Seminar, European Physical Society, Geneva, 1993, pp. 241–258.
[25] C.G. Granqvist, Proc. Soc. Photo-Opt. Instr. Eng. 2017 (1993) 84.
[26] C.G. Granqvist, J. Phys. IV (Paris) 3 (1993) 1367.
[27] C.G. Granqvist, Solar Energy Mater. Solar Cells 32 (1994) 369.
[28] C.G. Granqvist, Solid State Ionics 70/71 (1994) 678.
[29] C.G. Granqvist, Arkhimedes 2 (1994) 95.
[30] C.G. Granqvist, Renewable Energy 5 (1994) 141.
[31] C.G. Granqvist, Memoire di Scienze Fisiche e Naturali 112 (1994) 355.
[32] C.G. Granqvist, in: P.J. Gellings, H.J.M. Bouwmeester (Eds.), Handbook of Electrochemistry, CRC Press, Boca Raton, 1997, pp. 587–615.
[33] C.G. Granqvist, Proc. Soc. Photo-Opt. Instr. Eng. 2968 (1997) 158.
[34] C.G. Granqvist, Renewable Energy 15 (1998) 243.
[35] C.G. Granqvist, V. Wittwer, Solar Energy Mater. Solar Cells 54 (1998) 39.
[36] C.G. Granqvist, A. Azens, L. Kullman, D. Rönnow, Renewable Energy 8 (1996) 97.
[37] C.G. Granqvist, A. Azens, J. Isidorsson, M. Kharrazi, L. Kullman, T. Lindström, G.A. Niklasson, C.-G. Ribbing, D. Rönnow, M. Strømme Mattsson, M. Veszelei, J. Non-Cryst. Solids 218 (1997) 273.
[38] C.G. Granqvist, A. Azens, A. Hjelm, L. Kullman, G.A. Niklasson, D. Rönnow, M. Strømme Mattsson, M. Veszelei, G. Vaivars, Solar Energy 63 (1998) 199.
[39] M. Green, Chem. Ind. (1996) 641–644.
[40] C.B. Greenberg, J. Electrochem. Soc. 140 (1993) 3332.
[41] O.A. Harizanov, K.A. Gesheva, P.L. Stefchev, Ceram. Int. 22 (1996) 91.
[42] M. Klingler, W.F. Chu, W. Weppner, Solar Energy Mater. Solar Cells 39 (1995) 247.
[43] C.M. Lampert, Thin Solid Films 236 (1993) 6.
[44] C.M. Lampert, Solar Energy Mater. Solar Cells 52 (1998) 207.
[45] J. Livage, Mater. Res. Soc. Symp. Proc. 293 (1993) 261.
[46] G. Macrelli, Renewable Energy 15 (1998) 306.
[47] G. Macrelli, E. Poli, in: K.-C. Ho, C.B. Greenberg, D.M. MacArthur (Eds.), Proceedings of the Third Symposium on Electrochromic Materials, Vol. 96-24. The Electrochemical Society, Pennington, 1997, pp. 338–352.
[48] M. Mastragostino, in: B. Scrosati (Ed.), Applications of Electroactive Polymers, Chapman and Hall, London, 1993, pp. 223–249.

[49] J.G.H. Mathew, S.P. Sapers, M.J. Cumbo, N.A. O'Brien, R.B. Sargent, V.P. Raksha, R.B. Lahaderne, B.P. Hichwa, J. Non. Cryst. Solids 218 (1997) 342.
[50] P.M.S. Monk, R.J. Mortimer, D.R. Rosseinsky, Electrochromism: Fundamentals and Applications, VCH, Weinheim, 1995.
[51] P.M.S. Monk, R.J. Mortimer, D.R. Rosseinsky, Chem. Britain (1995) 380–382.
[52] R.J. Mortimer, Chem. Soc. Rev. 26 (1997) 147.
[52a] B. Orel, A. Surca, U. Opara Krasovec, Acta Chim. Slov. 45 (1998) 487.
[53] N. Ozer, C.M. Lampert, Solar Energy Mater. Solar Cells 54 (1998) 147.
[54] N. Ozer, C.M. Lampert, M. Rubin, in: R. Akcakava, N. Erinc, G. Albayrak, S. Isevi (Eds.), Proceedings of the International Symposium on Glass Problems, SISECAM and International Commission on Glass, Istanbul, 1996, pp. 513–518.
[55] S. Passerini, J. Scarminio, B. Scrosati, D. Zane, F. Decker, J. Appl. Electrochem. 23 (1993) 1187.
[56] J.P. Pereira-Ramos, R. Baddour-Hadjean, N. Kumagai, K. Tanno, Electrochim. Acta 38 (1993) 431.
[57] B. Scrosati, in: B. Scrosati (Ed.), Applications of Electroactive Polymers, Chapman and Hall, London, 1993, pp. 250–282.
[58] S.E. Selkowitz, M. Rubin, E.S. Lee, R. Sullivan, Proc. Soc. Photo-Opt. Instr. Eng. 2255 (1994) 226.
[59] H. Tada, J. Jpn Soc. Colour Mater. 66 (1993) 344.
[60] O. Tillement, Solid State Ionics 68 (1994) 9.
[61] J. Volke, V. Volkeová, Chem. Listy 90 (1996) 137.
[62] M.S. Whittingham, J.-D. Guo, R. Chen, T. Chirayil, G. Janauer, P. Zavalij, Solid State Ionics 75 (1995) 257.
[63] T. Yamase, Chem. Rev. 98 (1998) 307.
[64] R.A. Zoppi, M.-A. DePaoli, Quim. Nova 16 (1993) 560.
[65] D.W. Bullett, Solid State Commun. 46 (1983) 575.
[66] D.W. Bullett, J. Phys. C 16 (1983) 2197.
[67] N.E. Christensen, A.R. Mackintosh, Phys. Rev. B 35 (1987) 8246.
[68] F. Corà, H.G. Stachiotti, C.R.A. Catlow, C.O. Rodriguez, J. Phys. Chem. B 101 (1997) 3945.
[69] F. Detraux, C. Ghosez, X. Gonze, Phys. Rev. B 56 (1997) 983.
[70] A. Gutiérrez-Alejandre, J. Ramírez, G. Busca, Catal. Lett. 56 (1998) 29.
[71] A. Hjelm, C.G. Granqvist, J.M. Wills, Phys. Rev. B 54 (1996) 2436.
[72] L.F. Mattheiss, Phys. Rev. B 2 (1970) 3918.
[72a] A. Stachans, S. Lunell, Int. J. Quantum Chem. 63 (1997) 729.
[73] C.-G. Zhan, F. Zheng, J. Mol. Struct. 285 (1993) 89.
[74] O. Gunnarsson, B.I. Lundqvist, Phys. Rev. B 13 (1976) 4274.
[75] L. Hedin, B.I. Lundqvist, J. Phys. C 4 (1971) 2064.
[76] P. Hohenberg, W. Kohn, Phys. Rev. 136 (1964) B846.
[77] W. Kohn, L.J. Sham, Phys. Rev. 140 (1965) A1133.
[78] J.F. Janak, V.L. Moruzzi, A.R. Williams, Phys. Rev. B 12 (1975) 1257.
[79] U. von Barth, L. Hedin, J. Phys. C 5 (1972) 1629.
[80] D.L. Price, B.R. Cooper, Phys. Rev. B 39 (1989) 4945.
[81] J.M. Wills, B.R. Cooper, Phys. Rev. B 36 (1987) 3809.
[82] O.K. Andersen, Phys. Rev. B 12 (1975) 3060.
[83] H.L. Skriver, The LMTO Method, Springer, Berlin, 1984.
[84] D.D. Koelling, B.N. Harmon, J. Phys. C 10 (1977) 3107.
[85] D.J. Chadi, M.L. Cohen, Phys. Rev. B 8 (1973) 5747.
[86] S. Froyen, Phys. Rev. B 39 (1989) 3168.
[87] M. Figlarz, Proc. Solid State Chem. 19 (1989) 1.
[88] B. Gérand, L. Seguin, Solid State Ionics 84 (1996) 199.
[89] J.-D. Guo, M.S. Whittingham, Int. J. Mod. Phys. 7 (1993) 4145.
[90] L. Seguin, M. Figlarz, J. Pannetier, Solid State Ionics 63–65 (1993) 437.
[91] W. Sahle, M. Nygren, J. Solid State Chem. 48 (1983) 154.
[92] T. Nanba, I. Yasui, J. Solid State Chem. 83 (1989) 304.
[93] T. Nanba, Y. Nishiyama, I. Yasui, J. Mater. Res. 6 (1991) 1324.

[94] T. Nanba, T. Takahashi, J. Takada, A. Osaka, Y. Miura, I. Yasui, A. Kishimoto, T. Kudo, J. Non-Cryst. Solids 178 (1994) 233.
[95] T. Nanba, T. Takahashi, S. Takano, J. Takada, A. Osaka, Y. Miura, T. Kudo, I. Yasui, J. Ceram. Soc. Japan 103 (1995) 222.
[96] P.J. Wiseman, P.G. Dickens, J. Solid State Chem. 6 (1973) 374.
[97] S. Ayyappan, G.N. Subbanna, C.N.R. Rao, Chem. European J. 1 (1995) 165.
[98] S. Begin-Colin, G. Le Caër, M. Zandona, E. Bouzy, B. Malaman, J. Alloys Compounds 227 (1995) 157.
[99] W. Kondo, T. Manabe, T. Kumagai, S. Mizuta, Nippon Kagaku Kaishi (1993) 1034.
[100] Y.T. Zhu, A. Manthiram, J. Solid State Chem. 110 (1994) 187.
[101] B. Pequenard, H. Lecacheux, J. Livage, C. Julien, J. Solid State Chem. 135 (1998) 159.
[102] P.M. Woodward, A.W. Sleight, T. Vogt, J. Solid State Chem. 131 (1997) 9.
[103] W. Han, M. Hibino, T. Kudo, Bull. Chem. Soc. Japan 71 (1998) 933.
[104] W. Han, M. Hibino, T. Kudo, Denki Kagaku 66 (1998) 1230.
[105] N. Kumagai, N. Kumagai, Y. Umetzu, K. Tanno, J.P. Pereira-Ramos, Solid State Ionics 86–88 (1996) 1443.
[106] N. Kumagai, K. Kozawa, N. Kumagai, S. Komaba, A. Derja, Denki Kagaku 66 (1998) 1223.
[107] I. Tsuyumoto, A. Kishimoto, T. Kudo, Solid State Ionics 59 (1993) 211.
[108] J. Bludská, J. Vondrák, I. Jakubec, Collect. Czech. Chem. Commun. 62 (1997) 1177.
[109] T.I. Drobasheva, V.I. Snezhkov, Neorg. Mater. 34 (1998) 1377 [Inorg. Mater. 34 (1998) 1162].
[110] J. Oi, A. Kishimoto, T. Kudo, J. Solid State Chem. 103 (1993) 176.
[111] J. Oi, A. Kishimoto, T. Kudo, Solid State Ionics 72 (1994) 204.
[112] J. Bludská, J. Vondrák, I. Jakubec, Electrochim. Acta 39 (1994) 2045.
[113] X.-L. Xu, H.W. Schmalle, J.R. Günter, Solid State Ionics 76 (1995) 221.
[114] A. Driouiche, M. Figlarz, C. Delmas, Solid State Ionics 62 (1993) 113.
[115] S. Laruelle, M. Figlarz, J. Solid State Chem. 111 (1994) 172.
[116] Y.J. Li, P.P. Tsai, Solid State Ionics 86–88 (1996) 1001.
[117] S.F. Solodovnikov, N.V. Ivannikova, Z.A. Solodovnikova, E.S. Zolotova, Neorg. Mater. 34 (1998) 1011 [Inorg. Mater. 34 (1998) 845].
[118] A. Yu, N. Kumagai, H. Yashiro, Solid State Ionics 100 (1997) 267.
[119] A. Aird, E.K.H. Salje, J. Phys. Condens Matter. 10 (1998) L377.
[120] A.M. de la Cruz, F. Garcia-Alvarado, E. Morán, M.A. Alario-Franco, L.M. Torres-Martinez, J. Mater. Chem. 5 (1995) 513.
[121] J. Molenda, A. Kubik, Phys. Stat. Sol. B 191 (1995) 471.
[122] A. Polaczek, M. Pekala, Z. Obuszko, J. Phys: Condens. Matter 6 (1994) 7909.
[123] W. Zhou, J. Solid State Chem. 108 (1994) 381.
[124] F. Krumeich, Acta Crystallogr. B 54 (1998) 240.
[125] T. Miyano, J. Solid State Chem. 126 (1996) 208.
[126] T. Miyano, K. Kosuge, European J. Solid State Inorg. Chem. 31 (1994) 867.
[127] M. Sundberg, N.D. Zakharov, I.P. Zibrov, Yu.A. Barabanenkov, V.P. Filonenko, P. Werner, Acta Cryst. B 49 (1993) 951.
[128] L.A. Aleshina, S.V. Glazkova, L.A. Lugovskaya, V.P. Malinenko, A.D. Fofanov, Elektrokhim. 34 (1998) 988 [Russian J. Electrochem. 34 (1998) 887].
[129] L.A. Aleshina, L.A. Lugovskaya, Kristallografia 42 (1997) 343 [Crystalolog. Rep. 42 (1997) 303].
[130] J. Pfeifer, C. Guifang, P. Tekula-Buxbaum, B.A. Kiss, M. Farkas-Jahnke, K. Vadasdi, J. Solid State Chem. 119 (1995) 90.
[131] F. Krumeich, Z. Kristallogr. 212 (1997) 708.
[132] A.H. Yahaya, Z.A. Ibrahim, A.K. Arof, J. Alloys Compounds 241 (1996) 148.
[133] S.T. Triantafyllou, P.C. Christidis, C.B. Lioutas, J. Solid State Chem. 133 (1997) 479.
[134] E. Canadell, M.-H. Whangbo, Inorg. Chem. 33 (1994) 1864.
[135] K. Tatsumi, M. Hibino, T. Kudo, Solid State Ionics 96 (1997) 35.
[136] A. Martínez-de la Cruz, L.M. Torres-Martínez, F. García-Alvarado, E. Morán, M.A. Alario-Franco, J. Mater. Chem. 8 (1998) 1805.

[137] S.T. Triantafyllou, P.C. Christidis, C.B. Lioutas, J. Solid State Chem. 134 (1997) 344.
[138] X.-L. Xu, J.R. Günter, Solid State Ionics 74 (1994) 1.
[139] S.M. Montemayor, A.A. Mendez, A. Martinez de la Cruz, A.F. Fuentes, L.M. Torres Martinez, J. Mater. Chem. 8 (1998) 2777.
[140] F. Krumeich, T. Geipel, J. Solid State Chem. 124 (1996) 58.
[141] L. Dupont, D. Larcher, F. Potemer, M. Figlarz, J. Solid State Chem. 121 (1996) 339.
[142] J. Gopalakrishan, N.S.P. Bhuvanesh, A.R. Raju, Chem. Mater. 6 (1994) 373.
[142a] A. Yu, N. Kumagai, Z. Liu, Y. Lee, J. Solid State Electrochem. 2 (1998) 394.
[143] C.D.E. Lakeman, Y. Xia, J.-H. Kim, X. Wu, H.G. Eckert, F.F. Lange, J. Mater. Res. 3 (1998) 1596.
[144] B.V.R. Chowdari, P.P. Kumari, J. Mater. Sci. 33 (1998) 3591.
[145] G.G. Janauer, A. Dobley, J. Guo, P. Zavalij, M.S. Whittingham, Chem. Mater. 8 (1996) 2096.
[146] A. Sclafani, L. Palmisano, G. Marci, A.M. Venezia, Solar Energy Mater. Solar Cells 51 (1998) 203.
[147] M. Greenblatt, Int. J. Mod. Phys. B 7 (1993) 3937.
[148] R.A. Dixon, J.J. Williams, D. Morris, J. Rebane, F.H. Jones, R.G. Egdell, S.W. Downes, Surface Sci. 399 (1998) 199.
[149] R.G. Egdell, F.H. Jones, J. Mater. Chem. 8 (1998) 469.
[150] F.H. Jones, K. Rawlings, J.S. Foord, P.A. Cox, R.G. Egdell, J.B. Pethica, B.M.R. Wanklyn, Phys. Rev. B 52 (1995) R14392.
[151] F.H. Jones, K. Rawlings, J.S. Foord, R.G. Egdell, J.B. Pethica, B.M.R. Wanklyn, S.C. Parker, P.M. Oliver, Surface Sci. 359 (1996) 107.
[152] P.M. Oliver, S.C. Parker, R.G. Egdell, F.H. Jones, J. Chem. Soc. Faraday Trans. 92 (1996) 2049.
[153] F.H. Jones, K. Rawlings, S. Parker, J.S. Foord, P.A. Cox, R.G. Egdell, J.B. Pethica, Surface Sci. 336 (1995) 181.
[154] F.H. Potter, R.G. Egdell, J. Mater. Chem. 4 (1994) 1647.
[155] P.L. Wincott, A.F. Prime, P.J. Hardman, C.A. Muryn, G. Thornton, P. Bailey, Surface Sci. 402–404 (1998) 705.
[156] J. Kleperis, J. Zubkans, A. Lusis, Proc. Soc. Photo-Opt. Instrum. Engr. 2968 (1997) 186.
[157] M. Hybertsen, S.G. Louie, Comments Condens. Mater. Phys. 13 (1987) 5.
[158] M.J. Sienko, T.B.N. Truong, J. Am. Chem. Soc. 83 (1961) 3939.
[159] A. Azens, B. Stjerna, C.G. Granqvist, J. Gabrusenoks, A. Lusis, Appl. Phys. Lett. 65 (1994) 1988.
[160] A. Azens, A. Gutarra, B. Stjerna, C.G. Granqvist, J. Gabrusenoks, A. Lusis, Proc. Soc. Photo-Opt. Instr. Eng. 2255 (1994) 435.
[161] A. Azens, C.G. Granqvist, E. Pentjuss, J. Gabrusenoks, J. Barczynska, J. Appl. Phys. 78 (1995) 1968.
[162] A. Azens, B. Stjerna, C.G. Granqvist, Thin Solid Films 254 (1995) 1.
[163] A. Azens, C.G. Granqvist, Solar Energy Mater. Solar Cells. 44 (1996) 333.
[164] D. Le Bellac, A. Azens, C.G. Granqvist, Appl. Phys. Lett. 66 (1995) 1715.
[165] A. Azens, M. Kitenbergs, U. Kanders, Vacuum 46 (1995) 745.
[166] J.-G. Zhang, C.E. Tracy, D.K. Benson, S.K. Deb, J. Mater. Res. 8 (1993) 2649.
[167] S. Badilescu, P.V. Ashrit, N. Minh-Ha, G. Bader, F.E. Girouard, V.-V. Truong, Thin Solid Films 250 (1994) 47.
[168] I. Shiyanovskaya, M. Hepel, in: K.-C. Ho, C.B. Greenberg, D.M. MacArthur (Eds.), Proceedings of the Third Symposium on Electrochromic Materials, Vol. 96-24. The Electrochemical Society Pennington, 1997, pp. 119–130.
[169] I. Shiyanovskaya, M. Hepel, J. Electrochem. Soc. 145 (1998) 1023.
[170] S.A. Agnihotry, Rashmi, R. Ramchandran, S. Chandra, Solar Energy Mater. Solar Cells 36 (1995) 289.
[171] O. Bohnke, G. Frand, M. Fromm, J. Weber, O. Greim, Appl. Surf. Sci. 93 (1996) 45.
[172] J.D. Klein, A. Yen, Mater. Res. Soc. Symp. Proc. 293 (1993) 389.
[173] C. Cantalini, H.T. Sun, M. Faccio, M. Pelino, S. Santucci, L. Lozzi, M. Passacantando, Sensors and Actuators B 31 (1996) 81.
[174] L.J. LeGore, O.D. Greenwood, J.W. Paulus, D.J. Frankel, R.J. Lad, J. Vac. Sci. Technol. A 15 (1997) 1223.
[175] W. Wagner, F. Rauch, R. Feile, C. Ottermann, K. Bange, Thin Solid Films 235 (1993) 228.

[176] P.V. Ashrit, K. Benaissa, G. Bader, F.E. Girouard, V.-V. Truong, Solid State Ionics 59 (1993) 47.
[177] P.V. Ashrit, F.E. Girouard, V.-V. Truong, Solid State Ionics 89 (1996) 65.
[178] G. Bader, P.V. Ashrit, V.-V. Truong, Proc. Soc. Photo-Opt. Instrum. Engr. 2531 (1995) 70.
[179] C. Bechinger, B.A. Gregg, Solar Energy Mater. Solar Cells 54 (1998) 405.
[180] C. Bechinger, G. Oefinger, S. Herminghaus, P. Leiderer, J. Appl. Phys. 74 (1993) 4527.
[181] C. Bechinger, S. Herminghaus, P. Leiderer, Thin Solid Films 239 (1994) 156.
[182] C. Bechinger, E. Wirth, P. Leiderer, Appl. Phys. Lett. 68 (1996) 2834.
[183] C. Bechinger, J.N. Bullock, J.-G. Zhang, C.E. Tracy, D.K. Benson, S.K. Deb, H.M. Branz, J. Appl. Phys. 80 (1996) 1226.
[184] C. Bohnke, O. Bohnke, B. Vuillemin, Electrochim. Acta 38 (1993) 1935.
[185] O. Bohnke, A. Gire, J.G. Theobald, Thin Solid Films 247 (1994) 51.
[186] O. Bohnke, B. Vuillemin, C. Gabrielli, M. Keddam, H. Perrot, H. Takenouti, R. Torresi, Electrochim. Acta 40 (1995) 2755.
[187] E. Burattini, J. Purans, A. Kuzmin, Jpn. J. Appl. Phys. (Suppl. 32-1) (1993) 655.
[188] F. Carcenac, C. Vieu, A.M. Haghiri-Gosnet, G. Simon, M. Meijias, H. Launois, J. Vac. Sci. Technol. B 14 (1996) 4283.
[189] J. Chen, Z. Zhu, Y. Zhou, R. Wang, Y. Yan, Proc. Soc. Photo-Opt. Instr. Eng. 2531 (1995) 161.
[190] S.F. Cogan, R.D. Rauh, J.D. Klein, T.D. Plante, in: K.-C. Ho, D.A. MacArthur (Eds.), Proceedings of the Symposium on Electrochromic Materials II, The Electrochemical Society, Pennington, 1994, Vol. 94-2, pp. 269–277.
[191] S.F. Cogan, R.D. Rauh, J.D. Klein, N.M. Nguyen, R.B. Jones, T.D. Plante, in: J.B. Bates (Ed.), Proceedings of the Symposium on Thin Film Solid State Ionic Devices and Materials, Vol. 95-22, The Electrochemical Society, Pennington, 1995, pp. 113–124.
[192] S.F. Cogan, R.D. Rauh, J.D. Klein, N.M. Nguyen, R.B. Jones, T.D. Plante, J. Electrochem. Soc. 144 (1997) 956.
[193] D. Dini, F. Decker, in: K.-C. Ho, C.B. Greenberg, D.M. MacArthur (Eds.), Proceedings of the Third Symposium on Electrochromic Materials, Vol. 96-24, The Electrochemical Society, Pennington, 1997, pp. 275–282.
[194] D. Dini, F. Decker, E. Masetti, J. Appl. Electrochem. 26 (1996) 647.
[195] Y. Djaoued, V.H. Phong, S. Badilescu, P.V. Ashrit, F.E. Girouard, V.-V. Truong, Thin Solid Films 293 (1997) 108.
[196] A.I. Gavrilyuk, Pis'ma Zh. Tekh. Fiz. 19 (1993) 49 [Tech. Phys. Lett. 19 (1993) 720].
[197] A. Gavrilyuk, Proc. Soc. Photo-Opt. Instr. Eng. 2968 (1996) 213.
[198] A. Georg, D. Schweiger, D. Weisbrod, W. Graf, V. Wittwer, in: K.-C. Ho, C.B. Greenberg, D.M. MacArthur (Eds.), Proceeding of the Third Symposium on Electrochromic Materials, Vol. 96-24, The Electrochemical Society, Pennington, 1997, pp. 283–302.
[199] M. Green, Z. Hussain, J. Appl. Phys. 74 (1993) 3451.
[200] M. Green, K. Pita, Solar Energy Mater. Solar Cells 43 (1996) 393.
[201] E. Haro-Poniatowski, M. Jouanne, J.F. Morhange, C. Julien, R. Diamant, M. Fernández-Guasti, G.A. Fuentes, J.C. Alonso, Appl. Surf. Sci. 127–129 (1998) 674.
[202] M. Hashimoto, S. Watanuki, N. Koshida, M. Komuro, N. Atoda, Jpn. J. Appl. Phys. 35 (1996) 3665.
[203] M. Hashimoto, S. Watanuki, N. Koshida, M. Komuro, N. Atoda, Proceedings of the Nineth International Micro Process Conference Japan, 8–11 July, 1996.
[204] K.-C. Ho, T.G. Rukavina, C.B. Greenberg, J. Electrochem. Soc. 141 (1994) 2061.
[205] H. Inaba, M. Iwaku, T. Tatsuma, N. Oyama, Denki Kagaku 61 (1993) 783.
[206] H. Inaba, M. Iwaku, K. Nakase, H. Yasukawa, I. Seo, N. Oyama, Electrochim. Acta 40 (1995) 227.
[207] H. Inaba, M. Iwaku, T. Tatsuma, N. Oyama, J. Electroanal. Chem. 387 (1995) 71.
[208] M.D. Ingram, J.A. Duffy, P.M.S. Monk, J. Electroanal. Chem. 380 (1995) 77.
[209] J.I. Jeong, J.H. Hong, J.H. Moon, J.-S. Kang, Y. Fukuda, J. Appl. Phys. 79 (1996) 9343.
[210] E.E. Khawaja, S.M.A. Durrani, M.A. Daous, J. Phys. Cond. Matter 9 (1997) 9381.
[211] E. Kikuchi, K. Iida, A. Fujishima, K. Itoh, J. Electroanal. Chem. 351 (1993) 105.
[212] E. Kikuchi, N. Hirota, A. Fujishima, K. Itoh, M. Murabayashi, J. Electroanal. Chem. 381 (1995) 15.
[213] J.J. Kim, D.A. Tryk, T. Amemiya, K. Hashimoto, A. Fujishima, J. Electroanal. Chem. 435 (1997) 31.

[214] K. Kuwabara, Y. Noda, Solid State Ionics 61 (1993) 303.
[215] K. Kuwabara, M. Yamada, Solid State Ionics 59 (1993) 25.
[216] A. Kuzmin, J. Purans, J. Phys.: Cond. Matter 5 (1993) 2333.
[217] R. Lechner, L.K. Thomas, Solar Energy Mater. Solar Cells 54 (1998) 139.
[218] B.H. Loo, J.N. Yao, H.D. Coble, K. Hashimoto, A. Fujishima, Appl. Surface Sci. 81 (1994) 175.
[219] A. Lusis, E. Pentjuss, G. Bajars, J. Benders, V. Eglitis, Proc. Soc. Photo-Opt. Instrum. Engr. 2968 (1996) 234.
[220] G. Macrelli, E. Poli, H. Demiyront, R. Götzelmann, J. Non-Cryst. Solids 218 (1997) 296.
[221] J. Marti, S. Gimeno, A. Lousa, E. Bertran, Mater. Res. Soc. Symp. Proc. 403 (1996) 527.
[222] E. Masetti, D. Dini, F. Decker, Solar Energy Mater. Solar Cells 39 (1995) 301.
[223] P.M.S. Monk, J.A. Duffy, M.D. Ingram, Electrochim. Acta 38 (1993) 2759.
[224] P.M.S. Monk, J.A. Duffy, M.D. Ingram, Electrochim. Acta 43 (1998) 2349.
[225] H. Ohno, H. Yamazaki, Solid State Ionics 59 (1993) 217.
[226] E. Pascual, J. Marti, E. Garcia, A. Canillas, E. Bertran, Thin Solid Films 313–314 (1998) 682.
[227] E. Pentjuss, A. Rodinov, R. Kalendarev, G. Bajars, A. Lusis, Proc. Soc. Photo-Opt. Instr. Eng. 2968 (1996) 230.
[228] J. Purans, A. Kuzmin, E. Burattini, Jpn. J. Appl. Phys. (Suppl. 32-2) (1993) S64.
[229] H. Rafla-Yuan, J.G.H. Mathew, B.P. Hichwa, J. Electrochem. Soc. 143 (1996) 2341.
[230] D. Rauh, Solar Energy Mater. Solar Cells 39 (1995) 145.
[231] D. Schweiger, A. Georg, W. Graf, V. Wittwer, Solar Energy Mater. Solar Cells 54 (1998) 99.
[232] I.V. Shiyanovskaya, J. Non-Cryst. Solids 187 (1995) 420.
[233] I.V. Shiyanovskaya, T.A. Gavrilko, E.V. Gabrusenoks, J. Mol. Struct. 293 (1993) 295.
[234] I. Shiyanovskaya, H. Ratajczak, J. Baran, M. Marchewka, J. Mol. Struct. 348 (1995) 99.
[235] S.K. Srivastava, J. Mater. Sci. Lett. 13 (1994) 832.
[236] E.L. Tassi, M.-A. De Paoli, Electrochim. Acta 39 (1994) 2481.
[237] E.A. Tutov, V.I. Kukuev, A.A. Baev, E.N. Bormontov, E.P. Domashevskaya, Zh. Tekh. Fiz. 65 (1995) 117 [Tech. Phys. 40 (1995) 697].
[238] G. Vaivars, J. Kleperis, A. Lusis, Solid State Ionics 61 (1993) 317.
[239] K. von Rottkay, M. Rubin, S.-J. Wen, Thin Solid Films 306 (1997) 10.
[240] B. Vuillemin, O. Bohnke, Solid State Ionics 68 (1994) 257.
[241] L.S. Wang, B.P. Hichwa, S.P. Sapers, J.G.H. Mathew, N.A. O'Brien, in: J.B. Bates (Ed.), Proceedings of the Symposium on Thin Film Solid State Ionic Devices and Materials, Vol. 95-22, The Electrochemical Society, Pennington, 1995, pp. 63–75.
[242] B. Yagoubi, C.A. Hogarth, J. Mater. Sci. 28 (1993) 239.
[243] M. Yamamoto, Jpn. J. Appl. Phys. 33 (1994) 1518.
[244] J.N. Yao, P. Chen, A. Fujishima, J. Electroanal. Chem. 406 (1996) 223.
[245] Y. Yonghong, Z. Jiayu, G. Peifu, T. Jinfa, Solar Energy Mater. Solar Cells 46 (1997) 349.
[246] K.H. Yoon, J.W. Lee, Y.S. Cho, D.H. Kang, Appl. Phys. Lett. 68 (1996) 572.
[247] K.H. Yoon, J.W. Lee, Y.S. Cho, D.H. Kang, J. Appl. Phys. 80 (1996) 6813.
[248] K.H. Yoon, C.W. Chin, D.H. Kang, J. Appl. Phys. 81 (1997) 7024.
[249] K.H. Yoon, D.K. Seo, Y.S. Cho, D.H. Kang, J. Appl. Phys. 84 (1998) 3954.
[250] J.-G. Zhang, D.K. Benson, C.E. Tracy, S.K. Deb, J. Mater. Res. 8 (1993) 2657.
[251] J.-G. Zhang, D.K. Benson, C.E. Tracy, J. Webb, S.K. Deb, Proc. Soc. Photo-Opt. Instrum. Engr. 2017 (1993) 104.
[252] J.-G. Zhang, D.K. Benson, C.E. Tracy, S.K. Deb, A.W. Czanderna, R.S. Crandall, J. Electrochem. Soc. 141 (1994) 2795.
[253] J.-G. Zhang, D.K. Benson, C.E. Tracy, S.K. Deb, C. Bechinger, in: J.B. Bates (Ed.), Proceedings of the Symposium on Thin Film Solid State Ionic Devices and Materials, Vol. 95-22, The Electrochemical Society, Pennington, 1995, pp. 125–136.
[254] Y. Zhou, P. Gu, J. Tang, Proc. Soc. Photo-Opt. Instr. Eng. 2017 (1993) 155.
[255] S.-H. Lee, K.-H. Hwang, S.-K. Joo, in: K.-C. Ho, D.A. MacArthur (Eds.), Proceedings of the Symposium on Electrochromic Materials II, Vol. 94-2, The Electrochemical Society, Pennington, 1994, pp. 290–302.

[256] P.V. Ashrit, G. Bader, V.-V. Truong, Thin Solid Films 320 (1998) 324.
[257] H.-M. Lin, C.-Y. Tung, C.-M. Hsu, P.-Y. Lee, J. Mater. Res. 10 (1995) 1115.
[258] P. Lippens, P. Verheyen, in: Proceedings of the 37th Vacuum Coaters Technical Conference, Boston, May 1994.
[259] M. Burdis, J. Siddle, R. Batchelor, J. Gallego, Proc. Soc. Photo-Opt. Instr. Eng. 2531 (1995) 11.
[260] J. Göttsche, A. Hinsch, V. Wittwer, Solar Energy Mater. Solar Cells 31 (1993) 415.
[261] H.S. Witham, P. Chindaudom, I. An, R.W. Collins, R. Messier, K. Vedam, J. Vac. Sci. Technol. A 11 (1993) 1881.
[262] T. Kubo, Y. Nishikitani, J. Electrochem. Soc. 145 (1998) 1729.
[263] A. Georg, W. Graf, V. Wittwer, Solar Energy Mater. Solar Cells 51 (1998) 353.
[264] J.S. Hale, M. DeVries, B. Dworak, J.A. Woollam, Thin Solid Films 313–314 (1998) 205.
[265] J. Wang, J.M. Bell, Solar Energy Mater. Solar Cells 43 (1996) 377.
[266] J.D. Klein, S.L. Clauson, Mater. Res. Soc. Symp. Proc. 403 (1996) 521.
[267] T.A. Taylor, H.H. Patterson, Appl. Spectrosc. 48 (1994) 674.
[268] R.A. Batchelor, M.S. Burdis, J.R. Siddle, J. Electrochem. Soc. 143 (1996) 1050.
[269] I. An, R.W. Collins, H.V. Nguyen, K. Vedam, H.S. Witham, R. Messier, Thin Solid Films 233 (1993) 276.
[270] M. Antinucci, A. Ferriolo, Proc. Soc. Photo-Opt. Instrum. Engr. 2255 (1994) 395.
[271] M. Antinucci, B. Chevalier, A. Ferriolo, Solar Energy Mater. Solar Cells 39 (1995) 271.
[272] M.D. Antonik, J.E. Schneider, E.L. Wittman, K. Snow, J.F. Vetelino, R.J. Lad, Thin Solid Films 256 (1995) 247.
[273] C. Bechinger, M.S. Burdis, J.-G. Zhang, Solid State Commun. 101 (1997) 753.
[274] M.S. Burdis, J.R. Siddle, Thin Solid Films 237 (1994) 320.
[275] M.S. Burdis, I.R. Siddle, S. Taylor, Proc. Soc. Photo-Opt. Instr. Eng. 2255 (1994) 371.
[276] M.S. Burdis, J.R. Siddle, A.P. Mackenzie, S. Badilescu, P.C. Richard, P.V. Ashrit, G. Bader, F.E. Girouard, V.-V. Truong, Proc. Soc. Photo-Opt. Instr. Eng. 2531 (1995) 105.
[277] M.P. Cantão, A. Lourenco, A. Gorenstein, S.I. Córdoba de Torresi, R.M. Torresi, Mater. Sci. Eng. B 26 (1994) 157.
[278] S. Chao, Jpn. J. Appl. Phys. 37 (1998) L245.
[279] M.-A. De Paoli, A. Zanelli, M. Mastragostino, A.M. Rocco, J. Electroanal. Chem. 435 (1997) 217.
[280] L.E. Depero, S. Groppelli, I. Natali-Sora, L. Sangaletti, G. Sberveglieri, E. Tondello, J. Solid State Chem. 121 (1996) 379.
[281] L.E. Depero, I. Natali-Sora, C. Perego, L. Sangaletti, G. Sberveglieri, Sensors Actuators B 31 (1996) 19.
[282] M. Di Giulio, D. Manno, G. Micocci, A. Serra, A. Tepore, J. Phys. 30 (1997) 3211.
[283] D. Dini, S. Passerini, B. Scrosati, F. Decker, Proc. Soc. Photo-Opt. Instr. Eng. 2968 (1996) 201.
[284] M. Ferroni, V. Guidi, G. Martinelli, P. Nelli, G. Sberveglieri, Sensors Actuators B 44 (1997) 499.
[285] M. Ferroni, V. Guidi, G. Martinelli, G. Sberveglieri, J. Mater. Res. 12 (1997) 793.
[286] B. Frühberger, M. Grunze, D.J. Dwyer, Sensors Actuators B 31 (1996) 167.
[287] C. Gabrielli, M. Keddam, H. Perrot, R. Torresi, J. Electroanal. Chem. 378 (1994) 85.
[288] A. Georg, V. Wittwer, Proc. Soc. Photo. Opt. Instr. Eng. 2255 (1994) 314.
[289] R.B. Goldner, T.E. Haas, F.O. Arntz, S. Slaven, K.K. Wong, B. Wilkens, C. Shepard, W. Lanford, Appl. Phys. Lett. 62 (1993) 1699.
[290] H. Hosono, M. Miyakawa, H. Kawazoe, K.-I. Shimizu, J. Non-Cryst. Solids 241 (1998) 190.
[291] D.-J. Kim, S.-I. Pyun, Solid State Ionics 99 (1997) 185.
[292] D.-J. Kim, S.-I. Pyun, Y.-M. Choi, Solid State Ionics 109 (1998) 81.
[293] N. Leventis, Y.C. Chung, J. Mater. Chem. 3 (1993) 833.
[294] E. Masetti, S.E. Segre, S. Bosch, Thin Solid Films 313–314 (1998) 62.
[295] J.G.H. Mathew, S.P. Sapers, M.J. Cumbo, N.A. O'Brien, R.B. Sargent, V.P. Raksha, R.B. Lahaderne, B.P. Hichwa, in: K.-C. Ho, C.B. Greenberg, D.M. MacArthur (Eds.), Proceedings of the Third Symposium on Electrochromic Materials, Vol. 96-24. The Electrochemical Society, Pennington, 1997, pp. 311–324.
[296] F.M. Michalak, J.R. Owen, Solid State Ionics 86 (1996) 965.

[297] F.M. Michalak, J.R. Owen, in: K.-C. Ho, C.B. Greenberg, D.M. MacArthur (Eds.), Proceedings of the Third Symposium on Electrochromic Materials, Vol. 96-24, The Electrochemical Society, Pennington, 1997, pp. 385–397.
[298] M. Miyakawa, K.-I. Kawamura, H. Hosono, H. Kawazoe, J. Appl. Phys. 84 (1998) 5610.
[299] P. Nelli, L.E. Depero, M. Ferroni, S. Groppelli, V. Guidi, F. Ronconi, L. Sangaletti, G. Sberveglieri, Sensors Actuators B 31 (1996) 89.
[300] L.Q. Nguyen, P.V. Ashrit, G. Bader, F.E. Girouard, V.-V. Truong, Proc. Soc. Photo-Opt. Instr. Eng. 2017 (1993) 161.
[301] T. Nishide, F. Mizukami, Opt. Eng. 34 (1995) 3329.
[302] S. Panero, B. Scrosati, M. Baret, B. Cecchini, E. Masetti, Solar Energy Mater. Solar Cells 39 (1995) 239.
[303] J.-L. Paul, J.-C. Lassègues, J. Solid State Chem. 106 (1993) 357.
[304] M. Penza, L. Vasanelli, Sensors Actuators B 41 (1997) 31.
[305] M. Penza, C. Martucci, G. Cassano, Sensors Actuators B 50 (1998) 52.
[306] M. Penza, M.A. Tagliente, L. Mirenghi, C. Gerardi, C. Martucci, G. Cassana, Sensors Actuators B 50 (1998) 9.
[307] M.A. Petit, V. Plichon, J. Electrochem. Soc. 143 (1996) 2789.
[308] S.-I. Pyun, J.-S. Bae, J. Alloys Compounds 245 (1996) L1.
[309] S.-I. Pyun, D.-J. Kim, J.-S. Bae, J. Alloys Compounds 244 (1996) 16.
[310] A.M. Rocco, M.-A. De Paoli, A. Zanelli, M. Mastragostino, Electrochim. Acta 41 (1996) 2805.
[311] I. Ruokamo, T. Kärkkäinen, J. Huusko, T. Ruokanen, M. Blomberg, H. Torvela, V. Lantto, Sensors Actuators B 18–19 (1994) 486.
[312] G. Sberveglieri, L. Depero, S. Groppelli, P. Nelli, Sensors Actuators B 26–27 (1995) 89.
[313] P. Schlotter, G. Baur, R. Schmidt, U. Weinberg, Proc. Soc. Photo-Opt. Instr. Eng. 2255 (1994) 351.
[314] D.J. Smith, J.F. Vetelino, R.S. Falconer, E.L. Wittman, Sensors Actuators B 13–14 (1993) 264.
[315] P.A. van Nijnatten, C.I.M.A. Spee, J. Non-Cryst. Solids 218 (1997) 302.
[316] J.-I. Yamaki, H. Ohtsuka, T. Shodai, Solid State Ionics 86–88 (1996) 1279.
[317] K. Friestad, G. Hagen, S. Panero, B. Scrosati, in: K.-C. Ho, C.B. Greenberg, D. MacArthur (Eds.), Proceedings of the Third Symposium on Electrochromic Materials, Vol. 96-24, The Electrochemical Society, Pennington, 1997, pp. 353–368.
[318] K.H. Heckner, A. Rothe, Proc. Soc. Photo-Opt. Instr. Eng. 2255 (1994) 305.
[319] B.P. Jelle, G. Hagen, in: K.-C. Ho, D.A. MacArthur (Eds.), Proceedings of the Symposium on Electrochromic Materials II, Vol. 94-2, The Electrochemical Society, Pennington, 1994, pp. 324–338.
[320] B.P. Jelle, G. Hagen, S. Sunde, R. Ødegård, Synth. Met. 54 (1993) 315.
[321] B.P. Jelle, G. Hagen, S. Nødland, Electrochim. Acta 38 (1993) 1497.
[322] B.P. Jelle, G. Hagen, Ø. Birketveit, J. Appl. Electrochem. 28 (1998) 483.
[323] C.M. Lampert, S.J. Visco, M.M. Doeff, Y.P. Ma, Y. He, J.-C. Giron, Proc. Soc. Photo-Opt. Instr. Eng. 2017 (1993) 143.
[324] C.M. Lampert, S.J. Visco, M.M. Doeff, Y.P. Ma, Y. He, J.-C. Giron, Solar Energy Mater. Solar Cells 33 (1994) 91.
[325] P.M.S. Monk, R.D. Partridge, R. Janes, M.J. Parker, J. Mater. Chem. 4 (1994) 1071.
[326] M. Morita, Macromol. Chem. Phys. 195 (1994) 609.
[327] A. Pennisi, F. Simone, Appl. Phys. A 57 (1993) 13.
[328] A. Pennisi, F. Simone, Proc. Soc. Photo-Opt. Instr. Eng. 2255 (1994) 406.
[329] A. Pennisi, F. Simone, Solar Energy Mater. Solar Cells 39 (1995) 333.
[330] S.J. Visco, M. Liu, M.M. Doeff, Y.P. Ma, C. Lampert, L.C. De Jonghe, Solid State Ionics 60 (1993) 175.
[331] E.A. Meulenkamp, J. Electrochem. Soc. 144 (1997) 1664.
[332] E.A. Meulenkamp, R.J.J. de Groot, J.M.L. de Vries, Mater. Res. Soc. Symp. Proc. 451 (1997) 321.
[333] B.H. Pan, J.Y. Lee, J. Electrochem. Soc. 143 (1996) 2784.
[334] P.K. Shen, A.C.C. Tseung, J. Mater. Chem. 4 (1994) 1289.
[335] P.K. Shen, K.Y. Chen, A.C.C. Tseung, in: K.-C. Ho, D.A. MacArthur (Eds.), Proceedings of the Symposium on Electrochromic Materials II, Vol. 94-2, The Electrochemical Society, Pennington, 1994, pp. 14–19.

[336] P.K. Shen, K.Y. Chen, A.C.C. Tseung, J. Electrochem. Soc. 141 (1994) 1758.
[337] P.M.S. Monk, S.L. Chester, Electrochim. Acta 38 (1993) 1521.
[338] K. Ogura, M. Nakayama, N. Endo, J. Electroanal. Chem. 451 (1998) 219.
[339] S.R. Biaggio, R.C. Rocha-Filho, J.R. Vilche, F.E. Varela, L.M. Gassa, Electrochim. Acta 42 (1997) 1751.
[340] A. Goossens, D.D. Macdonald, J. Electroanal. Chem. 352 (1993) 65.
[341] D.-J. Kim, S.-I. Pyun, R.A. Oriani, Electrochim. Acta 40 (1995) 1171.
[342] D.-J. Kim, S.-I. Pyun, R.A. Oriani, Electrochim. Acta 41 (1996) 57.
[343] A.D. Modestov, T.M. Cheshko, A.D. Davydov, Elektrokhim. 34 (1998) 1468 [Russian J. Electrochem. 34 (1998) 1329].
[344] D. Davazoglou, A. Donnadieu, J. Non-Cryst. Solids 169 (1994) 64.
[345] D. Davazoglou, A. Moutsakis, V. Valamontes, V. Psykaris, D. Tsamakis, J. Electrochem. Soc. 144 (1997) 595.
[346] D. Davazoglou, K. Georgouleas, J. Electrochem. Soc. 145 (1998) 1346.
[347] K.A. Gesheva, D.S. Gogova, J. Phys. IV (Colloq. 3) 3 (1993) 475.
[348] D.S. Gogova, K.A. Gesheva, G.I. Stoyanov, Proc. Soc. Photo-Opt. Instr. Eng. 2255 (1994) 332.
[349] T. Maruyama, S. Arai, J. Electrochem. Soc. 141 (1994) 1021.
[350] U. Riaz, Thin Solid Films 235 (1993) 15.
[351] J.G. Eden, Photochemical Vapor Deposition, Wiley, New York, 1992.
[352] T. Maruyama, T. Kanagawa, J. Electrochem. Soc. 141 (1994) 2435.
[353] W.B. Henley, G.J. Sachs, J. Electrochem. Soc. 144 (1997) 1045.
[354] J. Arakaki, R. Reyes, M. Horn, W. Estrada, Solar Energy Mater. Solar Cells 37 (1995) 33.
[355] P.S. Patil, P.R. Patil, Solar Energy Mater. Solar Cells 33 (1994) 293.
[356] S. Badilescu, N. Minh-Ha, G. Bader, P.V. Ashrit, F.E. Girouard, V.-V. Truong, J. Mol. Struct. 297 (1993) 393.
[357] K. Nonaka, A. Takase, K. Miyakawa, J. Mater. Sci. Lett. 12 (1993) 274.
[358] O. Pyper, R. Schöllhorn, J.J.T.M. Donkers, L.H.M. Krings, Mater. Res. Bull. 33 (1998) 1095.
[359] L. Armelao, R. Bertoncello, G. Granozzi, G. Depaoli, E. Tondello, G. Battaglin, J. Mater. Chem. 4 (1994) 407.
[360] J.P. Cronin, D.J. Tarico, J.C.L. Tonazzi, A. Agrawal, S.R. Kennedy, Solar Energy Mater. Solar Cells 29 (1993) 371.
[361] L.H.M. Krings, W. Talen, Solar Energy Mater. Solar Cells 54 (1998) 27.
[362] H. Wang, M. Zhang, S. Yang, L. Zhao, L. Ding, Solar Energy Mater. Solar Cells 43 (1996) 345.
[363] T. Nishide, F. Mizukami, J. Mater. Sci. Lett. 15 (1996) 1149.
[364] J. Livage, G. Guzman, Solid State Ionics 84 (1996) 205.
[365] B. Yebka, B. Pecquenard, C. Julien, J. Livage, Solid State Ionics 104 (1997) 169.
[366] K. von Rottkay, N. Ozer, M. Rubin, T. Richardson, Thin Solid Films 308–309 (1997) 50.
[367] J. Stoch, M. Klisch, I. Babytch, Bull. Polish Acad. Sci. Chem. 43 (1995) 173.
[368] A.T. Baker, S.G. Bosi, J.M. Bell, D.R. MacFarlane, B.G. Monsma, I. Skryabin, J. Wang, Solar Energy Mater. Solar Cells 39 (1995) 133.
[369] J.M. Bell, G.B. Smith, D.C. Green, J. Barczynska, L. Evans, K.A. MacDonald, G. Voelkel, B.O. West, L. Spiccia, Proc. Soc. Photo-Opt. Instr. Eng. 2017 (1993) 132.
[370] J.H. Choy, Y.-I. Kim, S.-H. Choy, N.-G. Park, C. Campet, J. Portier, in: K.-C. Ho, C.B. Greenberg, D.M. MacArthur (Eds.), Proceedings of the Third Symposium on Electrochromic Materials, Vol. 96-24, The Electrochemical Society, Pennington, 1997, pp. 303–308.
[371] M. Denesuk, J.P. Cronin, S.R. Kennedy, K.J. Law, G.F. Nielson, D.R. Uhlmann, Proc. Soc. Photo-Opt. Instr. Eng. 2255 (1994) 52.
[372] M. Denesuk, J.P. Cronin, S.R. Kennedy, D.R. Uhlmann, J. Electrochem. Soc. 144 (1997) 888.
[373] M. Denesuk, J.P. Cronin, S.R. Kennedy, D.R. Uhlmann, J. Electrochem. Soc. 144 (1997) 1971.
[374] M. Denesuk, J.P. Cronin, S.R. Kennedy, D.R. Uhlmann, J. Electrochem. Soc. 144 (1997) 2154.
[375] S.M. Jones, S.E. Friberg, J. Mater. Sci. Lett. 15 (1996) 1172.
[376] P. Judeinstein, J. Livage, J. Chim. Phys. 90 (1993) 1137.
[377] K. Koseki, Y. Demizu, N. Ooto, S. Sakurada, Solid State Ionics 66 (1993) 337.

[378] T. Kudo, Y. Aikawa, Y.M. Li, A. Kishimoto, Solid State Ionics 62 (1993) 99.
[379] Y. Li, Y. Aikawa, A. Kishimoto, T. Kudo, Electrochim. Acta 39 (1994) 807.
[380] K.A. MacDonald, J.M. Bell, J. Barczynska, G. Voelkel, Proc. Soc. Photo-Opt. Instr. Eng. 2017 (1993) 95.
[381] M.A. Macêdo, M.A. Aegerter, J. Sol-Gel Sci. Technol. 2 (1994) 667.
[382] B. Munro, S. Krämer, P. Zapp, H. Krug, H. Schmidt, J. Non-Cryst. Solids 218 (1997) 185.
[383] B. Munro, P. Conrad, S. Krämer, H. Schmidt, P. Zapp, Solar Energy Mater. Solar Cells 54 (1998) 131.
[384] T. Nishide, F. Mizukami, Thin Solid Films 259 (1995) 212.
[385] N. Ozer, Thin Solid Films 304 (1997) 310.
[386] R. Reisfeld, M. Zayat, H. Minti, A. Zastrow, Solar Energy Mater. Solar Cells 54 (1998) 109.
[387] Z.A.E.P. Vroon, C.I.M.A. Spee, J. Non-Cryst. Solids 218 (1997) 189.
[388] C.N. Xu, M. Akiyama, P. Sun, T. Watanabe, Appl. Phys. Lett. 70 (1997) 1639.
[389] L.B. Kriksunov, D.D. Macdonald, P.J. Millett, J. Electrochem. Soc. 141 (1994) 3002.
[390] I. Saeki, N. Okushi, H. Konno, R. Furuichi, J. Electrochem. Soc. 143 (1996) 2226.
[391] C. Louro, A. Cavaleiro, J. Electrochem. Soc. 144 (1997) 259.
[392] J. Guo, Y.J. Li, M.S. Whittingham, J. Power Sources 54 (1995) 461.
[393] I. Bedja, S. Hotchandani, P.V. Kamat, J. Phys. Chem. 97 (1993) 11064.
[394] I. Bedja, S. Hotchandani, R. Carpenter, K. Vinodgopal, P.V. Kamat, Thin Solid Films 247 (1994) 195.
[395] S. Hotchandani, I. Bedja, R.W. Fessenden, P.V. Kamat, Langmuir 10 (1994) 17.
[396] P.V. Kamat, K. Vinodgopal, Langmuir 12 (1996) 5739.
[397] B. Karawowska, P.J. Kulesza, Electroanal. 7 (1995) 1005.
[398] A.A. Tomchenko, V.V. Khatko, E.I. Emelianov, Sensors Actuators B 46 (1998) 8.
[399] S. Chao, Jpn. J. Appl. Phys. 32 (1993) L1346.
[400] F. Beck, M. Dahlhaus, J. Appl. Electrochem. 23 (1993) 781.
[401] M. Dahlhous, F. Beck, J. Appl. Electrochem. 23 (1993) 957.
[402] S. Srinivasan, P. Pramanik, J. Mater. Sci. Lett. 13 (1994) 365.
[403] F. Michalak, P. Aldebert, Solid State Ionics 85 (1996) 265.
[404] K. Itoh, K. Yamagishi, M. Nagasono, M. Murabayashi, Ber. Bunsenges. Phys. Chem. 98 (1994) 1250.
[405] B. Orel, N. Groselj, U. Opara Krasovec, M. Gabrscek, P. Bukovec, R. Reisfeld, Sensors Actuators 50 (1998) 234.
[406] P.J. Kulesza, L.R. Faulkner, in: K.-C. Ho, D.A. MacArthur (Eds.), Proceedings of the Symposium on Electrochromic Materials II, Vol. 94-2, The Electrochemical Society, Pennington, 1994, pp. 20–29.
[407] U. Lavrencic Stangar, B. Orel, M.G. Hutchins, Proc. Soc. Photo-Opt. Instr. Eng. 2255 (1994) 260.
[408] U. Lavrencic Stangar, B. Orel, A. Régis, Ph. Colomban, J. Sol–Gel Sci. Technol. 8 (1997) 965.
[409] B. Orel, U. Lavrencic-Stangar, M.G. Hutchins, K. Kalcher, J. Non-Cryst. Solids 175 (1994) 251.
[410] S.J. Babinec, in: K.-C. Ho, D.A. MacArthur (Eds.), Proceedings of the Symposium on Electrochromic Materials II, Vol. 94-2, The Electrochemical Society, Pennington, 1994, pp. 30–46.
[411] K.V. Yumashev, A.M. Malyarevich, N.N. Posnov, I.A. Denisov, V.P. Mikhailov, M.V. Artemyev, D.V. Sviridov, Chem. Phys. Lett. 288 (1998) 567.
[412] E. Cazzanelli, C. Vinegoni, G. Mariotto, A. Kuzmin, J. Purans, in: K.-C. Ho, C.B. Greenberg, D.M. MacArthur (Eds.), Proceedings of the Third Symposium on Electrochromic Materials, Vol. 96-24. The Electrochemical Society, Pennington, 1997, pp. 260–274.
[413] M. Kharrazi, A. Azens, L. Kullman, C.G. Granqvist, Thin Solid Films 295 (1997) 117.
[414] M. Kharrazi, L. Kullman, C.G. Granqvist, Solar Energy Mater. Solar Cells 53 (1998) 349.
[415] M. Kharrazi Olsson, K. Macák, U. Helmersson, B. Hjörvarsson, J. Vac. Sci. Technol. A 16 (1998) 639.
[416] P.C. Johnson, in: J.L. Vossen, W. Kern (Eds.), Thin Film Processes II, Academic, San Diego, 1991, pp. 209–280.
[417] Y. Shigesato, Y. Hayashi, A. Masui, T. Haranou, Jpn. J. Appl. Phys. 30 (1991) 814.
[418] G.L. Harding, Solar Energy Mater. 12 (1985) 169.
[419] G.L. Harding, I. Hamberg, C.G. Granqvist, Solar Energy Mater. 12 (1985) 187.

[420] G.L. Harding, Thin Solid Films 138 (1986) 279.
[421] M.C. Peignon, C. Cardinaud, G. Turban, J. Appl. Phys. 70 (1991) 3314.
[422] M.C. Peignon, C. Cardinaud, G. Turban, J. Electrochem. Soc. 140 (1993) 505.
[423] R. Petri, D. Henry, N. Sadeghi, J. Appl. Phys. 72 (1992) 2664.
[424] G. Turban, J.F. Coulon, N. Mutsukura, Thin Solid Films 176 (1989) 289.
[425] P. Verdonck, J. Swart, G. Brasseur, P. De Geyter, J. Electrochem. Soc. 142 (1995) 1971.
[426] H.F. Winters, J. Vac. Sci. Technol. A 3 (1985) 700.
[427] H.F. Winters, J. Vac. Sci. Technol. B 3 (1985) 9.
[428] A.G. Dirks, H.J. Leamy, Thin Solid Films 47 (1977) 219.
[429] H.J. Leamy, G.H. Gilmer, A.G. Dirks, in: E. Kaldis (Ed.), Current Topics in Materials Science, Vol. 6, North-Holland, Amsterdam, 1980, pp. 309–340.
[430] S.A. Agnihotry, K.K. Saini, T.K. Saxena, S. Chandra, Thin Solid Films 141 (1986) 183.
[431] T. Miyoshi, K. Iwasa, SID Symp. Dig. 11 (1980) 126.
[432] M. Strømme Mattsson, Phys. Rev. B 58 (1998) 11015.
[433] L.I. Skatkov, Zh. Prikl. Khim. 70 (1997) 685 [Russian J. Appl. Chem. 70 (1997) 653].
[434] T. Kudo, M. Hibino, Solid State Ionics 84 (1996) 65.
[435] J. Vondrák, J. Bludská, Solid State Ionics 68 (1994) 317.
[436] J. Bludská, I. Jakubec, Z. Phys. Chem. 194 (1996) 69.
[437] N. Kumagai, M. Abe, N. Kumagai, K. Tanno, J.P. Pereira-Ramos, Solid State Ionics 70/71 (1994) 451.
[438] A. Vértes, R. Schiller, J. Appl. Phys. 54 (1983) 199.
[439] B.Sh. Galyamov, Yu.E. Roginskaya, Pris'ma Zh. Tekh. Fiz. 14 (1988) 280 [Soviet Tech. Phys. Lett. 14 (1988) 124].
[440] D.A. Hensley, S.H. Garofalini, J. Electrochem. Soc. 145 (1998) 669.
[441] D. Dini, F. Decker, Electrochim. Acta 43 (1998) 2919.
[442] B. Bouchet-Fabre, S. Laurelle, M. Figlarz, Nucl. Instrum. Phys. Res. B 97 (1995) 180.
[443] A. Kuzmin, J. Phys.: Condens. Matter 6 (1994) 5761.
[444] A. Kuzmin, J. Purans, J. Phys.: Condens. Matter 5 (1993) 267.
[445] A. Kuzmin, J. Purans, J. Phys.: Condens. Matter 5 (1993) 9423.
[446] A. Kuzmin, J. Purans, P. Parent, Physica B 208 (1995) 45.
[447] J. Purans, A. Kuzmin, P. Parent, H. Dexpert, Physica B 208–209 (1995) 307.
[448] J. Purans, A. Kuzmin, P. Parent, H. Dexpert, Physica B 208–209 (1995) 373.
[449] J. Purans, A. Kuzmin, P. Parent, H. Dexpert, Physica B 208–209 (1995) 707.
[450] J. Purans, A. Kuzmin, C. Guéry, Proc. Soc. Photo-Opt. Instr. Eng. 2968 (1996) 174.
[451] C. Guéry, C. Choquet, F. Dujeancourt, J.M. Tarascon, J.C. Lassègues, J. Solid State Electrochem. 1 (1997) 199.
[452] J. Gabrusenoks, Proc. Soc. Photo-Opt. Instr. Eng. 2968 (1996) 192.
[453] A. Katrib, F. Hemming, P. Wehrer, L. Hilaire, G. Maire, J. Electron Spectr. Related Phenomena 76 (1995) 195.
[454] Q. Zhong, J.R. Dahn, K. Colbow, Phys. Rev. B 46 (1992) 2554.
[455] A.J. Berlinsky, W.G. Unruh, W.R. McKinnon, R.R. Haering, Solid State Commun. 31 (1979) 135.
[456] W.R. McKinnon, in: P.G. Bruce (Ed.), Solid State Electrochemistry, Cambridge University Press, Cambridge, 1995, pp. 163–198.
[457] L. Kullman, D. Rönnow, C.G. Granqvist, Thin Solid Films 288 (1996) 330.
[458] T. Lindström, L. Kullman, D. Rönnow, C.-G. Ribbing, C.G. Granqvist, J. Appl. Phys. 81 (1997) 1464.
[459] D. Rönnow, L. Kullman, C.G. Granqvist, J. Appl. Phys. 80 (1996) 423.
[460] S.F. Cogan, T.D. Plante, M.A. Parker, R.D. Rauh, Solar Energy Mater. 14 (1986) 185.
[461] S.F. Cogan, T.D. Plante, M.A. Parker, R.D. Rauh, J. Appl. Phys. 60 (1986) 2735.
[462] F.O. Arntz, R.B. Goldner, B. Morel, T.E. Haas, K.K. Wong, J. Appl. Phys. 67 (1990) 3177.
[463] R.B. Goldner, G. Berrera, F.O. Arntz, T.E. Haas, B. Morel, K.K. Wong, in: M.K. Carpenter, D.A. Corrigan (Eds.), Proceedings of the Symposium on Electrochromic Materials, Vol. 90-2, The Electrochemical Society, Pennington, 1990, pp. 14–22.
[464] F. Wooten, Optical Properties of Solids, Academic, New York, 1972.

[465] F. Urbach, Phys. Rev. 92 (1953) 1324.
[466] M.E. Straumanis, S.S. Hsu, J. Am. Chem. Soc. 72 (1950) 4027.
[467] B.W. Brown, E. Banks, Phys. Rev. 84 (1951) 609.
[468] M. Kielwein, K. Saiki, G. Roth, J. Fink, G. Paasch, R.G. Egdell, Phys. Rev. B 51 (1995) 10320.
[469] J.S.E.M. Svensson, C.G. Granqvist, Appl. Phys. Lett. 45 (1984) 828.
[470] M.G. Calkin, P.J. Nicholson, Rev. Mod. Phys. 39 (1967) 361.
[471] E. Gerlach, J. Phys. C 19 (1986) 4585.
[472] A.S. Alexandrov, N. Mott, Polarons and Bipolarons, World Scientific, Singapore, 1995.
[473] H. Böttger, V.V. Bryksin, Hopping Conduction in Solids, VCH, Weinheim, 1985.
[474] N.F. Mott, Metal-Insulator Transitions, 2nd Edition, Taylor and Francis, London, 1990.
[475] E. Iguchi, H. Miyagi, J. Phys. Chem. Solids 54 (1993) 403.
[476] E.K.H. Salje, Eur. J. Solid State Inorg. Chem. 31 (1994) 805.
[477] S.K. Deb, Phys. Rev. B 16 (1977) 1020.
[478] P. Gérard, A. Deneuville, R. Courths, Thin Solid Films 71 (1980) 221.
[479] J.V. Gabrusenoks, P.D. Cikmach, A.R. Lusis, J.J. Kleperis, G.M. Ramans, Solid State Ionics 14 (1984) 25.
[480] J.J. Kleperis, P.D. Cikmach, A.R. Lusis, Phys. Stat. Sol. A 83 (1984) 291.
[481] J.H. Pifer, E.K. Sichel, J. Electronic Mater. 9 (1980) 129.
[482] Y. Shigesato, Jpn. J. Appl. Phys. 30 (1991) 1457.
[483] O. Bohnke, C. Bohnke, G. Robert, B. Carquille, Solid State Ionics 6 (1982) 121.
[484] O. Bohnke, C. Bohnke, G. Robert, B. Carquille, Solid State Ionics 6 (1982) 267.
[485] M. Denesuk, D.R. Uhlmann, J. Electrochem. Soc. 143 (1996) L186.
[486] J.-G. Zhang, D.K. Benson, C.E. Tracy, S.K. Deb, A.W. Czanderna, C. Bechinger, J. Electrochem. Soc. 144 (1997) 2022.
[487] J.-G. Zhang, D.K. Benson, C.E. Tracy, S.K. Deb, A.W. Czanderna, C. Bechinger, in: K.-C. Ho, C.B. Greenberg, D.M. MacArthur (Eds.), Proceedings of the Third Symposium on Electrochromic Materials, Vol. 96-24. The Electrochemical Society, Pennington, 1997b, pp. 251–259.
[488] P.K. Shen, H.T. Huang, A.C.C. Tseung, J. Mater. Chem. 2 (1992) 497.
[489] D. Rönnow, E. Veszelei, Rev. Sci. Instr. 65 (1994) 327.
[490] C.K. Carniglia, Opt. Eng. 18 (1979) 104.
[491] A. Duparré, in: R.E. Hummel, K.H. Gunther (Eds.), Handbook of Optical Properties, Vol. 1, CRC Press, Boca Raton, 1995, pp. 273–303.
[492] C. Amra, J. Opt. Soc. Am. A 10 (1993) 365.
[493] D. Le Bellac, G.A. Niklasson, C.G. Granqvist, J. Phys. D 28 (1995) 600.
[494] D. Le Bellac, G.A. Niklasson, C.G. Granqvist, J. Appl. Phys. 77 (1995) 6145.
[495] D. Le Bellac, G.A. Niklasson, C.G. Granqvist, J. Appl. Phys. 78 (1995) 2894.
[496] D. Le Bellac, G.A. Niklasson, C.G. Granqvist, Thin Solid Films 266 (1995) 94.
[497] G.W. Mbise, D. Le Bellac, G.A. Niklasson, C.G. Granqvist, Proc. Soc. Photo-Opt. Instr. Eng. 2255 (1994) 182.
[498] G.W. Mbise, G.A. Niklasson, C.G. Granqvist, J. Appl. Phys. 77 (1995) 2816.
[499] G.W. Mbise, G.A. Niklasson, C.G. Granqvist, S. Palmer, J. Appl. Phys. 80 (1996) 5361.
[500] G.W. Mbise, D. Le Bellac, G.A. Niklasson, C.G. Granqvist, J. Phys. D 30 (1997) 2103.
[501] S. Palmer, G.W. Mbise, G.A. Niklasson, C.G. Granqvist, Solar Energy Mater. Solar Cells 44 (1996) 397.
[502] J.M. Bell, J.P. Matthews, I.L. Skryabin, J. Wang, B.G. Monsma, Renewable Energy 15 (1998) 312.
[503] R. Sullivan, E.S. Lee, K. Papamichael, M. Rubin, S.E. Selkowitz, Proc. Soc. Photo-Opt. Instr. Eng. 2255 (1994) 443.
[504] D.E. Soule, J.-G. Zhang, D.K. Benson, Proc. Soc. Photo-Opt. Instr. Eng. 2531 (1995) 19.
[505] X. Ripoche, in: K.-C. Ho, D.A. MacArthur (Eds.), Proceedings of the Symposium on Electrochromic Materials II, Vol. 94-2, The Electrochemical Society, Pennington, 1994, pp. 315–323.
[506] F. Varsano, D. Cahen, F. Decker, J.F. Guillemoles, E. Masetti, J. Electrochem. Soc. 145 (1998) 4212.
[507] M. Moeck, E.S. Lee, M.D. Rubin, R.T. Sullivan, S.E. Selkowitz, Solar Energy Mater. Solar Cells 54 (1998) 157.

[508] J.N. Bullock, Y. Xu, D.K. Benson, H.M. Branz, Proc. Soc. Photo-Opt. Instr. Eng. 2531 (1995) 35.
[509] J.N. Bullock, C. Bechinger, D.K. Benson, H.M. Branz, J. Non-Cryst. Solids 198–200 (1996) 1163.
[510] S.-H. Lee, W. Gao, E. Tracy, H.M. Branz, D.K. Benson, S. Deb, J. Electrochem. Soc. 145 (1998) 3545.
[511] C. Bechinger, S. Herminghaus, W. Petersen, P. Leiderer, Proc. Soc. Photo-Opt. Instr. Eng. 2255 (1994) 467.
[512] Y.A. Yang, Y.W. Cao, P. Chen, B.H. Loo, J.N. Yao, J. Phys. Chem. Solids 59 (1998) 1667.
[512a] Y. Zhao, Z.-C. Feng, Y. Liang, Acta Phys. Sinica 7 (1998) 618.
[513] Y.Z. Xu, M.Q. Qiu, S.C. Qiu, J. Dai, G.J. Cao, H.H. He, J.Y. Wang, Solar Energy Mater. Solar Cells 45 (1997) 105.
[514] H.-M. Lin, C.-M. Hsu, H.Y. Yang, P.-W. Lee, C.-C. Yang, Sensors Actuators B 22 (1994) 63.
[515] C.W. Chu, M.J. Deen, R.H. Hill, J. Electrochem. Soc. 145 (1998) 4219.
[516] L. Sangaletti, E. Bontempi, L.E. Depero, R. Salari, M. Zocchi, P. Nelli, G. Sberveglieri, P. Galinetto, M. Ferroni, V. Guidi, G. Martinelli, J. Mater. Res. 13 (1998) 1568.
[517] J.L. Solis, V. Lantto, Sensors Actuators B 48 (1998) 322.
[518] J. Tamaki, Z. Zhang, K. Fujimori, M. Akiyama, T. Harada, N. Miura, N. Yamazoe, J. Electrochem. Soc. 141 (1994) 2207.
[519] V.N. Nguyen, T.B.N. Nguyen, V.H. Nguyen, Thin Solid Films 334 (1998) 113.
[520] X. Wang, S. Yee, P. Carey, Sensors Actuators B 13–14 (1993) 458.
[521] L.T. Dimitrakopoulos, T. Dimitrakopoulos, P.W. Alexander, D. Logic, D.B. Hibbert, Anal. Commun. 35 (1998) 395.
[522] M. Hashimoto, T. Koreeda, N. Koshida, M. Komuro, N. Atoda, J. Vac. Sci. Technol. B 16 (1998) 2767.
[523] A. Lusis, Proc. Soc. Photo-Opt. Instr. Eng. 2968 (1996) 167.
[524] R.D. Rauh, S.F. Cogan, J. Electrochem. Soc. 140 (1993) 378.
[525] J.C.L. Tonazzi, C. Pershing, in: K.-C. Ho, D.A. MacArthur (Eds.), Proceedings of the Symposium on Electrochromic Materials II, Vol. 94-2, The Electrochemical Society, Pennington, 1994, pp. 339–353.
[526] P. Baudry, A.C.M. Rodriguez, M.A. Aegerter, L.O. Bulhões, J. Non-Cryst. Solids 121 (1990) 319.
[527] D. Camino, D. Deroo, J. Salardenne, N. Treuil, Solar Energy Mater. Solar Cells 39 (1995) 349.
[528] Z. Crnjak Orel, B. Orel, Proc. Soc. Photo-Opt. Instr. Eng. 2255 (1994) 285.
[529] Z. Crnjak Orel, B. Orel, Phys. Stat. Sol. B 186 (1994) K33.
[530] M.A.B. Gomes, D. Goncalves, E.C. Perieira de Souza, B. Valla, M.A. Aergerter, L.O. Bulhões, Electrochim. Acta 37 (1992) 1653.
[531] D. Kéomani, C. Poinsignon, D. Deroo, Solar Energy Mater. Solar Cells 33 (1994) 429.
[532] D. Kéomani, J.-P. Petit, D. Deroo, Proc. Soc. Photo-Opt. Instr. Eng. 2255 (1994) 363.
[533] D. Kéomani, J.-P. Petit, D. Deroo, Solar Energy Mater. Solar Cells 36 (1995) 397.
[534] U. Lavrencic Stangar, B. Orel, I. Grabec, B. Ogorvec, Proc. Soc. Photo-Opt. Instr. Eng. 1728 (1992) 118.
[535] U. Lavrencic Stangar, B. Orel, I. Grabec, B. Ogorvec, K. Kalcher, Solar Energy Mater. Solar Cells 31 (1993) 171.
[536] M.A. Macêdo, L.H. Dall'Antonia, B. Valla, M.A. Aegerter, J. Non-Cryst. Solids 147/148 (1992) 792.
[537] J.C.L. Tonazzi, B. Valla, M.A. Macedo, P. Baudry, M.A. Aegerter, A.C.M. Rodriguez, L.O. Bulhões, Proc. Soc. Photo-Opt. Instr. Eng. 1328 (1990) 375.
[538] B. Valla, J.C.L. Tonazzi, M.A. Macedo, L.H. Dall'Antonia, M.A. Aegerter, M.A.B. Gomes, L.O. Bulhões, Proc. Soc. Photo-Opt. Instr. Eng. 1536 (1991) 48.
[539] A. Azens, L. Kullman, D.D. Ragan, C.G. Granqvist, B. Hjörvarsson, G. Vaivars, Appl. Phys. Lett. 68 (1996) 3701.
[540] A. Azens, L. Kullman, D.D. Ragan, M. Strømme Mattsson, C.G. Granqvist, in: K.-C. Ho, C.B. Greenberg, D. MacArthur (Eds.), Proceedings of the Third Symposium on Electrochromic Materials, Vol. 96-24, The Electrochemical Society, Pennington, 1997, pp. 218–228.
[541] A. Azens, L. Kullman, D.D. Ragan, C.G. Granqvist, Solar Energy Mater. Solar Cells 54 (1998) 85.
[542] L. Kullman, A. Azens, C.G. Granqvist, J. Appl. Phys. 81 (1997) 8002.
[543] L. Kullman, M. Veszelei, D.D. Ragan, J. Isidorsson, G. Vaivars, U. Kanders, A. Azens, S. Schelle, B. Hjörvarsson, C.G. Granqvist, Proc. Soc. Photo-Opt. Instr. Eng. 2968 (1997) 219.

[544] M. Strømme Mattsson, A. Azens, G.A. Niklasson, C.G. Granqvist, J. Purans, J. Appl. Phys. 81 (1997) 6432.
[545] M. Veszelei, L. Kullman, M. Strømme Mattsson, A. Azens, C.G. Granqvist, J. Appl. Phys. 83 (1998) 1670.
[546] M. Veszelei, L. Kullman, C.G. Granqvist, K. von Rottkay, M. Rubin, Appl. Opt. 37 (1998) 5993.
[546a] K. von Rottkay, T. Richardson, M. Rubin, J. Slack, L. Kullman, Solid State Ionics 113–115 (1998) 425.
[547] A. Azens, L. Kullman, G. Vaivars, H. Nordborg, C.G. Granqvist, Solid State Ionics 113–115 (1998) 449.
[548] W. Estrada, A.M. Andersson, C.G. Granqvist, J. Appl. Phys. 64 (1988) 3678.
[549] J.S.E.M. Svensson, C.G. Granqvist, Appl. Phys. Lett. 49 (1986) 1566.
[550] J.S.E.M. Svensson, C.G. Granqvist, Appl. Opt. 26 (1987) 1554.
[551] M. Chigane, M. Ishikawa, J. Electrochem. Soc. 141 (1994) 3439.
[552] M. Chigane, M. Ishikawa, Electrochim. Acta 42 (1997) 1515.
[553] J.I. Cisneros, R.M. Torresi, A. Lourenco, F. Decker, A. Gorenstein, J. Phys.: Condens. Matter 5 (1993) A323.
[554] Z. Crnjak Orel, M.G. Hutchins, G. McMeeking, Solar Energy Mater. Solar Cells 30 (1993) 327.
[555] I.C. Faria, R. Torresi, A. Gorenstein, Electrochim. Acta 38 (1993) 2765.
[556] I.C. Faria, M. Kleinke, A. Gorenstein, M.C.A. Fantini, M.H. Tabacniks, J. Electrochem. Soc. 145 (1998) 235.
[557] F.F. Fereira, M.H. Tabacniks, M.C.A. Fantini, I.C. Faria, A. Gorenstein, Solid State Ionics 86–88 (1996) 971.
[558] M. Kitao, K. Izawa, K. Urabe, T. Komatsu, S. Kuwano, S. Yamada, Jpn. J. Appl. Phys. 33 (1994) 6656.
[559] M. Kitao, K. Izawa, S. Yamada, Solar Energy Mater. Solar Cells 39 (1995) 115.
[560] F. Kong, R. Kostecki, F. McLarnon, R.H. Muller, Thin Solid Films 313–314 (1998) 775.
[561] F. Kong, R. Kostecki, F. McLarnon, J. Electrochem. Soc. 145 (1998) 1174.
[562] T. Maruyama, S. Arai, Solar Energy Mater. Solar Cells 30 (1993) 257.
[563] E.L. Miller, R.E. Rocheleau, J. Electrochem. Soc. 144 (1997) 1995.
[564] K. Murai, T. Mihara, S. Mochizuki, S. Tamura, Y. Sato, Solid State Ionics 86–88 (1996) 955.
[565] J. Nagai, Solar Energy Mater. Solar Cells 31 (1993) 291.
[566] C. Natarajan, S. Ohkubo, G. Nogami, Solid State Ionics 86–88 (1996) 949.
[567] C. Natarajan, H. Matsumoto, G. Nogami, J. Electrochem. Soc. 144 (1997) 121.
[568] Y. Sato, S. Tamura, K. Murai, Jpn. J. Appl. Phys. 35 (1996) 6275.
[569] Y. Sato, M. Ando, K. Murai, Solid State Ionics 113–115 (1998) 443.
[570] P.K. Sharma, M.C.A. Fantini, A. Gorenstein, Solid State Ionics 113–115 (1998) 457.
[571] A. Surca, B. Orel, B. Pihlar, P. Bukovec, J. Electroanal. Chem. 408 (1996) 83.
[572] D.A. Wruck, M. Rubin, J. Electrochem. Soc. 140 (1993) 1097.
[573] J.N. Bullock, H.M. Branz, Proc. Soc. Photo-Opt. Instr. Eng. 2531 (1995) 152.
[574] K. Yoshimura, T. Miki, S. Tanemura, Jpn. J. Appl. Phys. 34 (1995) 2440.
[575] S. Hüfner, Adv. Phys. 43 (1994) 183.
[576] H.L. Tuller, D.P. Button, D.R. Uhlmann, J. Non-Cryst. Solids 40 (1980) 93.
[577] G.B. Smith, G.A. Niklasson, J.S.E.M. Svensson, C.G. Granqvist, J. Appl. Phys. 59 (1986) 571.
[578] A. Talledo, C.G. Granqvist, J. Appl. Phys. 77 (1995) 4655.
[579] V. Eyert, K.-H. Höck, Phys. Rev. B 57 (1998) 12727.
[580] I. Hamberg, C.G. Granqvist, Appl. Opt. 22 (1983) 609.
[581] I. Hamberg, C.G. Granqvist, J. Appl. Phys. 60 (1986) R123.
[582] R.B. Goldner, F.O. Arntz, T.E. Haas, Solar Energy Mater. Solar Cells 32 (1994) 421.
[583] R.B. Goldner, F.O. Arntz, K. Dickson, M.A. Goldner, T.E. Haas, T.Y. Liu, S. Slaven, G. Wei, K.K. Wong, P. Zerigian, Solid State Ionics 70/71 (1994) 613.
[584] R.B. Goldner, F.O. Arntz, K. Dickson, M.A. Goldner, T.E. Haas, T.Y. Liu, S. Slaven, G. Wei, K.K. Wong, P. Zerigian, in: K.-C. Ho, D.A. MacArthur (Eds.), Proceedings of the Symposium on Electrochromic Materials II, Vol. 94-2, The Electrochemical Society, Pennington, 1994c, pp. 237–243.
[585] P.M.M.C. Bressers, E.A. Meulenkamp, J. Electrochem. Soc. 145 (1998) 2225.
[586] J.P. Coleman, J.J. Freeman, A.T. Lynch, P. Madhukar, J.H. Wagenknecht, Acta Chem. Scand. 52 (1998) 86.

[587] R.D. Varjian, M. Shabrang, S.J. Babinec, in: K.-C. Ho, D.A. MacArthur (Eds.), Proceedings of the Symposium on Electrochromic Materials II, Vol. 94-2, The Electrochemical Society, Pennington, 1994, pp. 278–289.
[588] K.-C. Ho, T.G. Rukavina, C.B. Greenberg, in: K.-C. Ho, D.A. MacArthur (Eds.), Proceedings of the Symposium on Electrochromic Materials II, Vol. 94-2, The Electrochemical Society, Pennington, 1994b, pp. 252–268.
[589] M.C. Bernard, A. Hugot le Goff, W. Zeng, Electrochim. Acta 44 (1998) 781.
[590] B.P. Jelle, G. Hagen, J. Appl. Electrochem. 28 (1998) 1061.
[591] S. Passerini, B. Scrosati, V. Herrmann, C.A. Holmblad, T. Bartlett, in: K.-C. Ho, D.A. MacArthur (Eds.), Proceedings of the Symposium on Electrochromic Materials II, Vol. 94-2, The Electrochemical Society, Pennington, 1994, pp. 244–250.
[592] S. Passerini, A.L. Tipton, W.H. Smyrl, Solar Energy Mater. Solar Cells 39 (1995) 167.
[593] J.-G. Béraud, D. Deroo, Solar Energy Mater. Solar Cells 31 (1993) 263.
[594] M.A. Habib, S.P. Maheswari, J. Appl. Electrochem. 23 (1993) 44.
[595] L. Su, Z. Lu, Appl. Spectrosc. 51 (1997) 1587.
[596] L. Su, Z. Lu, J. Phys. Chem. Solids 59 (1998) 1175.
[597] L. Su, J. Fang, B. Liang, Z. Lu, Jpn. J. Appl. Phys. 36 (1997) L684.
[598] L. Su, J. Fang, Z. Lu, Jpn. J. Appl. Phys. 36 (1997) 5747.
[599] L. Su, J. Fang, Z. Lu, Mater. Chem. Phys. 51 (1997) 85.
[600] L. Su, J. Fang, Z. Xiao, Z. Lu, Thin Solid Films 306 (1997) 133.
[601] L. Su, Z. Xiao, Z. Lu, Thin Solid Films 320 (1998) 285.
[602] L. Su, Z. Lu, Y. Wei, Chinese Sci. Bull. 43 (1998) 944.
[603] L. Su, Z. Xiao, Z. Lu, Mater. Chem. Phys. 52 (1998) 180.
[604] L. Su, Q. Hong, Z. Lu, J. Mater. Chem. 8 (1998) 85.
[605] L. Su, H. Wang, Z. Lu, Mater. Chem. Phys. 56 (1998) 266.
[606] L. Su, J. Fang, Z. Lu, J. Appl. Polym. Sci. 70 (1998) 1955.
[607] L. Su, H. Wang, Z. Lu, Supramol. Sci. 5 (1998) 657.
[608] S.-H. Lee, S.-K. Joo, Solar Energy Mater. Solar Cells 39 (1995) 155.
[609] S.-H. Lee, B.-I. Lee, S.-K. Joo, in: K.-C. Ho, C.B. Greenberg, D.A. MacArthur (Eds.), Proceedings of the Third Symposium on Electrochromic Materials, Vol. 96-24, The Electrochemical Society, Pennington, 1997, pp. 191–205.
[610] S.-H. Lee, Y.-S. Park, S.-K. Joo, Solid State Ionics 109 (1998) 303.
[611] B. Orel, U. Opara Krasovec, U. Lavrencic Stangar, P. Judeinstein, J. Sol–Gel Sci. Technol. 11 (1998) 87.
[612] P. Olivi, E.C. Pereira, E. Longo, J.A. Varella, L.O. de S. Bulhoes, J. Electrochem. Soc. 140 (1993) L81.
[613] U. Opara Krasovec, B. Orel, S. Hocevar, I. Musevic, J. Electrochem. Soc. 144 (1997) 3398.
[614] B. Orel, U. Lavrencic Stangar, K. Kalcher, J. Electrochem. Soc. 141 (1994) L127.
[615] J. Isidorsson, C.G. Granqvist, Solar Energy Mater. Solar Cells 44 (1996) 375.
[616] J. Isidorsson, M. Strømme, G. Gåhlin, G.A. Niklasson, C.G. Granqvist, Solid State Commun. 99 (1996) 109.
[617] J. Isidorsson, C.G. Granqvist, L. Häggström, E. Nordström, J. Appl. Phys. 80 (1996) 2367.
[618] J. Isidorsson, C.G. Granqvist, K. von Rottkay, M. Rubin, Appl. Opt., in press.
[619] M. Strømme Mattsson, G.A. Niklasson, C.G. Granqvist, J. Appl. Phys. 80 (1996) 233.
[620] M. Veszelei, L. Kullman, A. Azens, C.G. Granqvist, B. Hjörvarsson, J. Appl. Phys. 81 (1997) 2024.
[621] A. Azens, A. Talledo, A.M. Andersson, G.A. Niklasson, B. Stjerna, C.G. Granqvist, J.R. Stevens, Proc. Soc. Photo-Opt. Instr. Eng. 1728 (1992) 103.
[622] C. Bechinger, S. Ferrere, A. Zaban, J. Sprague, B.A. Gregg, Nature 383 (1996) 608.
[623] A. Hagfeldt, M. Grätzel, Chem. Rev. 95 (1995) 49.
[624] M.K. Nazeeruddin, A. Kay, I. Rodicio, R. Humphry, E. Müller, P. Liska, N. Vlachopoulos, M. Grätzel, J. Am. Chem. Soc. 115 (1993) 6382.
[625] B. O'Regan, M. Grätzel, Nature 353 (1991) 737.
[626] D.R. MacFarlane, J. Sun, M. Forsyth, J.M. Bell, L.A. Evans, I.L. Skryabin, Solid State Ionics 86–88 (1996) 959.